UNIVERSITÉ DU LUXEMBOURG

Faculty of Science, Technology and Medicine

Master in Integrated Systems Biology

MASTER thesis

by

Daniela María VEGA GUTIÉRREZ
Born on 27 February 1989 in Costa Rica

Usage of an ENS-Intestine Assembloid to Reveal α-synuclein Transport from the Intestine to the Nervous System

UNIVERSITÉ DU LUXEMBOURG

Faculty of Science, Technology and Medicine

Master in Integrated Systems Biology

MASTER thesis

by

Daniela María VEGA GUTIÉRREZ
Born on 27 February 1989 in Costa Rica

Usage of an ENS-Intestine Assembloid to Reveal α-synuclein Transport from the Intestine to the Nervous System

Defense:	16 November 2022 in Luxembourg
Supervisor(s):	Jens Schwamborn, PhD, Full Professor in Cellular and Developmental Biology, University of Luxembourg
Jury members:	Paul Wilmes, PhD, Full Professor in Systems Ecology, University of Luxembourg Elisabeth Letellier, PhD, Principal Investigator and Co-Head of the Molecular Disease Mechanisms Group, University of Luxembourg

Table of Contents

Preamble and Acknowledgements

Herewith I would like to declare that portions of this thesis were adapted from my previously written document “Research Practical Report” for the course ISB902 - Research Practical, specifically for the Introduction and some immunofluorescence images of brain organoids.

This thesis would not have been possible without the support and guidance from several individuals whom I want to give an enormous amount of thanks: Dr. Jens Schwamborn for supervising this project and giving me the opportunity to work in his research team; Gemma Gomez, for her excellent guidance since my internship and throughout my thesis, the knowledge provided constituted the foundation for the execution of this project. Dr. Paul Antony for the vital support in image acquisition and analysis and the never-ending availability to teach, this significantly enriched this project and my coding knowledge; Dr. Graham Robertson for the provision of the 3D-printed inserts and the valuable insights for improvement; Dr. Elisabeth Letellier and Dr. Paul Wilmes for reviewing this thesis; and, of course, all the members of the Developmental and Cell Biology group for welcoming me as part of the team and all the assistance provided with data analysis, lab work and general support throughout my time at the Luxembourg Centre for Systems Biomedicine.

Abstract

Parkinson's disease (PD) is characterized by the loss of dopaminergic neurons exhibiting Lewy Pathology (LP) in the *substantia nigra*. It has been suggested that LP to occurs at the gastrointestinal tract long before than in the brain. Braak's hypothesis postulates that external agents in the gut come in contact with enteric neurons triggering α-synuclein misfolding and aggregation, which then propagates through the vagal nerve towards the brain. Numerous preclinical and clinical studies support this hypothesis; however, it is yet impossible to observe this process in a human *in vivo*. To overcome this, this project proposed the construction of an *in vitro* assembloid model of the intestine and the enteric nervous system based on iPSC-derived organoids. The assembloid, composed of intestinal organoids (iHOs) and enteric neurons (ENS), was used to visualize the pathological spread of α-synuclein. Two different approaches were followed to build the assembloids. The first one involved the co-cultivation of the iHOs and ENS in a single well subdivided by an insert (iHO-ENS assembloid). Intracellular and extracellular α-synuclein were quantified using blotting techniques. The second strategy involved combining both cell types at earlier differentiation stages and culturing them in 3D conditions to obtain iHOs with integrated ENS (iHO-ENC assembloid). In this case, α-synuclein was measured using high content microscopy and an own-developed computational algorithm. This algorithm was first created for the analysis of brain organoids and later adapted to the assembloids. In the iHO-ENS assembloid, direct contact within the different cell types could not be detected, and even though extracellular α-synuclein measurements suggested that iHO-secreted α-synuclein might be up taken by the ENS, this could not be confirmed by intracellular α-synuclein tests. By contrast, an increased content of α-synuclein was detected in neurons co-cultured with PD iHOs in the iHO-ENC assembloid. Furthermore, aggregate size within the neurons conveyed early stages of LP. Interestingly, in the iHOs α-synuclein expression was detected mostly within enteroendocrine cells, which have been proposed as α-synuclein misfolding induction sites in the gut. Additionally, analysis of PD brain organoids revealed an increased content of α-synuclein phosphorylated at S129 in nuclei, supporting the function of this modification as a nuclear localization tag, and providing insight into its pathological implications. Furthermore, in this model Lewy body-like aggregates expanded over time mimicking pathological progression. Overall, findings of this project encompass the novel characterization of α-synuclein expression in iHOs and, preliminarily, the foremost observation of α-synuclein propagation from the intestine to the enteric nervous system in a human organoid-based model. Both the cellular and computational models created can serve as the foundation for further disease modeling and drug screening studies.

List of Abbreviations

PD - Parkinson's Disease
REM - Rapid Eye Movement
MPTP - 1-methyl-4-fenyl-1,2,3,6-tetrahydropyridine)
MPPP - desmethylprodine
α-synuclein - alpha-synuclein
LBs - Lewy bodies
LNs - Lewy neurites
SNpc -*substantia nigra pars compacta*
LP - Lewy pathology
DNs - dopaminergic neurons
CNS - Central Nervous System
NAC - non-amyloid component
PTMs - post-translational modifications
pS129 - phosphorylation at Serine residue 129
SN - *substantia nigra*
DMV - dorsal motor nucleus of the *vagus*
iPSCs - induced pluripotent stem cells
MOs - midbrain organoids
iHOs - human intestinal organoids
Wnt - Wingless/Integrated
RA - Retinoic Acid
EGF - Epidermal Growth Factor
ENS - enteric neurons
ENCs - enteric neural precursors
BMP - Bone Morphogenic Protein
AA - Ascorbic Acid
GDNF - Glial cell line-Derived Neurotrophic Factor
HCI - High Content Imaging
HCA - High Content Analysis
GFP - Green Fluorescent Protein
E8 - Essential 8
P/S - Penicillin-Streptomycin
DMEM/F-12 - Dulbecco's Modified Eagle Medium/Nutrient Mixture F-12
ROCK inhibitor - Rho-associated kinase inhibitor Y27632
WT - Wild Type
SNCAx3 - Triplication of the *SNCA* gene
SNCA KO - *SNCA* gene knock-out
WT-GFP - Wild Type- GFP
bFGF- basic Fibroblast Growth Factor
RPMI - Roswell Park Memorial Institute
MEM NEAA - Minimum Essential Medium Non-Essential Amino Acids
LY - LY294002
CHIR - CHIR99021
PE2 - Prostaglandin E2
GFR - Growth Factor Reduced
PBS - phosphate-buffered saline
HEPES - (4-(2-hydroxyethyl)-1-piperazineethanesulfonic acid
hiPSC - human induced pluripotent stem cell
E6 - Essential 6 medium
LDN - LDN193189
SB - SB431542
Ri - ROCK inhibitor
FACS - fluorescence activated cell sorting
CD49d - Integrin α-4
ULA - ultralow adhesion
NB - Neurobasal
BSA - Bovine Serum Albumin
DoD - days of differentiation
PFA - paraformaldehyde
NGS - Normal Goat Serum
RT - room temperature

RT-qPCR - quantitative real time polymerase chain reaction

RPL37A - Ribosomal Protein L37a

HOXB2 - Homeobox B2

PHOX2A - Paired Like Homeobox 2A

PHOX2B - Paired Like Homeobox 2B

SOX10 - SRY-Box Transcription Factor 10

TUJ1 - class III β-tubulin

MASH1 - Achaete-scute homolog 1

Ct - Cycle threshold

DTT - dithiothreitol

PVDF - polyvinylidene fluoride

p-α-synuclein - α-synuclein phosphorylated at S129

IgG - immunoglobulin G

MAP2 - Microtubule-associated Protein 2

CBC - Crypt Base Columnar

5-HT$_{2c}$ - 5-hydroxytryptamine

ChAT - Choline acetyltransferase

GABA - gamma-Aminobutyric acid

TH - Tyrosine hydroxylase

VIP - Vasoactive Intestinal Peptide

EECs - enteroendocrine cells

WB - Western Blot

DSP - dithiobis(succinimidylpropionate)

1 Introduction

1.1 Parkinson's Disease

Parkinson's disease (PD) is the second most common age-related neurodegenerative disorder, surpassed only by Alzheimer's disease[1]. Diagnosis for PD commonly occurs upon the appearance of the first motor symptoms: resting tremor, muscular rigidity, bradykinesia, and postural instability. Nonetheless, these might be preceded by non-motor symptoms for more than a decade and include constipation, Rapid Eye Movement (REM) sleep behavior disorder, loss of taste and smell, fatigue, and mood disturbances. The type and severity of non-motor symptoms differs greatly between patients, but they remain present as other symptoms appear during disease progression, usually becoming even more problematic for the patient than the motor symptoms[2], evidencing the significant impact that PD has on the patient's quality of life.

The risk of suffering from PD becomes increasingly prevalent with age, as demonstrated in a meta-analysis performed by Hirsch *et al.* (2016)[3] based on 27 international studies. In a comparison between individuals aged 40-49 and aged 80 or more, they revealed that PD incidence increased over 30-fold in women and 70-fold in men. Having mentioned that, in about 3-5% of cases disease onset occurs before the age of 40 due to secondary reasons, such as environmental factors or (less frequently) genetic causes, a condition known as Early-onset Parkinson's Disease[4]. Even so, PD is considered an age-related disease.

Independently of the age of onset, PD is classified as familial or sporadic according to its source. Sporadic PD cases represent an 85% of the total[5], yet its causes remain elusive, with potential sources pointing to genetic and environmental elements. For instance, the prodrug MPTP (1-methyl-4-fenyl-1,2,3,6-tetrahydropyridine), a neurotoxic by-product of the manufacturing of the synthetic opioid MPPP (desmethylprodine), and the pesticides Rotenone and Paraquat have been demonstrated to cause PD[6,7]. On the other hand, familial PD is caused by alterations in genes such as *SNCA*, *LRRK2*, *GBA*, *PRKN*, among others, of which *SNCA* was the first to be linked to PD[5]. This gene codes for the protein alpha-synuclein (α-synuclein), and its alterations are comprised of point mutations (e.g. A30P, A53T, and E46K) or copy number variations (locus duplication or triplication)[8]. Still, having a mutation for one the mentioned genes does not lead to PD in a 100% of the cases[5], complicating the distinction between genetic predisposition in familial

and sporadic PD. It seems most likely that genetic risk factors create a susceptibility that, in interplay with aging and environmental factors, lead to familial or sporadic PD.

Despite affecting more than 6 million people around the world[9], treatment options for PD remain limited and focus primarily on symptom relief. Motor symptoms are mainly treated with dopamine-related medication (Levodopa, dopamine agonists, and monoamine oxidase-B inhibitors) and physical therapy. Advanced therapies such as deep brain stimulation and MRI-focused ultrasound have shown to be beneficial, but they are applicable to patients with a specific profile and require a highly specialized health infrastructure[9]. Research is under way to better understand the disease from a genetic and mechanistic point of view, with the aim to be translated into an increase in treatment options for physicians and their patients.

From a neuropathological perspective, PD is characterized by the presence of abnormal proteinaceous inclusions, Lewy bodies (LBs), and spindle or thread-like Lewy neurites (LNs) in involved neurons. Notably, a significant loss of dopaminergic neurons with LBs in the *substantia nigra pars compacta* (SNpc) of the midbrain occurs early during disease development, before symptoms appear. The death of dopaminergic nigrostriatal neurons exhibiting Lewy pathology (LP), and the subsequent dopamine deficiency, are considered the primary cause of classical Parkinsonian motor impairment[2] and the neuropathological hallmarks of this disease (Figure 1).

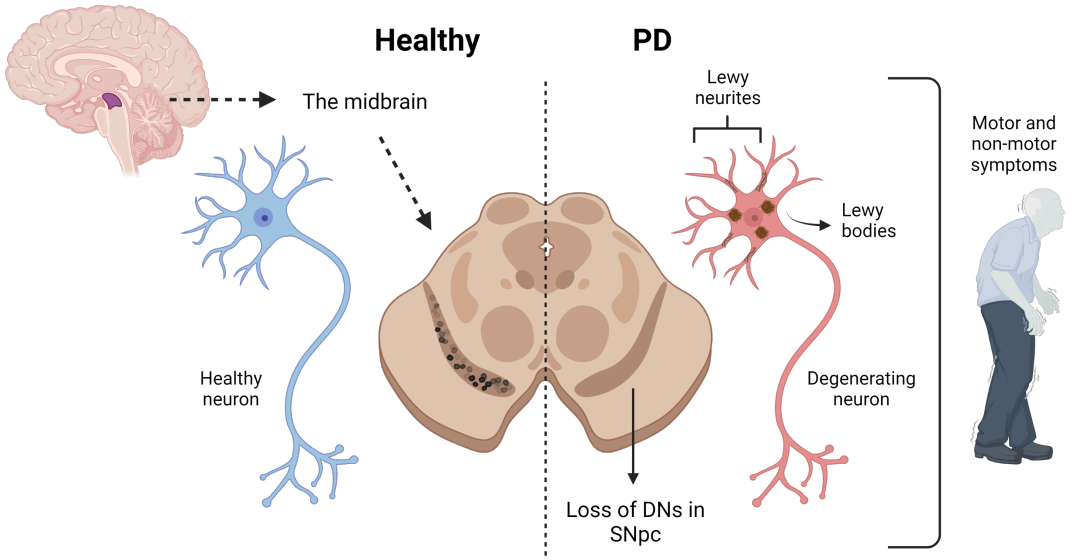

Figure 1. The neuropathological hallmarks of Parkinson's Disease (PD). PD is characterized by the loss of dopaminergic neurons (DNs) in the *substantia nigra pars compacta* (SNpc) containing Lewy bodies and Lewy neurites. This neurodegeneration leads to classical symptoms. Created with BioRender.

1.2 α-synuclein and Parkinson's Disease

α-synuclein is the main protein component of LBs and LNs. It is particularly highly expressed in the Central Nervous System (CNS), making up approximately 1% of the proteins in the brain, where it is abundant in presynaptic vesicles[10]. As explained by Kawahata *et al.* (2022)[10], the protein was first reported in cholinergic synaptic vesicles from the electric organ of the Pacific electric ray (*Torpedo californica*). Its expression distribution, in presynapses and nuclei, gave rise to the name "synuclein". This protein's functions have not been fully unraveled, but experiments with knock out cell lines and animal models have revealed roles related to synaptic vesicle release and trafficking, enzyme and transporter regulation, and binding of fatty acids[11].

Structurally, α-synuclein is 140-amino acids long and consists of three domains: an amphipathic α-helical N-terminal domain, a hydrophobic non-amyloid center, and a hydrophilic C-terminal domain[10,11] (Figure 2). As indicated by Meade *et al.* (2019), the precise native structure of α-synuclein is still highly debated, with studies describing it as intrinsically disordered, helical, or a combination of both. The current paradigm is that it exists in an equilibrium mixture of unstructured monomers and helical oligomers in interaction with phospholipid membranes[12].

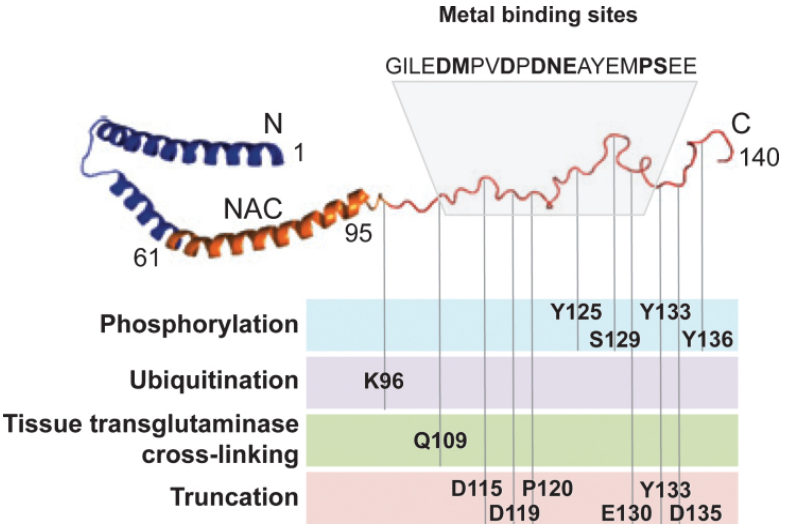

Figure 2 Structure of α-synuclein and summary of post translational modifications of the C-terminal and metal binding sites. N: N-terminal region; NAC: non-amyloid component; C: C-terminal region. Taken from Oueslati *et al.* (2022)[13].

Lewy body-contained α-synuclein is subjected to multiple post-translational modifications (PTMs) that include ubiquitination, phosphorylation, nitration, truncation, and cross-linking (Figure 2). The C-terminal tail of α-synuclein contains most of these PTM sites, and since this region is instrumental in the protein's

interactions with ligands (e.g. proteins and metal ions), it has been deducted that they normally regulate the protein's physiological structure and functions[13]. Among these PTMs, a special focus has been given to the phosphorylation at the Serine residue 129 (pS129) due to its prominent accumulation in the brains of patients suffering from synucleopathies, where it represents about 90% of the insoluble α-synuclein. In contrast, only around 4% of α-synuclein is phosphorylated in this way in the brain of healthy individuals[10,13]. These findings support the hypothesis that pS129 plays an important role in α-synuclein aggregation, formation of LBs and neurotoxicity.

Under pathological conditions, α-synuclein's structure is altered causing its misfolding. This in turn leaves the protein susceptible to aggregation, resulting in the formation of soluble oligomers that afterwards progress into insoluble fibrils. These fibrils are composed of β-sheets made up of two or more polypeptide chains linked to each other by hydrogen bonds[11] (Figure 3). As pointed out in a review by Koh and collaborators (2018), although fibrils are the main component of LBs, several studies suggest that soluble oligomers are actually more toxic, possibly because they can be more easily transmitted from cell to cell[11].

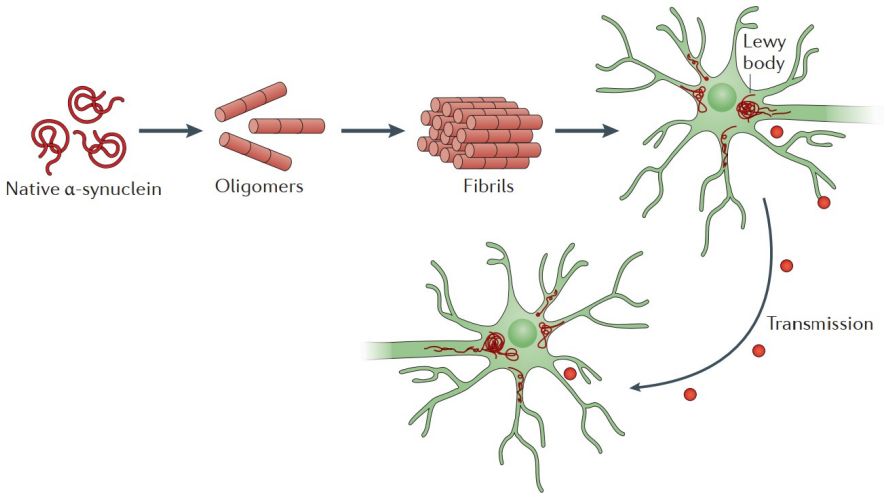

Figure 3. α-synuclein aggregation. Under normal physiological conditions α-synuclein exists as monomers, but under pathological conditions it becomes misfolded and tends to form oligomers and then fibrils. These further aggregate into Lewy bodies. Evidence suggests that aggregates are transmitted from cell to cell, leading to spread of the pathology. Obtained from Kingwell (2017)[14].

1.3 Braak's hypothesis for Parkinson's Disease

Recently, it has been uncovered that PD-associated pathology seems to occur at the gastrointestinal tract at much earlier time points than in the CNS[15]. In particular, LP

has been described as beginning at specific induction sites and advancing in a defined pattern through the nervous system. The hypothesis, postulated by Braak *et al.* in 2003, originally stated that PD was triggered by an unknown pathogen (e.g. a virus or bacteria) present in the gut[16]. Then, these researchers proposed a staging system based on the sequence followed by α-synuclein as it spreads through the body[17]. The proposal was later expanded to a dual-hit hypothesis indicating that PD can begin at two locations: the nasal cavity and the gut[18,19]. At these sites, microbial substances are thought to come in contact with olfactory and/or enteric neurons triggering the misfolding and aggregation of α-synuclein. Aggregated α-synuclein then propagates through the olfactory bulb and the vagal nerve towards the CNS, eventually reaching the *substantia nigra* (SN) of the midbrain (Figure 4). This is now known as Braak's hypothesis for Parkinson's Disease.

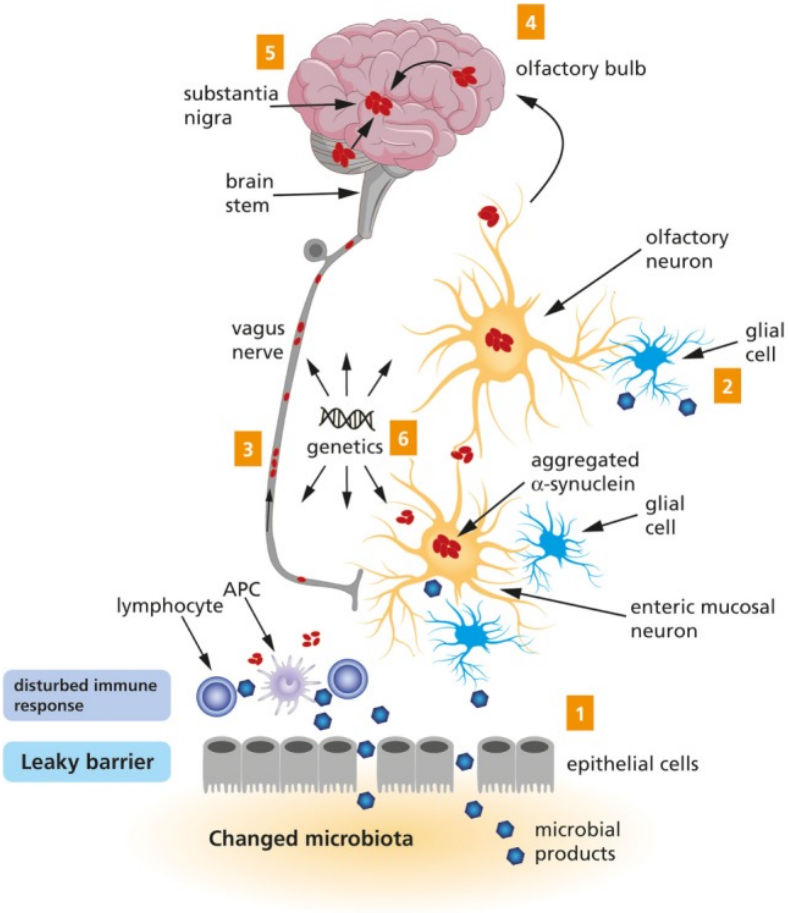

Figure 4. Illustration of Braak's hypothesis of Parkinson's Disease. Microbial agents come in contact with enteric and olfactory neurons triggering α-synuclein aggregation (1&2). Aggregates then travel through the *vagus* nerve (3) or olfactory bulb (4) to the brain, eventually reaching the *substantia nigra* (5) of the midbrain. A genetic predisposition is likely to contribute to PD (6). PD: Parkinson's Disease; APC: antigen presenting cell. Taken from Rietdijk *et al.* (2017)[8].

In a detailed review by Rietdijk and group (2017)[8], they summarize the preclinical and clinical evidence supporting this hypothesis. As mentioned, a key part of the hypothesis is the propagation of LP from the enteric nervous system to the CNS through the *vagus* nerve and the dorsal motor nucleus of the *vagus* (DMV). Within the CNS, LP is described to move from the lower brainstem regions towards the SN, reaching lastly the neocortex. In accordance with this, LP has been detected in the vagal nerves and the DMV before occurring in other regions of the CNS, and truncal vagotomy has been associated with a decreased risk of developing PD. In animal models, the spread α-synuclein to the *vagus* nerve and DMV has been observed upon the injection of the protein in the stomach and duodenum of rats. Similarly, gastric administration of Rotenone in mice, led to occurrence of LP in the enteric nervous system, the DMV and the SN, with neurodegeneration in the latter. Crucially, this spread was prevented by the execution of vagotomies[8]. All of these findings support the idea that α-synuclein indeed propagates to the CNS from the enteric nervous system via the *vagus* nerve.

1.4 Disease Modeling

The impossibility to study neurodegenerative diseases *in vivo* in humans, as demonstrated by the fact that definitive diagnosis is only possible post-mortem[17], is an obstacle for their mechanistic understanding and their timely management. In this regard, disease models have been developed with the aim to imitate pathological events in a non-human context. The usage of animal systems and classical cell lines as models in biomedical research, has yielded invaluable findings in the unravelling of pathological progression and mechanisms, cellular signaling pathways, and drug screening[20]. Yet, several biological phenomena are specific to humans and hence difficult, if not impossible, to be reproduced in animal models. A clear instance of this is the human brain, which is extremely complex and exhibits species-specific developmental processes. Furthermore, several types of cells are completely or nearly absent in frequently used models including mice, as is the case of the cells of the outer radial glia[21]. Human physiology also differs greatly, affecting for instance drug metabolism studies. As an example, the common drug ibuprofen, prescribed in humans as an anti inflammatory, is metabolized so distinctly in rats that it results toxic[22]. These disadvantages of animal models constitute a bottleneck for the translation of research results into the clinic.

Novel technologies have been developed to overcome these obstacles, namely, human cell-based *in vitro* models. An major leap in this area of research was the

discovery made in 2007 by Takahashi and collaborators of a method involving the transduction of transcription factors Oct 3/4, SOX2, Klf4, and c-Myc to reprogram differentiated cells into pluripotent, precursor states, called induced pluripotent stem cells (iPSCs)[23]. Today, easily available cells from patients, such as fibroblasts, can be dedifferentiated into iPSCs, and these in turn can be repurposed into a variety of cell lineages. Consequentially, the development of iPSCs has made possible the generation of individual-specific models for, in principle, any desired cell type.

The generation of iPSCs is now routinely done in laboratories, but their application in disease modelling is still in progress[20]. Initial efforts aimed to differentiate iPSCs into specific cell types and succeed at their monolayer culture. Currently, more advanced methods seek to recapitulate embryonic organ development for the generation of 3D self-organizing tissue structures which mimic a mature organ's anatomy[20], the so-called "organoids". These models were first developed for the small intestine[24], and since then numerous organs or organ regions have been represented in this way, as is the case of cerebral[25], midbrain[26], neuromuscular[27], and kidney[28] organoids. Organoids permit, among other aspects, to study cell-to-cell interactions between distinct cell types organized in a tridimensional structure that more closely resembles human physiology.

1.4.1 Brain organoids

Brain organoids are three-dimensional structures that resemble the human fetal brain structurally and functionally. In them, iPSCs differentiate into multiple cell types that are present in the brain and self-organize in a specific spatial disposition that recapitulates human embryonic development[15].

Protocols for the generation of brain organoids that mimic different brain regions have been published, including the cerebral cortex[29], the cerebellum[30], the midbrain[26,31], the forebrain, and the hypothalamus[32]. These models have been used increasingly to explore the human brain development and associated genetic and infectious diseases[26,33]. Regarding PD, midbrain organoids (MOs) are of particular interest since dopaminergic neuronal loss is a hallmark trait of the disease. Recently, these have been generated from iPSCs derived from patients harbouring PD-related genetic alterations, and have successfully recapitulated disease-relevant phenotypes[34,35]. These findings validated the model's relevance to study PD, and represented a huge step-forward in our knowledge of the pathology.

1.4.2 Intestinal organoids

Human intestinal organoids (iHOs) were originally generated from primary intestinal epithelium containing self-renewing stem cells[24]. Today, these 3D structures that imitate the epithelial lining of the human gut are derived from iPSCs using a stepwise differentiation process that simulates embryonic intestinal development. In it, iPSCs are first derived into definitive endoderm, which is later differentiated into hindgut spheroids; these will lastly grow to generated three-dimensional intestinal structures. iHOs possess a lumen-surrounding polarized epithelium and the characteristic cell types found in the human intestinal epithelium[36] (Figure 5).

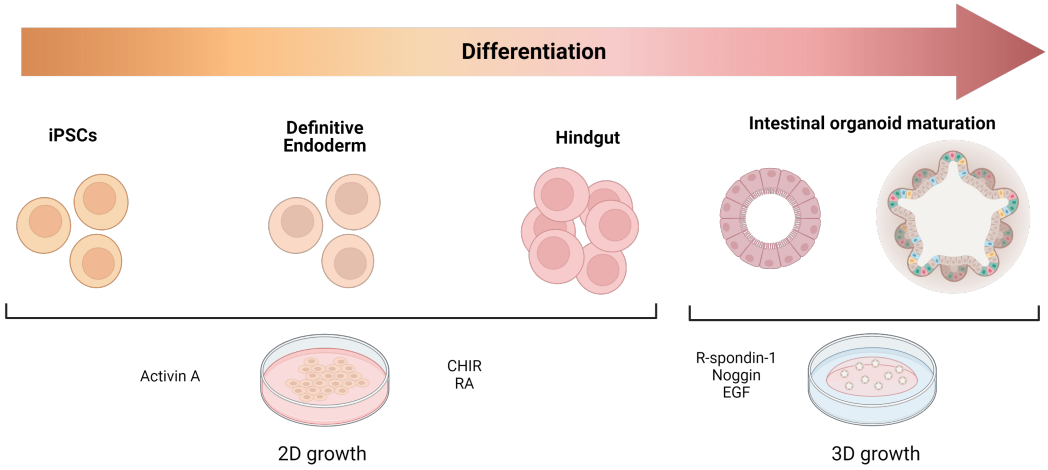

Figure 5. Intestinal organoid differentiation. iPSCs are differentiated into iHOs in a step wise manner: first into endoderm, then into hindgut, and lastly into organoids in a 3D culture system. iPSCs: induced pluripotent stem cells; iHOs: intestinal organoids; CHIR: CHIR99021; RA: Retinoic Acid; EGF: Epidermal Growth Factor; 2D: two-dimensional; 3D: three-dimensional. Created with BioRender.

Growth factors used for iHO derivation vary significantly between protocols[36–39]. In general, Activin A is used to promote differentiation into definitive endoderm[36], whereas an active Wingless/Integrated (Wnt) signaling (achieved with CHIR99021) in conjunction with Retinoic Acid (RA) are used to induce hindgut formation[40]. For spheroid development into intestinal tissue, three-dimensional culture conditions that had previously been employed for adult intestinal epithelium are used. Briefly, these consist in embedding the spheroids in Matrigel and the usage of R-spondin-1, Epidermal Growth Factor (EGF), and Noggin as growth factors[24,36] (Figure 5).

iHOs have been applied, for example, to identify the molecular basis of human congenital gut defects[36], and to model the intestinal epithelial response to enteric infections[37].

1.4.3 Enteric neurons

The enteric nervous system has long been considered a second brain due to its independent functionality, its important cellular population size, and the chemical and functional resemblance of neurons to those of the CNS[15]. Developmentally, the enteric nervous system is generated from vagal and sacral neural crest, but the former gives rise to the majority of cells that migrate and colonize the entire length of the bowel[41].

Scientists have also developed *in vitro* models for the enteric nervous system. They are based on the generation of vagal enteric neuronal precursors from iPSCs, which are later differentiated into enteric neurons (ENS). Similarly to iHOs, this procedure follows a staged methodology comprised of 2D and 3D culture phases. First, enteric neural precursors (ENCs) are derived from iPSCs in a monolayer fashion by the use of different combinations of RA, Bone Morphogenic Protein (BMP) and Wnt signaling. Then, cells are cultured as free-floating spheroids to enrich ENC populations. Finally, spheroids are plated in the presence of Ascorbic Acid (AA) and Glial cell line-Derived Neurotrophic Factor (GDNF) for neuronal induction[41,42] (Figure 6).

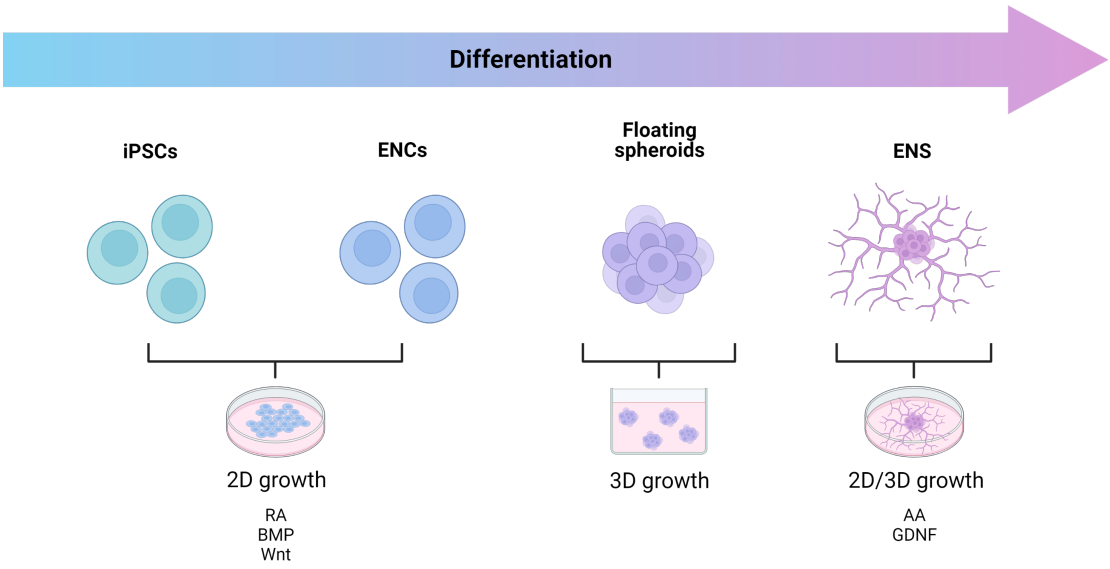

Figure 6 Differentiation of enteric neurons. To generate enteric neurons (ENS), iPSCs are first differentiated into enteric neuron precursors (ENCs), then cultivated as floating spheroids which are later plated to stimulate the outgrowth of neurons. iPSCs: induced pluripotent stem cells; RA: Retinoic Acid; BMP: Bone Morphogenic Protein signaling; Wnt: Wingless/Integrated signaling; AA: Ascorbic Acid; GDNF: Glial cell line-Derived Neurotrophic Factor; 2D: two-dimensional; 3D: three-dimensional. Created with BioRender

iPSC-derived enteric neural lineages are a powerful tool for developmental studies, disease modeling, and drug screening of the enteric nervous system. For instance,

neuronal precursors obtained through this process have demonstrated successful *in vivo* engraftment and migration in chicken and mice, have been able to differentiate into functional enteric neurons, and have been used as a disease model for Hirschsprung disease[41].

Despite the mentioned progress, it has to be considered that organoids, as any other type of model, have advantages and limitations. As mentioned, patient-derived organoids have a huge potential as models for disease mechanisms, drug screening and drug safety studies, which could ideally lead to the discovery of successful treatments. Moreover, organoids could be potentially used in regenerative medicine. On the other hand, these organ models generally lack proper irrigation and immune and nervous systems, failing to represent these relevant physiological aspects. Other issues that remain unsolved are the resolution and complexity with which disease manifestations can be examined, the epigenetic and environmental memories of employed cells, and their unsuitability to approach multi-tissue or multi-organ diseases in terms of system interactions[43].

1.4.4 Assembloids

Different tactics have been followed to address organoid-bound limitations. For example, cells of different lineages have been combined before organoid formation in an attempt to incorporate vasculature or immune cells. However, it has been found that organoids with a defined spatial organization are not obtained following this strategy[44]. Assembloids constitute a promising solution: in them, organoids of different regional identity are fused together with the purpose of reproducing inter-regional and inter-cellular interactions[33]. For example, as described by Makrygianni and Chrousos (2021)[33] the study of the interaction of cortical glutamatergic neurons and GABAergic interneurons was achieved in a multi-region assembloid generated by the fusion of dorsal and ventral forebrain organoids. Furthermore, the mentioned review illustrates a diverse range of brain assembloids that have been constructed, including multi-region and region-specific assembloids.

As previously stated, the generation of MOs from iPSCs derived from PD patients has significantly contributed to our understanding of PD-related pathophysiology. However, to comprehend its systemic implications, it has become necessary to upgrade the complexity of existent models. This could be accomplished, for example, by the generation of assembloids that incorporate additional brain regions to the midbrain. Similarly, brain organoids with vasculature or and immune system would better mimic physiological conditions. In this thesis project, we proposed to undertake

this challenge by the development of an assembloid that integrates the human intestine and enteric nervous system, with the purpose to better understand the interplay of both systems in PD pathology.

1.5 High content imaging and high content analysis

Traditionally, cellular biology data has been reported as an average response for a cell population. It is only in the last decade that computing power and data storage capabilities have developed sufficiently for scientist to be able to monitor single cells within a population. High content imaging (HCI) has proven instrumental to study specimens in a way that permits to unravel cellular heterogeneity within a sample, in terms of protein expression and response to stimuli[45].

HCI is done with the aim is to extract as much data as possible (high content data) from imaging of a biological sample. The "content' of the data can include information such as size, quantity, shape, color, brightness and location. As an example, while a standard cell biology experiment involves analyzing average protein expression in a small number of cells, in HCI this expression is studied in hundreds or thousands of cells, individually, for better statistical analysis. HCI often involves cell biology experiments in combination with a highly automated three-step process: image acquisition, image processing, and image analysis.

1.5.1 Image acquisition

The image acquisition technology involved in HCI seeks to create a sharp image automatically. This requires ultra-fast focusing and sample detection, precision-motion modules, and optimized acquisition speeds. High content imagers typically consist of automated microscopes contained in a box, equipped with image management packages (to store images on a server or data storage system) and an image analysis software (Figure 7.a). They generate image sets and associated meta-data of substantial size in the range of Tera-bytes[46].

There are several manufacturers of high content imaging systems[45,46], and most offer wide-field and confocal imagers. In this project, a confocal microscope with a dual spinning disc technology was used. Confocal microscopes use a fixed or adjustable pinhole to block out-of-focus light resulting in improved depth resolution and contrast, although, most of the light used to excite fluorescence in the sample is lost. Additionally, this mechanism can only image a single point at a time resulting in the need to scan the light beam and pinhole across the sample. To solve this, spinning disks have multiple small pinholes to increase illumination and the number of points

that can be scanned simultaneously. In this way, regions of interest can be scanned within an few hundred milliseconds. Furthermore, the dual spinning disc technology devised by Yokogawa consists in a first disk with lenses that focus the light on the pinholes of the second disk (Figure 7.b), increasing the illumination of the sample and reducing image acquisition time[46].

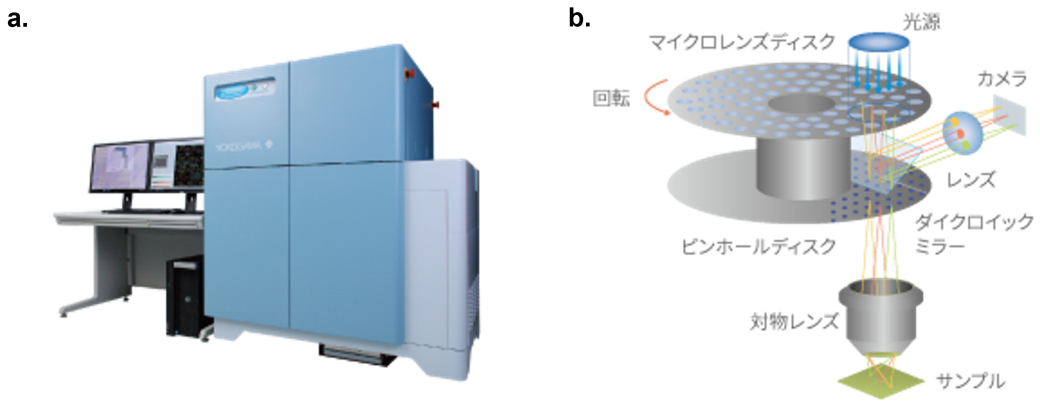

Figure 7. Yokogawa CV8000 high content imager. a. A high content imager is typically composed of an automated microscope contained in a box, equipped with image management and image processing software. **b.** The dual spinning disc technology consists of a first disk with lenses that focus the light on the pinholes of the second disk. Taken from www.yokogawa.com[47].

1.5.2 Image processing

Once acquired, images are automatically processed. Common processing operations include image stitching, Z-stack processing, and correction for noise and illumination errors. Image stitching is the joining of adjacent fields of view into a single image to visualize a large area of the sample. Z-stack processing reduces the three-dimensional visualized volume into a two-dimensional image (e.g. through the selection of specific planes of interest). Noise sources are diverse and include random photon emission from the background, staining artifacts or optic aberrations. Noise can be corrected by applying filters which smooth images through kernel-based methodologies. Filters can be linear (e.g. median or Gaussian filters) or non-linear[48].

1.5.3 Image analysis

Once images are processed, automated image analysis extracts the data of interest, a process known as High Content Analysis (HCA). It begins with the segmentation of images to identify objects of interest, followed by the extraction of measurements for each object, such as intensity, count and morphology information. The image

analysis process described next, is a summary of the guidelines for image-based High Content Screening, HCA and HCI published by Buchser *et al.* (2014)[46].

The first step in object identification is to distinguish the signal from the background. This is done by defining a threshold is that eliminates the pixels that are too dim, considering them as background. The result of thresholding is a binary image, a mask, with only negative or positive pixels. After thresholding, segmentation can classify positive pixels into separate objects. For this, an algorithm is used that scans the image until a positive pixel is found, then it identifies all connected positive pixels and assigns them to the first object. The process continues until all positive pixels in the image are allocated to an object. A further segmentation step allows to separate two adjacent objects. This can be achieved by applying a water shed algorithm that "fills" the image with water until boundaries are established, or by searching for intensity peaks, among other strategies. New and improved segmentation algorithms are continuously being developed.

The measurements that are obtained from an image are called "features". This are usually object-based measurements such as count, size, shape, intensity, or texture. Some commonly used features are explained below.

- **Intensity measurements** are related to the amount of photons captured in the sensor during exposure time, called intensity units. Intensities are reported for a unit of area, such as a pixel or an object area. Usually, the total and mean intensity are reported. The total intensity represents the sum of all pixel intensities of the area, while mean intensity is the average intensity of the pixels of a particular area.
- **Nuclear features:** nuclear staining is a frequently used marker for cell identification because of its distinct edge detection and uniform staining (Figure 8). Nuclear area and nuclear intensity are commonly calculated features. In this project for example, nuclear area is used to normalize other features according to the number of cells.
- **Regional analysis:** measuring specific regions within or around a cell or a sample can be of interest; for instance, to separate the nucleus from the cytoplasm or to discriminate cellular subtypes in a tissue. Algorithms for regional analysis usually use a mask or a halo which is dilated out or contracted in from the original object. For example, a nuclear mask can be built by directly considering the object detected in the applicable channel, or, more commonly, by constricting one or two pixels from the object (Figure

8.A). On the other hand, a cytosolic mask can be constructed by dilating a few pixels away from the nucleus and then considering an additional width of pixels (Figure 8.A, bottom). Alternatively, a cell area can be determined by implementing algorithms that use information from additional channels that demark the cytoplasm, the cytoskeleton or the cell membrane (Figure 8.B).

- **Spot identification:** feature extraction procedures often involve the identification of "spots" or sub-regions within a main object (Figure 8.B). This is usually done by establishing another threshold (for another channel), and sub-objects are identified within the boundary defined by a mask. But other characteristics such as size or shape of the object can be utilized for spot identification.

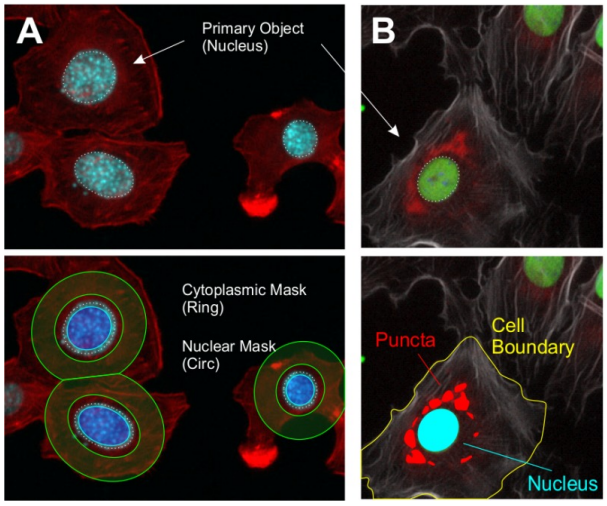

Figure 8. Image analysis feature extraction examples. A. Cells immunostained for markers that identify the nuclei and the cell body. The image in the bottom shows examples of a nuclear mask (circ: circular) and a cytoplasmic mask (ring). **B.** Cells immunostained for markers that identify the nuclei, the cell body, and a protein of interest. The image in the bottom shows examples for cell boundary, nucleus and spot (puncta) identification. Taken from Buchser *et al.* (2014)[46].

The power of HCA is that, once the pipeline of analysis is established, it can be applied to several data sets. Overall, the computer-driven automation in HCI and HCA accelerates repetitive operations and eliminates human bias, allowing Tera-bytes of imaged data to be acquired, processed, and analyzed in a short period of time.

High content approaches are instrumental for high through put applications such as drug discovery, where variations of several molecules of interest can be imaged simultaneously, or imaging of 3D tissues at high magnifications, where a significant amount of images are assembled together to analyze the complete sample.

1.6 Study aims

As previously discussed, PD is a complex and multifaced pathology with a systemic impact in human health. The proposed staged spread of LP from the enteric nervous system to the CNS, and the multi-organ symptomatologic profile, demonstrate the need for tools that are equally intricate to achieve a comprehensive understanding of the disease. In this sense, assembloids represent a promising opportunity to better unravel the mechanistic and molecular processes involved in PD, with the advantage that these models allow to simulate the interaction between different cell types and even diverse organs.

An ample range of evidence supports Braak's hypothesis for PD from the clinical, preclinical, and experimental lens, as described before. Even so, there are important knowledge gaps on the biological events that take place during LP spread through the human body and how this relates to the development of symptoms. This is due in great measure to the impossibility to study these processes in a living human being; but also, regarding what can be done *in vitro*, there is still the lack of an appropriate human model with the required complexity level.

It is within this context that this thesis project was conceived, with two main aims:

- Build an assembloid model for PD representing the enteric nervous system and the intestine.
- Use the developed assembloid to investigate α-synuclein propagation under PD pathological conditions.

To achieve this, an iPSC-derived organoid approach was used. Since the proposed path of α-synuclein spread in PD is from the intestine to the nervous system, the main concept of the project was to derive intestinal organoids from iPSCs carrying a PD-associated genetic alteration and co-cultivate them in an assembloid with iPSC-derived enteric neurons from a healthy individual. As can be seen in Figure 9 and as detailed in the methodology section of this thesis, two different approaches were followed to build the assembloids. The first one involved the co-cultivation of the iHOs and ENS in a single well subdivided by an insert, where each cell type would grow in a semi-separate compartment (Figure 9.a). The second strategy involved combining both cell types at earlier stages of differentiation and culturing them in a 3D system to achieve the development of intestinal organoids with integrated enteric neurons (Figure 9.b).

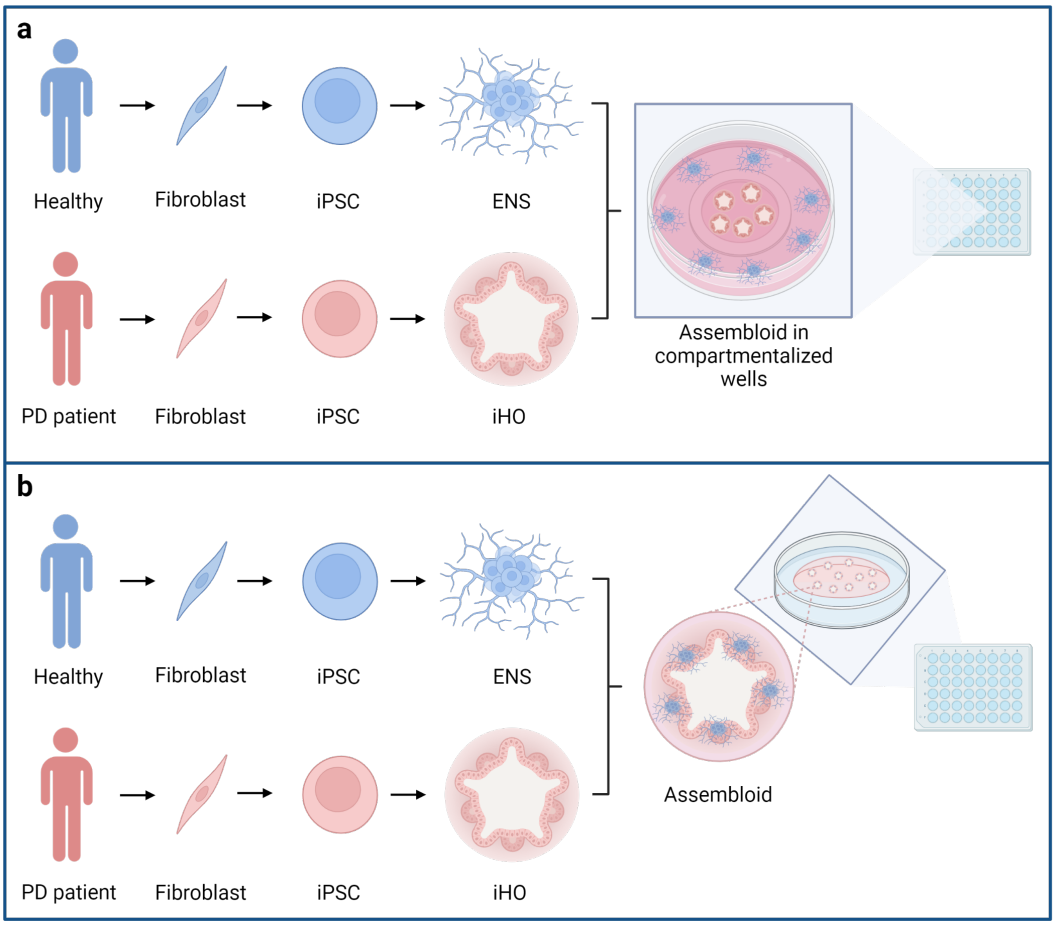

Figure 9. Assembloid models to simulate Parkinson's Disease pathology in the gut. a. intestinal organoids and enteric neurons are co-cultivated in semi-separate compartments. **b.** Intestinal organoids and enteric neurons develop together in a 3D system. iPSCs: induced pluripotent stem cells; ENS: enteric neurons; iHO: intestinal organoid; PD: Parkinson's Disease. Figure created with BioRender.

We hypothesized that enteric neurons co-cultivated with a PD intestinal organoid would have a greater content of α-synuclein in comparison to enteric neurons co-cultivated with a healthy iHO, demonstrating the pathological spread of this protein from the intestinal to the neuronal components of the assembloid, in a way that mirrors the events that occur in the human intestine and enteric nervous system.

The proposed model was developed with the intent of contributing to the elucidation of the first stages of disease progression, as once the progression of α-synuclein within the assembloids is characterized, the cellular and molecular mechanisms for this spread can be further investigated. The disease model itself can function as a foundation for additional research, such as the study of different genetic PD backgrounds or the impact of PD-associated toxins in the gut environment. All of this has the potential to shed light on new targets and treatment options for this burdensome neurodegenerative disease.

2 Materials and Methods

2.1 Cell Culture

2.1.1 iPSC maintenance

Human iPSCs from two healthy individuals, one PD patient (carrying a triplication for the *SNCA* gene), one knock-out for the *SNCA* gene, and one Green Fluorescent Protein (GFP)-expressing cell line (Table 1) were used in this project. They were maintained in Matrigel (Corning, 354277) or GelTrex (Thermo Fisher, A1413302)-coated 6-well plates (Thermo Fisher, 145380) with Essential 8 (E8) basal medium containing 2% E8 supplement (Thermo Fisher, A1517001) and 1% Penicillin-Streptomycin (P/S; Thermo Fisher 15140122), with daily medium changes. Cells were incubated at 37°C, 5% CO_2 and passaged at 80-90% confluence. For this, cells were detached by incubation in 750 µL of Accutase (Sigma-Aldrich, A6964-500ML) for 5 min at 37°C. Then, cells were transferred to a conical tube (Sigma-Aldrich, T1943-1000EA) with 5 mL of Dulbecco's Modified Eagle Medium/Nutrient Mixture F-12 (DMEM/F-12; Fisher Scientific, 21331046) and centrifuged for 3 min at 300 x g. Pellets were resuspended in supplemented E8 medium with Rho-associated kinase inhibitor Y27632 (ROCK inhibitor; CliniSciences, A11001-50) 1:2000 and 200.000 cells were seeded per well into pre-coated 6-well plates.

Table 1. iPSCs used for cell differentiation and organoid generation. GFP: Green Fluorescent Protein.

Database number	Description	Condition	Gender	Age of onset	Age of sampling
232	Wild Type (WT)	Healthy	Female	-	53
362	Wild Type (WT)	Healthy	Male	-	30
336	Triplication of the *SNCA* gene (SNCAx3)	PD	Female	50	55
320	*SNCA* gene knock-out (SNCA KO)	KO	Male	-	67
312	Wild Type- GFP (WT-GFP)	Healthy	Female	-	56

2.1.2 Derivation of intestinal organoids

iHOs were derived from iPSCs following an adapted procedure from the protocol by Lees *et al.* (2019)[37]. The differentiation process was started after iPSCs reached 80-90% of confluence, and it involved daily medium exchanges for the first ten days. During the first five days (days 0 to 4) the basal medium was E8 Flex with 2% E8 Flex supplement (Thermo Fisher, A2858501), and 1% P/S. On day 0 and 1, this media was supplemented with Activin A (10 ng/mL; Thermo Fisher, PHC9564) and basic Fibroblast Growth Factor (bFGF; 12 ng/mL; Peprotech, 100-18B 1mg). On day 2, the medium was supplemented with Activin A (100 ng/mL), bFGF (100 ng/mL), BMP-4 (10 ng/mL; R&D Systems, 314-BP-010), LY294002 (10 Mm; PreproTech, 1543664), and CHIR99021 (3 µM; Axon, CT 99021). The following day, endoderm specification was induced by addition of Activin A (100 ng/mL), bFGF (100 ng/mL), BMP-4 (10 ng/mL), and LY294002 (10 µM) to the medium. On days 4 to 9, the basal medium was replaced by Roswell Park Memorial Institute (RPMI)/B27 composed by RPMI medium (Thermo Fisher, 11875-093) with 2% B27 supplement with vitamin A (Thermo Fisher, 17504044), 1% L-glutamine (Promega, J8021), 1% P/S, and 1% Minimum Essential Medium Non-Essential Amino Acids (MEM NEAA; Life Technologies, 11140-050). On day 4 this medium was supplemented with Activin A (100 ng/mL) and bFGF (100 ng/mL). The next day Activin A (50 ng/mL) was added to the medium. On days 6 to 9, the medium contained CHIR99021 (6 µM) and RA (3 Mm; Sigma R2625), to induce hindgut formation (Figure 10).

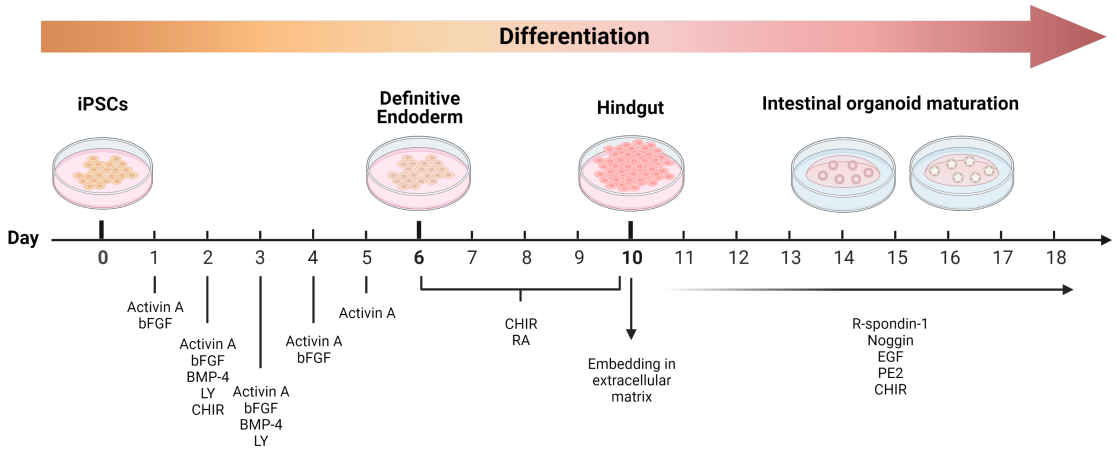

Figure 10. Derivation of intestinal organoids. iHO derivation implies the usage of several growth factors during definitive endoderm induction. Hindgut derivation is mainly done with CHIR and RA from day 6. After hindgut embedding at day 10, a cocktail of growth factors for intestinal organoid differentiation is used. iHO: intestinal organoid; bFGF: basic Fibroblast Growth Factor; BMP-4: Bone Morphogenic Protein 4; LY: LY294002; CHIR: CHIR99021; RA:

Retinoic Acid; EGF: Epidermal Growth Factor; PE2: Prostaglandin E2. Created with BioRender

On Day 10, the hindgut was embedded in Matrigel Growth Factor Reduced (GFR; Corning, 356231). Medium was removed and collected in a conical tube, plates were washed once with phosphate-buffered saline (PBS) without Calcium or Magnesium (Thermo Fisher, 14190250), also collecting this PBS on the tube. Attached hindgut was incubated in 1 mL of collagenase solution at 37°C for 5 min. The collagenase solution was composed of 0.1% collagenase type IV (Thermo Fisher, 17104-019), L-glutamine (2mM), and 0.7% 2-mercaptoethanol (Thermo Fisher, 31350-010) diluted in a combination of 20% knockout serum replacement (Thermo Fisher, 10828010) and 80% DMEM/F-12. Detached cells were transferred to a conical tube with 5 mL of iHO base growth medium; the previously collected hindgut-containing-medium/PBS was added to this tube and centrifuged at 240 x g for 2 min. iHO base growth medium was composed of Advanced DMEM/F12 (Thermo Fisher, 12634010) with 2% B27 supplement with vitamin A, 1% N2 supplement (Thermo Fisher, 17502001) , 10 mM HEPES (4-(2-hydroxyethyl)-1-piperazineethanesulfonic acid; Sigma, H0887-20ml), and 1% P/S. The pellet was resuspended in 3 mL of this medium, pipetting gently to break up the hindgut into smaller fragments, and centrifuged at 95 x g for 2 min. This was repeated once to wash the cells. The hindgut was resuspended in 1:2 mixture of iHO base growth medium with growth factors and Matrigel GFR kept on ice. Growth factors were R-spondin-1 (500 ng/mL; Stem Cell Technologies, 78213.1), Noggin (100 ng/mL; Stem Cell Technologies, 78060), EGF (100 ng/mL; PreproTech, 100-20), CHIR99021 (3 μM), Prostaglandin E2 (PE2; 2.5 Mm; Peprotech, 3632464), and ROCK inhibitor (10 μM). 20 to 30 μL droplets of suspended hindgut were placed in 48-well plates (Sigma-Aldrich, SIAL0548-100EA) and incubated at 37°C for 30 min. One well of a 6-well plate of hindgut was usually embeded in eight droplets or domes. Afterwards, 250 μL of iHO base growth medium with growth factors were added to each well. iHOs were kept at 37°C, 5% CO_2, with medium exchanges twice per week (omitting the ROCK inhibitor). iHOs were passaged weekly; for this, iHO-containing domes were detached by carefully pipetting with the medium, transferred to a conical tube, and allowed to settle for 2-3 min. The supernatant was removed and iHOs were resuspended in 2 mL of iHO base growth medium, pipetting gently to break down the iHOs. The suspension was centrifuged at 95 xg for 2 min and iHOs were embeded in Matrigel GFR droplets as previously described.

2.1.3 Derivation of enteric neurons

The derivation of ENS from iPSCs was performed following protocols by Fattahi *et al.* (2016)[41] and "Option B" in Barber *et al.* (2019)[42] with adaptations. After comparing the derivation efficiency of both protocols, only one was used to build the assembloids (see section 3.2).

2.1.3.1 Protocol by Fattahi et al. (2016), with adaptations

The process was started after iPSCs reached a 70-80% of confluence. During the first ten days, media was exchanged every other day, with Essential 6 medium (Thermo Fisher, A1516401) being replaced gradually by N2 medium. N2 medium was composed of DMEM/F12, 1% N2 supplement, 1% L- glutamine, 1% P/S, and 1% MEM NEAA. The medium was supplemented with LDN193189 (100 Nm; Sigma-Aldrich, SML0559-5MG), SB431542 (10 µM; Sigma, ab120163), CHIR99021 (3 µM), and RA (1 µM) in the combinations showed in Figure 11.

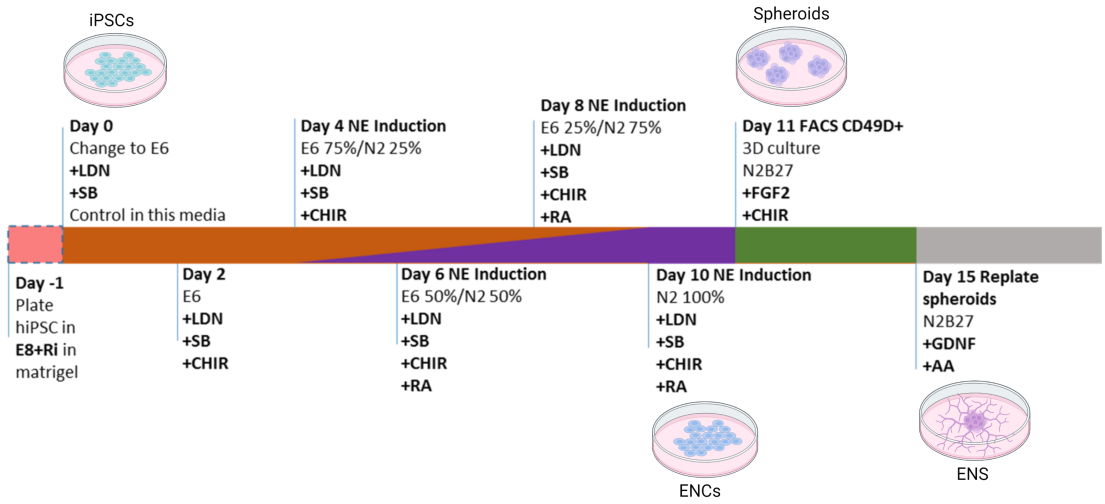

Figure 11. Derivation of enteric neurons from iPSCs as described by Fattahi *et al.* (2016), with adaptations. hiPSC: human induced pluripotent stem cell; E8: Essential 8 medium; Ri: ROCK inhibitor; E6: Essential 6 medium; LDN: LDN193189; SB:SB431542; CHIR: CHIR99021; NE: enteric neuron; N2: N2 medium; RA: Retinoic Acid; FACS: fluorescence activated cell sorting; N2B27: N2B27 medium; FGF2: basic Fibroblast Growth Factor; GDNF: Glial cell line-derived neurotrophic factor; AA: Ascorbic Acid. Modified with BioRender.

At day 11, cells were sorted for CD49d (Integrin α-4) positive (CD49d+) cells as described in section 2.1.3.3. At this stage, cells were considered as ENCs. 3 to 6 million positive cells were seeded into one well of a 6-well ultralow adhesion (ULA) plate (Corning, 3471) in 5 mL of N2B27 media supplemented with bFGF (10 nM) and CHIR99021 (3µM). N2B27 medium consisted of Neurobasal medium (Thermo

Fisher, 21103049) with 0.5% N2 supplement, 1% L-glutamine, 1% P/S and 1% B27 supplement without vitamin A (Thermo Fisher, 12587001). At day 13, a media exchange was performed. At day 15, spheroids formed in the ULA plate were plated in 6-well plates previously coated with poly-L-ornithine (Sigma-Aldric, P0671-25MG), laminin (BioLamina, LN111-02) and fibronectin (Sigma-Aldrich, F2006-1MG) with N2B27 medium supplemented with GDNF (25 ng/mL; PeproTech, 450-10-1mg) and AA (100 µM; Sigma-Aldrich, A4544-100G). From this point forward, neuronal differentiation was started; media was replaced twice per week.

2.1.3.2 Protocol by Barber et al. *(2019), Option B, with adaptations*

This procedure resembles the one described in section 2.1.3.1, with media exchanges every other day and a similar growth factor composition. After iPSCs reached a confluence of around 90%, media was exchanged to Essential 6 medium for the first ten days of differentiation, with growth factor concentration and combination as detailed in Figure 12. In contrast to the previous protocol, BMP-4 was used at 1 ng/mL during the first two days of differentiation.

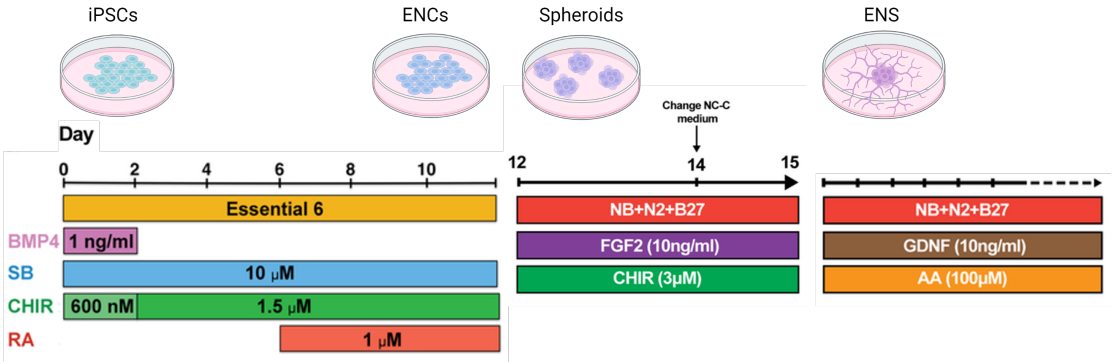

Figure 12. Derivation of enteric neurons from iPSCs as described by Barber *et al.* (2019). BMP4: Bone Morphogenic Protein 4; SB:SB431542; CHIR: CHIR99021; RA: Retinoic Rcid; NB: Neurobasal; N2: N2 supplement; B27: B27 supplement; FGF2: basic Fibroblast Growth Factor; GDNF: Glial cell line-Derived Neurotrophic Factor; AA: Ascorbic Acid. Adapted from Barber *et al.*(2019), modified with BioRender.

At day 11 or 12, cells were sorted for CD49d+ cells as described in section 2.1.3.3. As discussed in the results section 3.2, sorting was only done for the first derivation, afterwards proceeding directly to spheroid formation at day 12. From day 12 on, the basal media was composed of Neurobasal medium supplemented with N2 supplement (10 µL/mL), B27 supplement (20 µL/mL), GlutaMAX (10 µL/mL; Thermo Scientific, 35050061), MEM NEAA (10 µL/mL). Medium for spheroid formation contained bFGF (10 ng/mL) and CHIR99021 (3µM). Medium for enteric neuron

differentiation was supplemented with GDNF (10ng/mL) and AA (100μM). In all other respects, the procedure followed the steps described in section 2.1.3.1.

2.1.3.3 Fluorescence Activated Cell Sorting (FACS)

Cells were detached by incubation in 750 μL of Accutase for 5 min at 37˚C, transferred to conical tubes with 5 mL of DMEM/F-12, and centrifuged at 400 x g for 5 min. The pellet was resuspended in 2% Bovine Serum Albumin (BSA; Bioke, B9000S) in PBS and centrifuged to wash the cells, twice. Each sample was incubated with either 0.4 μg of PE/Cy7 anti-human CD49d Antibody (Biolegend, 304314), 0.4 μg of the isotype control antibody PE/Cy7 Mouse IgG1, κ (Biolegend, 400125) or 2% BSA as untreated control for 45 min at 4˚C with shaking. Samples were washed twice using 2% BSA and centrifugation at 400 x g for 5 min. The sorting was performed in a BD FACSAria™III (BD Biosciences) cell sorter.

2.1.4 Assembloid building

Assembloids were built utilizing two approaches: an in-house developed methodology that will be referred to as “iHO-ENS assembloid”, and a procedure based on the protocol described by Loffet *et al.* (2020)[39], that will be referenced as “iHO-ENC assembloid”.

2.1.4.1 iHO-ENS Assembloid

iHOs at passage seven and ENS with 21 days of differentiation (DoD) were co-cultured in 24-well imaging plates (Fisher Scientific, 15600547) pre-coated with poly-L-ornithine, laminin, and fibronectin (Figure 13.c). Each well was divided into two connected compartments by placing in them 3D-printed inserts made up of Clear Resin V4 (Formlabs, FLGPCL04), designed and provided by the postdoctoral researcher Graham Robertson. This compartmentalization had the purpose to allow the provision of the different culture medias to the different types of organoids/cells while allowing contact between them by channels localized at the bottom of the well (see Figure 13.a & b).

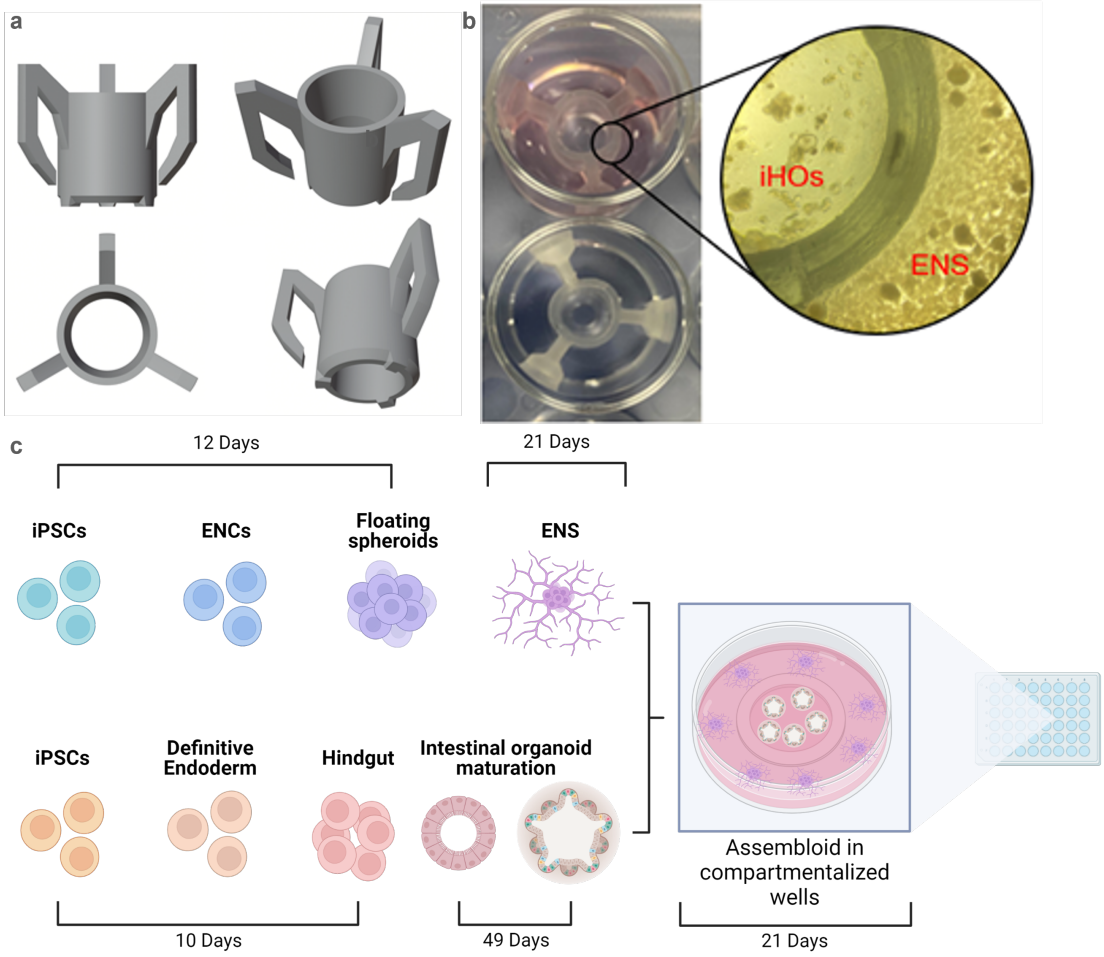

Figure 13. Establishment of an iHO-ENS co-culture system. **a.** Digital image of the 3D-printed inserts used for well compartmentalization. **b.** 3D-printed inserts, iHOs and ENS positioned inside a 24-well plate. **c.** Diagram of the iHO-ENS assembloid, 21-days-old ENS are co-cultivated with 7-week-old iHOs in compartmentalized wells for 21 days. Created with BioRender. iPSC: induced pluripotent stem cell; ENS: enteric neuron; PD: Parkinson's Disease; iHO: intestinal organoid.

The co-culture was performed following two different procedures, one involved plating the ENS before the iHOs and the second one consisted of seeding both types of cells simultaneously. For the first approach, ENS were seeded in all the compartments of the well one week before placing the iHOs in the central compartment. For both approaches, two confluent wells of a 6-well plate containing ENS were detached by incubation in 750 µL of Accutase for 5 min at 37˚C and resuspended in 4 mL of enteric neuron differentiation medium. 800 µL of the ENS suspension was placed on each well. On the other hand, iHO containing domes were detached from 48-well plates by gently pipetting with PBS, transferred to conical tubes and allowed to settle for 2-3 min. The supernantant was removed and iHOs were resuspended in 2 mL of iHO base growth medium without growth factors, pipetting gently to break up the iHOs. The iHO suspension was centrifuged at 95 x g

for 2 min and the pellet was resuspended in a mixture of 1:2 of iHO growth medium with growth factors and Matrigel GFR. 20 to 30 µL droplets were seeded in the central compartment of the well and allowed to polymerize at 37˚C for 30 min. One dome of a 48-well plate was seeded in one well of the co-culture. 100 µl of supplemented iHO base growth medium was placed in the central compartment and 750 µl of medium for neuron differentiation was added to the peripheral compartment. Co-cultures were kept at 37˚C and 5% CO_2 for 21 days.

Intestinal organoids from cell lines 232 (WT) and 336 (SNCAx3) were co-cultured with enteric neurons from the cell line 232 (WT) in two biological replicates.

2.1.4.2 iHO-ENC Assembloid, adapted from Loffet et al. (2020)

For this approach, iHOs and ENCs were derived from iPSCs until early stages of differentiation and then embedded together in an extracellular matrix to simultaneously initiate 3D-culture (Figure 14). Intestinal organoids were derived as described in section 2.1.2 until day 10 of differentiation, a stage in which cells form 3D hindgut structures. Enteric neurons were derived as described in section 2.1.3.2 until day 11/12 of differentiation, the ENC phase.

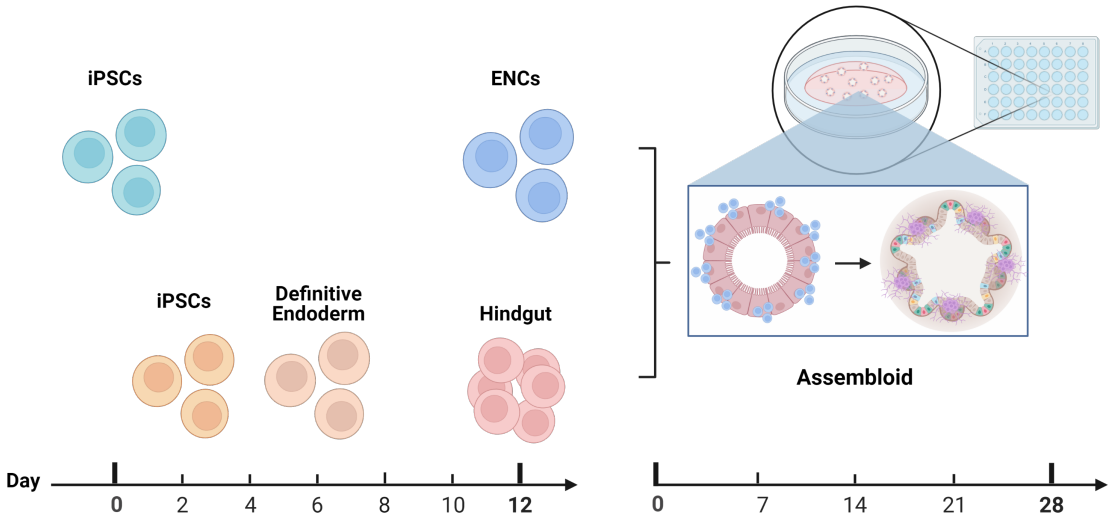

Figure 14. Diagram of the iHO-ENC co-culture system. Enteric neuron precursors (ENCs) are combined with hindgut in a 3D culture system. Resulting assembloids are co-cultured for 35 days. iPSC: induced pluripotent stem cell; ENC: enteric neuron precursor; PD: Parkinson's Disease; iHO: intestinal organoid. Created with BioRender.

For hindgut collection, medium was removed and collected in a conical tube, plates were washed once with PBS without Calcium or Magnesium and this effluent was also collected on the tube. Attached hindgut was incubated in 1 mL of collagenase solution at 37°C for 5 min. Detached cells were transferred to a conical tube with 5

mL of iHO base growth medium together with the previously collected hindgut-containing-medium/PBS and centrifuged at 240 x g for 2 min. The pellet was resuspended in 2 mL of iHO base growth medium, pipetting gently to break up the hindgut into smaller fragments, and centrifuged at 95 x g for 2 min. The hindgut was resuspended in 1 mL of iHO base growth medium and kept in an incubator at 37°C awaiting for ENC collection.

For ENC recovery, cells were detached by incubation in 750 µL of Accutase for 5 min at 37˚C and transferred to a conical tube with 4 mL of day 10 medium. After centrifugation at 300 x g for 3 min, ENCs were resuspended in 1 mL of day 10 medium and counted with a Countess II Automated Cell Counter (Invitrogen). Enough volume of ENC suspension was added to the iHO suspension to keep a ratio of 1-2 x 10^5 ENCs per dome and the mixture was centrifuged at 300 x g for 2 min. iHOs + ENCs were embeded and passaged as described for the intestinal organoids. Four passages were performed. Asembloids were kept at 37˚C and 5% CO_2 for 35 days.

Intestinal organoids from cell lines 232 (WT), 336 (SNCAx3), and 320 (SNCA KO) were co-cultured with enteric neuron precursors from the cell lines 232 (WT), 320 (SNCA KO) and 312 (WT-GFP). Due to cell death during cell differentiation, different biological replicates were performed per combination, as detailed in Table 2 (Initial replicates). However, after four weeks of passaging, only some of the co-cultures presented intestinal organoids, and therefore only those were used for further analysis (Table 2, Final replicates). Co-culture of iHOs with cell line 312 (WT-GFP) was only done once to evaluate the ENC origin of assembloid and their presence in the assembloids after four passages.

Table 2. Biological replicates of iHO-ENC assembloids. iHO: intestinal organoid; ENC: enteric neuron precursor.

iHO	**336**		**232**			**320**		
ENC	**232**	**320**	**232**	**320**	**312**	**232**	**320**	**312**
Initial Replicates	4	4	5	5	1	2	2	1
Final Replicates	0	1	1	4	1	0	0	0

2.2 Characterization of iHOs, ENCS and assembloids.

2.2.1 Immunocytochemistry

All samples were fixed with 4% paraformaldehyde (PFA; Sigma, 1.00496.5000) overnight at 4˚C with shaking, washed three times with PBS and stored in PBS with 0.1% sodium azide (Carl Roth, K305.1) at 4˚C.

Domes containing iHOs and iHO-ENC assembloids were embeded in 3% low melting point agarose (Biozym, 840100) and sectioned into 60 µm slices using with a Vibratome VT1000 S (Leica Biosystems). Sections were collected in PBS with 0.1% sodium azide and stored at 4˚C.

Permeabilization and blocking were performed simultaneously by incubation in 5% Normal Goat Serum (NGS; Thermo Fisher, 10000C), 0.5% Triton X-100 (Carl Roth, 3051.3), 0.1% sodium azide in PBS for 2 hours at room temperature (RT). Incubation of primary antibodies diluted in antibody solution was performed for 48 h at 4°C under shaking. Antibody solution contained 5% NGS, 0.01% Triton X-100, 0.1% sodium azide in PBS. Sections were washed three times with washing solution (0.01% Triton X-100 in PBS) for 5 min at RT on a shaker. Sections were incubated in secondary antibody diluted in antibody solution for 2 h at RT and washed three times with washing solution. One additional wash was done with Milli-Q water. When applicable, stained sections were mounted on slides with 4 or 8 mm grids (De Beer Medicals, BM-9244 and BM-9418). The complete list of antibodies used can be seen in appendix 6.1.

Images were acquired on a Zeiss LSM 710 AxioObserver confocal microscope and the ZEN Blue edition software (Carl Zeiss Microscopy GmBH) was used for image processing.

2.2.2 Quantitative real time PCR (RT-qPCR)

To compare derivation efficiency of the protocols for ENS differentiation, gene expression of specific markers was analyzed through quantitative real time polymerase chain reaction (RT-qPCR) in ENCs (day 12 of derivation) and ENS (21 DoD) derived using the protocols by Fattahi *et al*. (2016) and Barber *et al*. (2019), with modifications.

One confluent well of a 6-well plate was detached by incubation in 750 µL of Accutase for 5 min at 37˚C and transferred to 5 mL of DMEM/F-12 medium. After centrifugation at 300 x g for 3 min, cells were resuspended in PBS and centrifuged

again. The pellet was resuspended in RLT buffer (Qiagen, 79216) with 1% 2-mercaptoethanol and frozen overnight at -80˚C for cell lysis. RNA was extracted using the RNeasy Mini Kit (Qiagen, 217004) according to manufacturer's instructions and quantified using a Nanodrop 2000C spectrophotometer (Thermo Fisher Scientific).

Two micrograms of RNA were used for cDNA synthesis using the High Capacity RNA-to-cDNA synthesis kit (Invitrogen, 4387406) and following the manufacturer's instructions. The synthesis reaction was done at 37˚C for 60 min, followed by 5 min at 95˚C to stop the reaction, in a TProfessionnal basic gradient 96 Thermocycler (Biometra). Samples were stored at -20˚C until further use.

The mRNA expression of genes of interest was quantified using 2 µL of a 1/10 dilution of cDNA, 0.3 µM of the forward and reverse primers and 18 µL of Maxima SYBR Green qPCR Mater Mix (Thermo Fisher Scientific, K0252). Cycling was performed at 95˚C for 10 min, then 45 repeats at 95˚C for 15s, 60˚C for 30 s, and 72˚C for 30s in an AriaMx Real-Time PCR Lightcycler (Agilent). The housekeeping gene used was Ribosomal Protein L37a (*RPL37A)*.

The primer sequences used can be seen in Table 3.

Table 3. Primer sequences of markers used for ENS and ENC characterization. *RPL37A:* Ribosomal Protein L37a; HOXB2: Homeobox B2; PHOX2A: Paired Like Homeobox 2A; PHOX2B: Paired Like Homeobox 2B; SOX10: SRY-Box Transcription Factor 10; TUJ1: class III β-tubulin; MASH1: Achaete-scute homolog 1.

Gene	Primer	Sequence (5'-3')
RPL37A	Forward	GTGGTTCCTGCATGAAGACAGTG
	Reverse	TTCTGATGGCGGACTTTACCG
HOXB2	Forward	GCCGACTCCTGTCTCCAGCTAT
	Reverse	ACTGCAGGTCGATGGCACAG
PHOX2A	Forward	TTTTCGCTGAGACCCACTACC
	Reverse	CTCCTTGGAATCGTCGTCCTC
PHOX2B	Forward	AACCCGATAAGGACCACTTTTG
	Reverse	AGAGTTTGTAAGGAACTGCGG
SOX10	Forward	CCTCACAGATCGCCTACACC
	Reverse	CATATAGGAGAAGGCCGAGTAGA

TUJ1	Forward	CCGACAACTTTATCTTTGG
	Reverse	ACGACATCTAGGACTGAG
MASH1	Forward	GTCCTGTCGCCCACCATCTC
	Reverse	CCCTCCCAACGCCACTGAC

Relative mRNA expression was calculated using the $2^{-\Delta\Delta Ct}$ method. Cycle threshold (Ct) values were obtained in duplicate for one biological replicate. The mean of these values was used to calculate ΔCt as $Ct_{(gene\ of\ interest)}$- $Ct_{(housekeeping\ gene)}$. Afterwards, ΔΔCt was obtained by $\Delta Ct_{control}$- $\Delta Ct_{experimental}$. The control condition was the derivation following the protocol by Fattahi *et al*. (2016) and the experimental condition was the derivation with the protocol by Barber *et al*. (2019).

2.3 Study of intracellular and extracellular α-synuclein in iHO-ENS assembloids

2.3.1 Intracellular α-synuclein - Western Blotting

ENS coming from a single well of the 24-well plate after 21 days of co-culture of the iHO-ENS assembloid were pelleted and then lysed using Radioimmunoprecipitation assay (RIPA) buffer (Abcam, ab156034) with 4% Protease Inhibitor Cocktail (Sigma-Aldrich, 11697498001) and 2% Phosphatase Inhibitor Cocktail (Sigma-Aldrich, 524629-1ML) in ice for 5 min. Cells were resuspended by pipetting and sonicated 10 times for 30 s periods. After centrifugation at 16.000 x g for 20 min at 4˚C the supernatant was used for protein quantification using the Pierce™ BCA Protein Assay Kit (Thermo Fisher, 23225), following the manufacturer's instructions.

Samples were heated at 95˚C for 5 min with 6X loading dye (Thermo Fisher, R0611) with 0.1 M dithiothreitol (DTT, Thermo Fisher, R0861) before loading them in a Bolt™ 4-12%, Bis-Tris gel (Thermo Fisher, NW04122BOX). Samples were run at 120 V with MES (2-[N-morpholino] ethanesulfonic acid) propanesulfonic acid; Thermo Fisher, B000202) running buffer and transferred to polyvinylidene fluoride (PVDF) membranes (Thermo Fisher, IB24001) using an iBlot 2 Gel Transfer Device (Life Technologies). Membranes were fixed with 0.4% PFA for 30 min at RT, washed three times with Milli-Q water, blocked for 60 min at RT with 5% milk (Carl Roth, T145.2) and 0.02% Tween-20 (AppliChem, A1389) in PBS, and washed again with Milli-Q water. Primary antibodies diluted in antibody solution (5% BSA and 0.02% Tween-20 in PBS) were incubated at 4°C overnight and afterwards washed three

times with washing buffer (0.02% Tween-20 in PBS). Secondary antibodies diluted in antibody solution were incubated for 60 min at RT and afterwards washed three times with washing buffer.

All antibodies' dilution was used according to the manufacturer's instructions. Antibodies used are shown in Table 4.

Table 4. Antibodies used for the Western Blots. p-α-synuclein: α-synuclein phosphorylated at S129; IgG: immunoglobulin G.

Antibody	Source	Catalog number
α-synuclein	Santa Cruz	sc-12767
p-α-synuclein	Cell Signaling	23706S
β- actin	Cell Signaling	3700
Goat anti-rabbit IgG 800	Cell Signaling	5151
Goat anti-mouse IgG 680	Cell Signaling	5470

Membranes were visualized using the Odyssey® XF Imaging System (LI-COR, inc.) and quantified using the Image Studio Lite (LI-COR, inc.) software. Data was graphed using Microsoft Excel 2019.

The experiments were performed in 2 biological replicates, of which one representative example is shown.

2.3.2 Extracellular α-synuclein- Dotblotting

Medium from ENS collected after 21 days of co-culture of the iHO-ENS assembloid was centrifuged at 15.000 x g for 1 min and vacuum-filtered into a nitrocellulose membrane (Biorad, 1620115) previously hydrated with PBS using a Whatman™ Minifold I (Merck, WHA10447850). The membrane was fixed, blocked, stained, and visualized as indicated in section 2.3.1.

The primary antibody used was α-synuclein (Santa Cruz, sc-7011-R) and the secondary antibody was goat anti-rabbit IgG 800 (Cell Signaling, 5151).

The experiments were executed in 2 biological replicates, of which one representative example is shown.

2.4 High through put quantification of α-synuclein in organoids and assembloids.

Brain organoids at 30, 60, and 90 DoD (provided by the post-doctoral researcher Gemma Gomez Giro) and domes containing 4-week-old iHO-ENC assembloids were sectioned and immunofluorescently stained as indicated in section 2.2.1. Brain organoids were stained to identify α-synuclein and α-synuclein phosphorylated at S129 (p-α-synuclein) within neurons, using the MAP2 (Microtubule-associated Protein 2) neuronal marker. iHO-ENC assembloids were immunostained to identify α-synuclein within the iHOs and the enteric neurons using Villin and MAP2 as intestinal and neuronal markers, respectively (see antibody detail in Table 5). High content imaging was performed on a CellVoyager CV8000 High-Content Screening System (Yokogawa Electric Corporation).

Table 5. Antibodies used for high-content imaging studies. p-α-synuclein: α-synuclein phosphorylated at S129; IgG: immunoglobulin G; MAP2: Microtubule-associated Protein 2.

Antibody	Source	Catalog number
Brain organoids		
α-synuclein	NOVUS Biologicals	NBP1-05194
p-α-synuclein	Cell Signaling	23706S
Goat anti- chicken IgG 488	Invitrogen	A-11039
Goat anti- mouse IgG1 568	Invitrogen	A21124
Goat anti- Rabbit IgG 647	Invitrogen	A-21244
iHO-ENC assembloids		
α-synuclein	ab138501	Abcam
Villin	Santa Cruz	sc-58897
Goat anti- mouse IgG1 488	Thermo Scientific	A-21121
Goat anti- Rabbit IgG 568	Invitrogen	A11036
Goat anti- chicken IgY 647	Invitrogen	A-21449
Both		
MAP2	Abcam	ab92434
Hoechst	Invitrogen	62249

A custom-developed image analysis algorithm was fist developed for the brain organoids and then adapted to the assembloids. It was done using Matlab (2021a, Mathoworks).

Biological replicates for the brain organoids are indicated in Table 6. Biological replicates for the iHO-ENC assembloids are the final replicates indicated in Table 2.

Table 6. Biological replicates used for the high-content imaging analysis of brain organoids. DoD: Days of differentiation

	Time point		
Cell line	**30 DoD**	**60 DoD**	**90 DoD**
320	1	2	2
336	3	4	3
232	5	5	3
362	5	5	3

2.4.1 Image analysis of brain organoids

Organoids were segmented based on fluorescence intensities in Hoechst, Alexa488, Alexa568, and Alexa647 channels. The intensity threshold for each channel was selected based on the intensities shown by a positive control (a brain organoid from cell line 336 SNCAx3) and a negative control (a brain organoid from cell line 320 SNCA KO).

Organoids were segmented by a linear combination of images of the mentioned channels. Afterwards an organoid mask was created with a threshold of 175, connected components with fewer than 100 pixels were removed. To remove gaps, dilations with a disk-shaped structuring element of radius 50, and with a sphere-shaped structuring element of radius 5 were applied, and holes were filled. Connected components with fewer than 1.000.000 pixels were removed (Figure 15.c).

To segment the nuclei, a mask was created in which intensities from the Hoechst channel were median filtered with a 3 x 3 filter. An intensity threshold of 400 was set, and connected components smaller than 500 pixels were excluded. Only nuclei detected within the Organoid mask were considered (Figure 15.a).

To segment MAP2, a differential of gaussians was calculated. The raw MAP2 channel was filtered with a Gaussian filter of size 105 and standard deviation 1, a

second Gaussian filter of size 105 and standard deviation 35, and the first one was substracted from the second one. The mask was created with an intensity threshold of 100. Only MAP2 contained within the Organoid mask was considered (Figure 15.b).

For α-synuclein and p-α-synuclein segmentation, an intensity threshold of 500 and 2000 was set, respectively. Connected components smaller than 27 pixels were excluded and only objects within the Organoid mask were considered (Figure 15.d & g).

A spot detection method was developed to identify α-synuclein and p-α-synuclein aggregates. For both, a differential of gaussians was calculated. The raw α-synuclein and p-α-synuclein channels were filtered with a Gaussian filter of size 55 and standard deviation 1, a second Gaussian filter of size 55 and standard deviation 5, and the first one was substracted from the second one. To create the mask, an intensity threshold of 400 and 1000 was selected for α-synuclein and p α-synuclein, respectively (Figure 15.e, f, h & i).

To study the subcellular localization of α-synuclein and p-α-synuclein spots, masks were created to identify neuronal nuclei and extranuclear neuronal areas. For neuronal nuclei, a mask was created that included colocalization of the nuclear mask and the MAP2 mask. For the extranuclear area, a mask was created that included the MAP2 mask and excluded the nuclei mask. Finally, masks were created that included colocalization of the α-synuclein and p α-synuclein spots with the neuro-nuclear and extranuclear area, and excluded connected components of less than 7 pixels (Figure 15.f & i).

To study the subcellular localization of α-synuclein and p-α-synuclein, masks were created that identified colocalization of the nuclear mask and the α-synuclein and p-α-synuclein masks, as well as colocalization of the proteins with the extranuclear neuronal mask.

The scripts with the extracted features can be found at:

https://git-r3lab.uni.lu/paul.antony/irishcsprojects/-/tree/master/DanielaVega/Organoids_SNCA_TH_GPU_Hindbrain

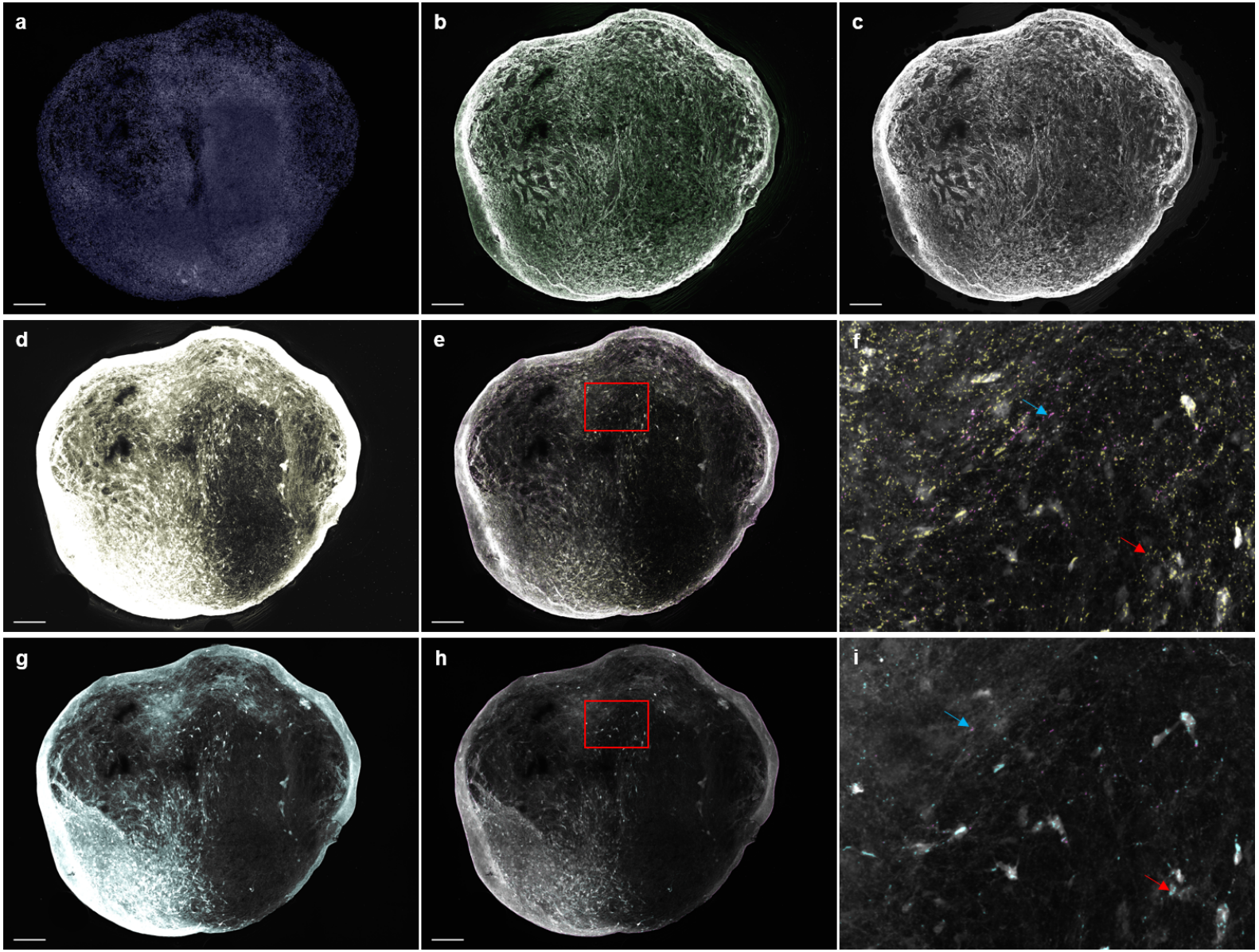

Figure 15. Segmentation of brain organoids. a. Preview of the nuclear mask**. b.** Preview of the MAP2 mask. **c.** Preview of the Organoid mask. **d**. Preview of the α-synuclein mask. **e.** Preview of the α-synuclein spot mask. **f.** Magnified view of the signaled area in e. **g.** Preview of the p- α-synuclein mask. **h**. Preview of the p-α-synuclein spot mask. **i.** Magnified view of the signaled area in h. The light blue arrows in f. and i. point to spots localized in the extracellular neuronal area, while red arrows indicate a spot localized in a nucleus. MAP2: Microtubule-associated Protein 2. Scale bar: 200 μm.

2.4.2 Image analysis of iHO-ENC assembloids

In this case, the intestinal and neuronal elements of the assembloids were segmented separately.

For the nuclei, a mask was created in which intensities from the Hoechst channel were median filtered with a 3 x 3 filter. An intensity threshold of 250 was set, and connected components smaller than 27 pixels were excluded (Figure 16.a).

The intestinal organoids were segmented by establishing an intensity threshold of 500 for the Villin channel, and connected components smaller than 25.000 pixels were excluded. Since a single dome section might have had more than one Villin organoid, identified objects were labeled to be analyzed separately (Figure 16.d & g).

Assembloids were identified as intestinal organoids with a surrounding area in which enteric neurons were expected to be in contact with the organoid. For this, a dilation with a disk-shaped structuring element of radius 200 was applied to the Villlin mask. This was visualized as a perimeter surrounding the intestinal organoid (Figure 16.g).

For the enteric neuronal element of the assembloid, the MAP2 channel intensities were median filtered with a 3 x 3 filter, then the intensity threshold was set at 2.500 and connected component of less than 100 pixels were excluded. To completely exclude the intestinal element, a dilation with a disk-shaped structuring element of radius 5 was applied to the Villlin mask and excluded from the neuronal mask. Connected components of less than 100 pixels were excluded. Lastly, the mask was reconstructed considering the nuclear mask colocalization with the neuronal mask, (with connected components larger than 250 pixels) and the previously defined neuronal mask (Figure 16.b).

For α-synuclein segmentation, an intensity threshold of 3.000 was set, and connected components smaller than 27 pixels were excluded. Spot detection was applied as previously described, with an intensity threshold of 500 (Figure 16. e & h). Then, the α-synuclein mask was redefined to include the area of the detected spots (Figure 16.c).

Neuronal, intestinal and assembloid nuclei were defined as the nuclear mask colocalized with the neuronal, intestinal organoid, and assembloid masks, respectively. Similarly, colocalization of α-synuclein and α-synuclein spots with these three areas was defined to study α-synuclein distribution within the assembloids.

The script with the extracted features can be found at: https://git-r3lab.uni.lu/paul.antony/irishcsprojects/-/tree/master/DanielaVega/ENS_intestine

2.4.3 Graphical and statistical analysis of high through put data

Statistical analysis performed on each data set is mentioned in each figure. The statistical analysis and graphing of the data were implemented in R (R Foundation for Statistical Computing).

The scripts for the statistical analysis and graphs can be consulted at: https://gitlab.lcsb.uni.lu/dvb/vega_2022

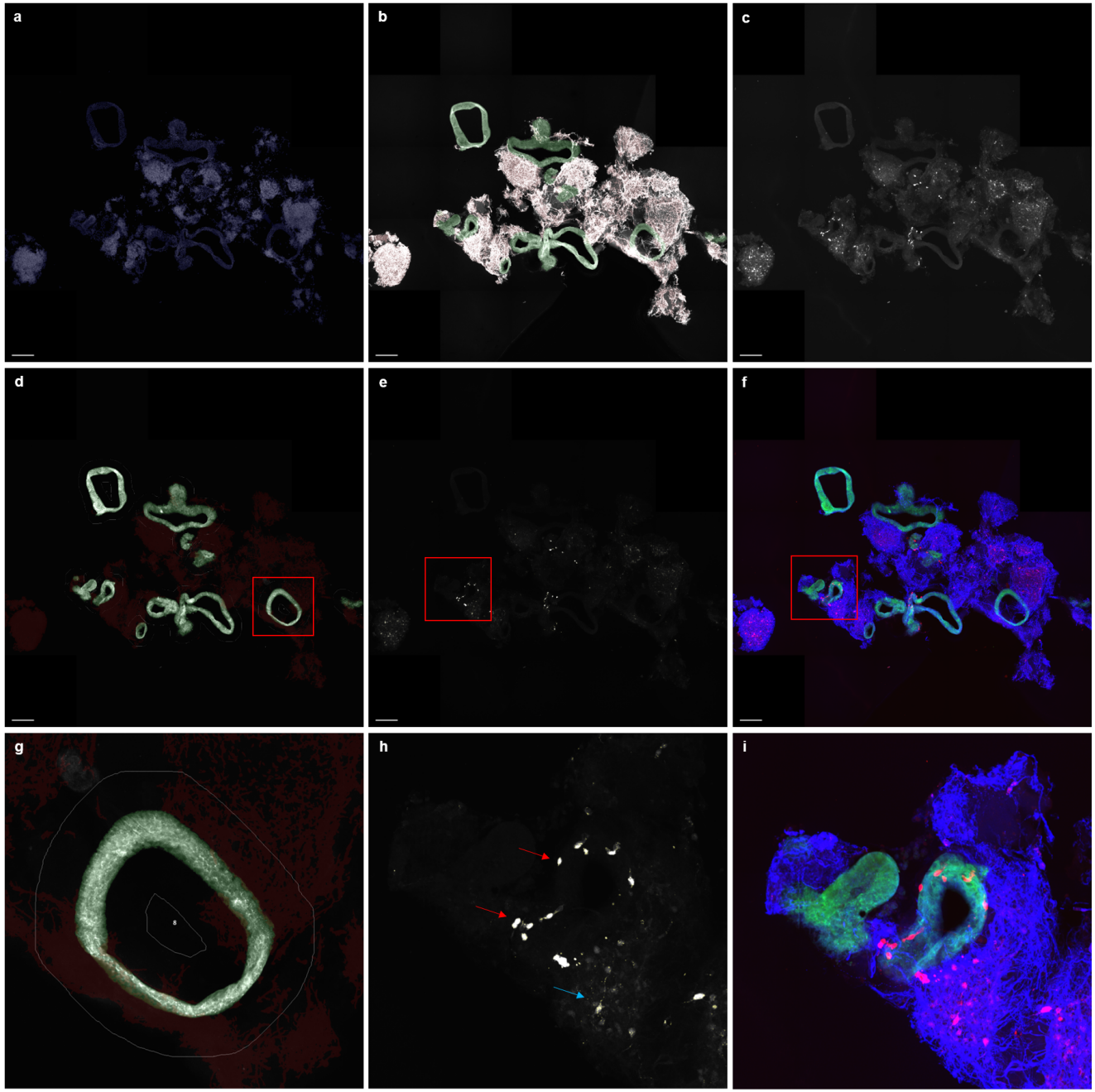

Figure 16. Segmentation of iHO-ENC assembloids. a. Preview of the nuclear mask. **b.** Preview of the MAP2 mask shown in white (Villin mask shown in green). **c.** Preview of the α-synuclein mask. **d.** Preview of the Villin mask shown in green (MAP2 mask shown in dark red). **e.** Preview of the α-synuclein spot mask. **f.** RGB view of the assembloid, Villin is shown in green, α-synuclein in red and MAP2 in blue. **g.** Magnified view of the area signaled in d., the perimeter around Villin is illustrated by a white line, this delimits the area considered as an assembloid. The assembloid is labeled by a number (in this case 8). **h.** Magnified view of the area signaled in e., spots localized within the iHO are pointed by red arrows. A spot within the ENCs is signaled by a light blue arrow. **i.** Magnified view of the area signaled in **f.** iHO: intestinal organoid; ENC: enteric neuron precursor; MAP2: microtubule-associated protein 2; RGB: red, green, blue. Scale bar: 200 µm.

3 Results

Intestinal organoids and enteric neurons were derived to build iHO-ENS and iHO-ENC assembloids. Later, the built assembloids were studied using analytic and computational tools to understand if α-synuclein transmission from the intestinal to the neuronal component was evidenced. To build the computational pipeline, brain organoids available beforehand were used. Results obtained are detailed in the following sections.

3.1 Intestinal organoids exhibit intestinal markers and morphology.

In this project, intestinal organoid derivation efficiency varied greatly between cell lines. As can be inferred from Table 2, iHO derivation was most efficient in cell line 232 (WT) with a 80% of success, less efficient in cell line 336 (SNCAx3) with 25% of success, and unsuccessful in cell line 320 (SNCA KO). Though, for the latter cell line, only two attempts of derivation were performed.

Derived iHOs consisted of a central lumen lined by a single-cell layer. They showed mainly a globular shape after 4 weeks of passage, exhibiting a more budded morphology after 7 weeks (Figure 17).

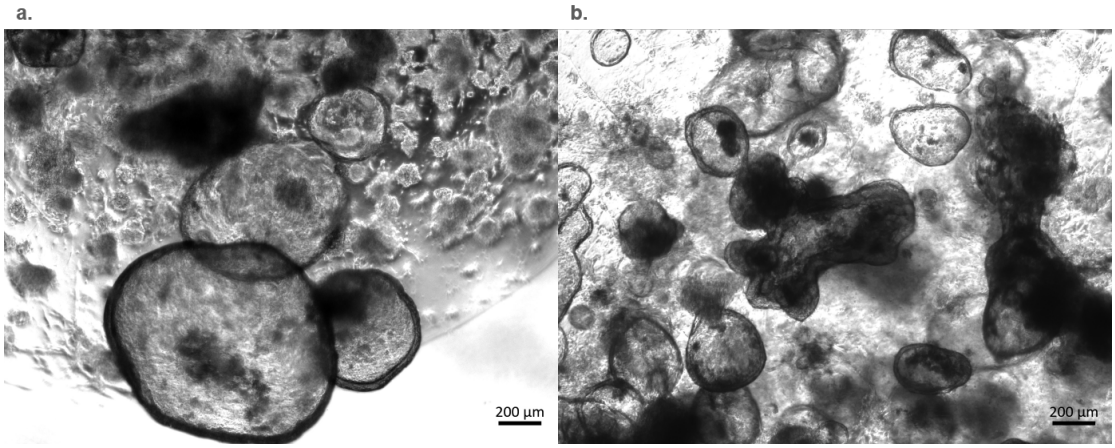

Figure 17. Intestinal organoids display globular (a) and budded (b) morphologies. iHOs derived from cell line 232 (WT) after four (a) and eight (b) weekly passages are shown. iHO: intestinal organoid; WT: Wild Type. Scale bar: 200 µm.

Derived iHOs were characterized through immunofluorescence to determine if they displayed markers expected for an intestinal epithelial lineage. Intestinal organoids were positive for Villin (Figure 18.a), a protein found in the microvilli that make up the

brush borders of enterocytes[49]. They were also stained for Epithelial cadherin (E-cadherin; Figure 18.a), a cell adhesion protein of epithelial cell junctions[49], and Occludin (Figure 18.b), a protein of the plasma membrane localized at tight junctions that plays a key role in barrier function[50]. iHOs also showed markers for enteroendocrine cells (Chromogranin A, a neuroendocrine secretory protein localized in secretory vesicles of neurons and endocrine cells[51]; Figure 18.c), Goblet cells (Mucin, a mucus gel-forming protein prominent in the gut[49]; Figure 18.d), Paneth cells (Lysozyme, an antimicrobial enzyme that catalyzes the destruction of bacterial cell walls[49]; Figure 18.c), and Crypt Base Columnar (CBC) stem cells (Ki67, a marker of cell proliferation[49]; Figure 18.d). Some iHOs were also positive for Vimentin, a major cytoskeletal component of non-epithelial cells, especially mesenchymal cells[49] (Figure 18. b & c).

To be capable of transmitting α-synuclein, derived iHOs should first express the protein. Immunoflurescence staining was performed to detect this expression, revealing that intestinal organoids were indeed positive for α-synuclein (Figure 18. a & b). It was observed that this staining occurred mainly within specific cells of the iHO, and the staining done for several cellular subtypes unveiled that most of these cells were also positive for Chromogranin A (Figure 19), therefore identifying them as enteroendocrine cells (EECs)

Figure 18. Intestinal organoid characterization. iHOs from cell line 336 (SNCAx3) and 232 (WT) were immunostained after 8 passages. **a.** iHOs stained for Hoechst, Villin, E-cadherin and α-synuclein. **b.** Immunofluorescence staining of Hoechst, α-synuclein, Occludin and Vimentin. **c.** iHOs stained for Hoechst, Lysozyme, Chromogranin A and Vimentin. **d.** iHOs stained for Hoechst, Ki67, and Mucin. iHOs: intestinal organoids; WT: Wild Type. Scale bar: 100 µm.

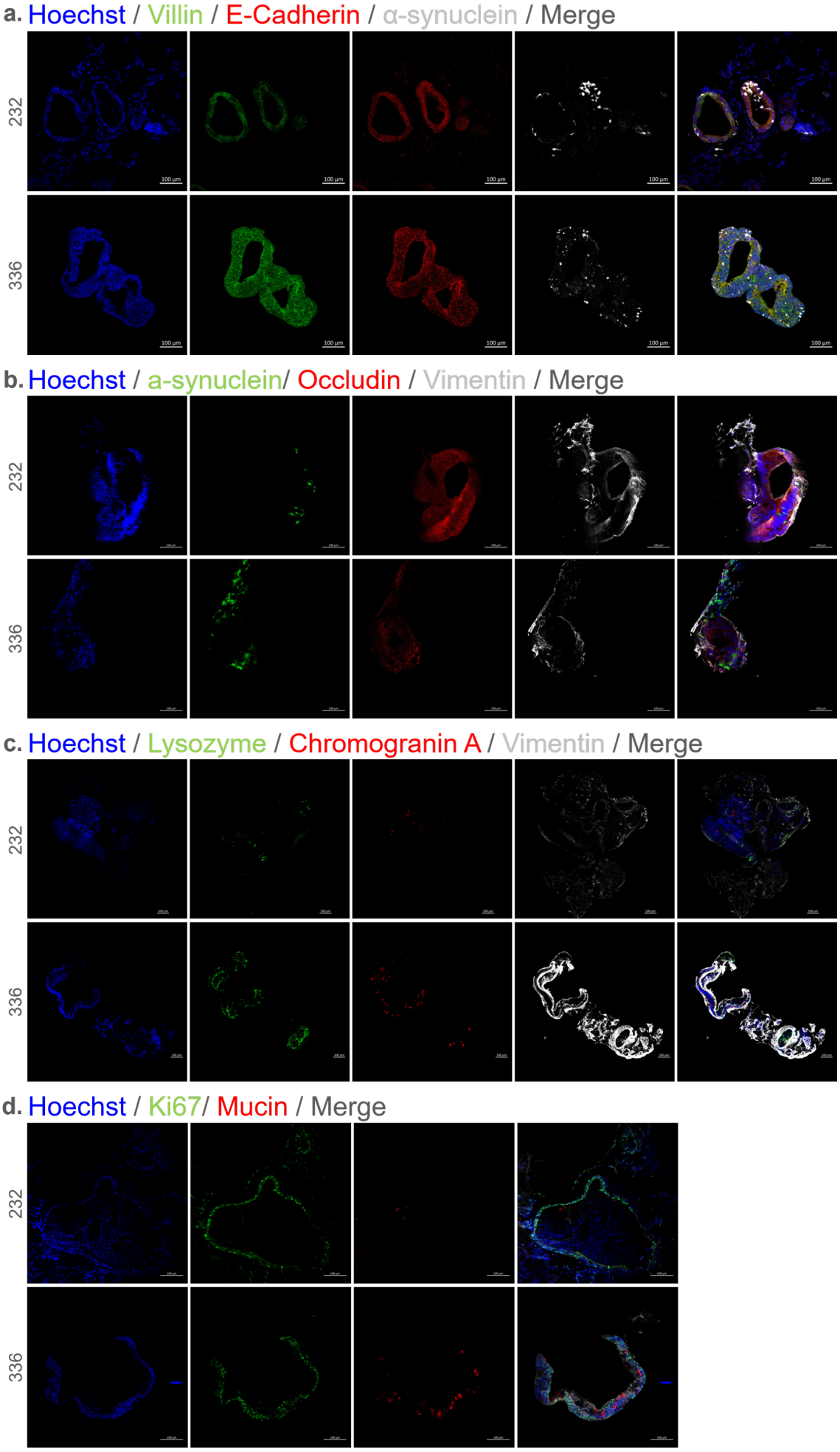
a. Hoechst / Villin / E-Cadherin / α-synuclein / Merge
232
336
b. Hoechst / a-synuclein/ Occludin / Vimentin / Merge
232
336
c. Hoechst / Lysozyme / Chromogranin A / Vimentin / Merge
232
336
d. Hoechst / Ki67/ Mucin / Merge
232
336

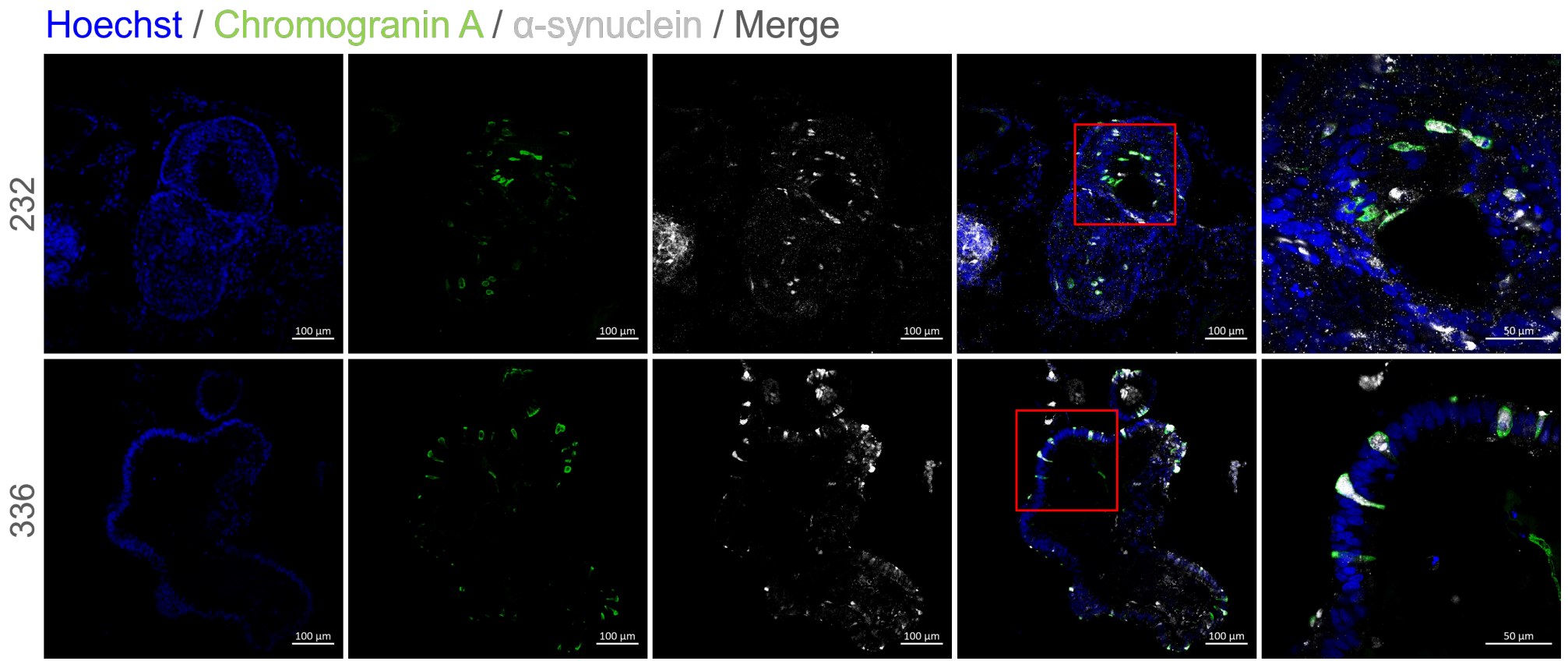

Figure 19. α-synuclein identification within intestinal organoids. Eight-week-old-iHOs from cell line 336 (SNCAx3) and 232 (WT) were immunostained for Hoechst, Chromogranin A, and α-synuclein. α-synuclein is greatly colocalized with Chromogranin A. An amplified view of the areas marked in a red box is shown to the right of each image. iHOs: intestinal organoids; WT: Wild Type; SNCAx3: Triplication of the *SNCA* gene. Scale bar as shown in each view.

3.2 Enteric precursors derived with the protocol by Barber et al. (2019) exhibit higher expression of enteric neuron precursor markers.

As mentioned, two protocols were tested for the derivation of ENS. To compare the derivation efficiency of the two used protocols (Fattahi *et al.,* 2016 and Barber *et al.,* 2019), simultaneous derivations from the same vial of iPSCs from cell line 232 (WT) were performed. At day 12 of differentiation, the cells were sorted to identify CD49d+ cells, which has been previously identified as a reliable marker for early neural crest lineages positive for SRY-Box Transcription Factor 10 (SOX10)[41,42]. As can be seen in Figure 20.a., 97,8% of the cells derived with the protocol by Barber *et al.* (2019) were CD49d+ while only a 6,84% of CD49d+ cells was obtained with the protocol by Fattahi *et al.* (2016). Such a high percentage of CD49d+ cells deemed the flow cytometry step unnecessary for derivations with this cell line.

To further evaluate derivation efficiency, not only at the enteric precursor stage, but also at the enteric neuron stage, RT-qPCR was performed on the ENCs at 12 DoD, after CD49d+ sorting, and on 21-days-old-ENS derived using both protocols. ENCs and ENS derived with the Barber *et al.* (2019) protocol showed an important upregulation of the enteric neuron precursor markers SOX10, Paired Like Homeobox 2B (PHOX2B), and Achaete-scute homolog 1 (MASH1), which was more pronounced at the ENC stage. On the other hand, the enteric precursor marker Paired Like Homeobox 2A (PHOX2A) and the neuronal cell marker MAP2 were downregulated with this protocol, specially at the ENS phase. It should be noted that the comparison of CD49d+ cells and gene expression levels between protocols was only done once.

To understand the robustness of the protocol by Barber *et al.* (2019), cell sorting was also performed in ENCs from cell lines 320 (SNCA KO) and 312 (WT-GFP), as well as in ENCs from the cell line 232 (WT) maintained in culture as precursors and passaged 3 times. Flow cytometry results (Figure 21) show that derivation efficiency varies between cell lines, presenting high levels of CD49d+ cells with WT cell lines (such as the 312 GFP, with 97,8%) and lower ones for cell line 320 (SNCA KO) at 49,5%. However, it is worth noting that this is still much higher percentage than the one achieved previously with the Fattahi *et al.* (2016) protocol (6,84%). It was also observed that, after 3 passages, the 232 (WT) ENCs showed only 31,4% of CD49d+ cells. The determination of CD49d+ cells in these types of samples was done once. According to the protocol by Barber *et al.* (2019), FACS should be done for samples

with a percentage of 60% CD49d+ cells or lower to obtain a pure ENC population; additionally, they state that this step is optional for samples derived with “Option B”, as the derivation is more reliable. Because of this, it was concluded that it is recommended to perform flow cytometry for cell line 320 (SNCA KO) or for ENCs that have been passaged more than once.

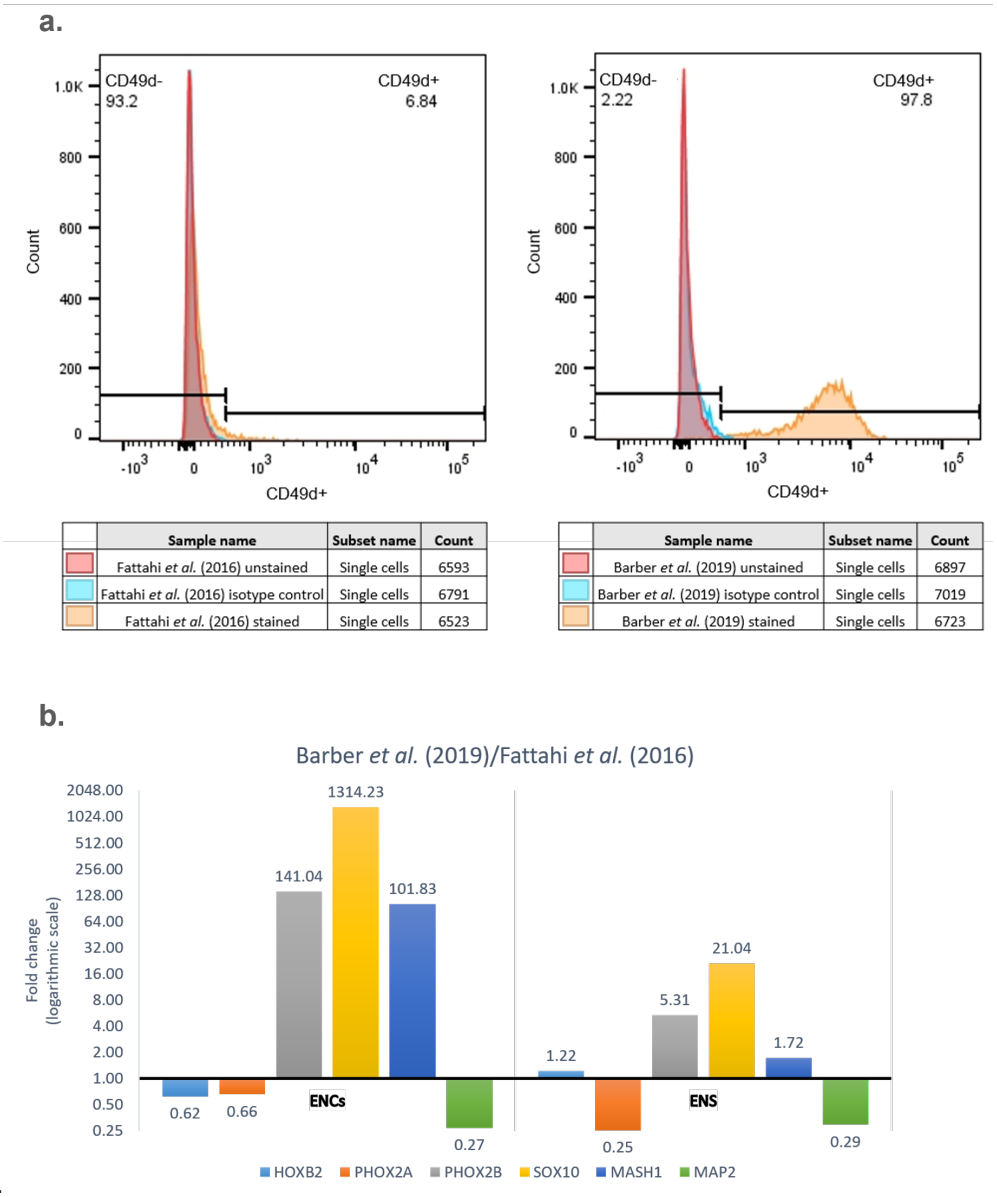

Figure 20. Comparison of the derivation efficiency of enteric neural precursors and enteric neurons with the protocols by Fattahi *et al.* (2016) and Barber *et al.* (2019). a. Flow cytometry results of ENCs derived with the Fattahi *et al.* (2019) protocol (left) and the Barber *et al. (*2019) protocol (right). **b.** Fold change expression of enteric neuron precursor and neuronal markers between the two mentioned protocols. CD49d: Integrin α-4; ENCs: enteric neural precursors; ENS: enteric neurons; HOXB2: Homeobox B2; PHOX2A: Paired Like Homeobox 2A; PHOX2B: Paired Like Homeobox 2B; SOX10: SRY-Box Transcription Factor 10; MASH1: Achaete-scute homolog 1; MAP2: Microtubule-associated Protein 2.

a.

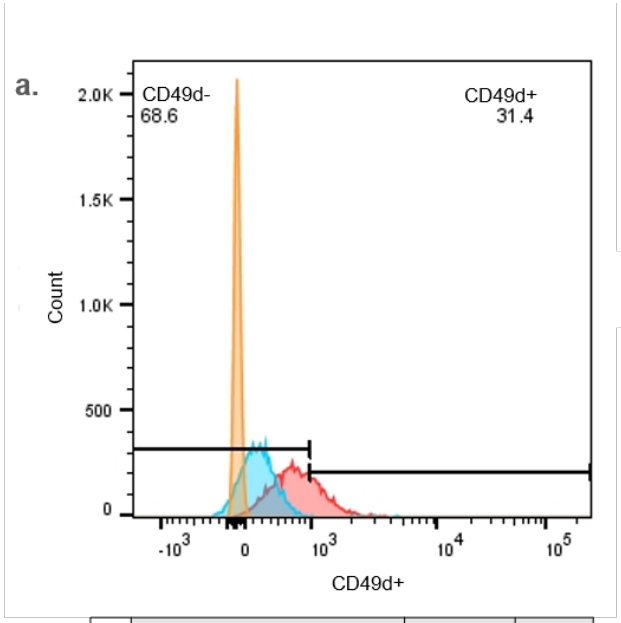

	Sample name	Subset name	Count
	ENCs 232 P3 stained	Single cells	8868
	ENCs 232 P3 isotype control	Single cells	8856
	ENCs 232 P3 unstained	Single cells	8816

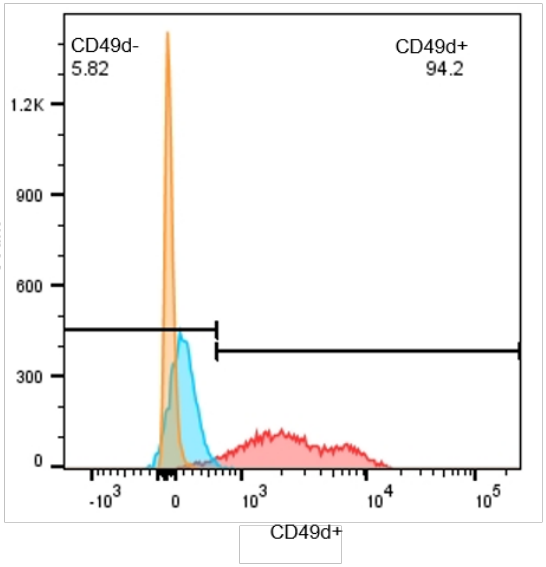

	Sample name	Subset name	Count
	ENCs 312 (GFP) P0 stained	Single cells	7970
	ENCs 312 (GFP) P0 isotype control	Single cells	8064
	ENCs 312 (GFP) P0 unstained	Single cells	7952

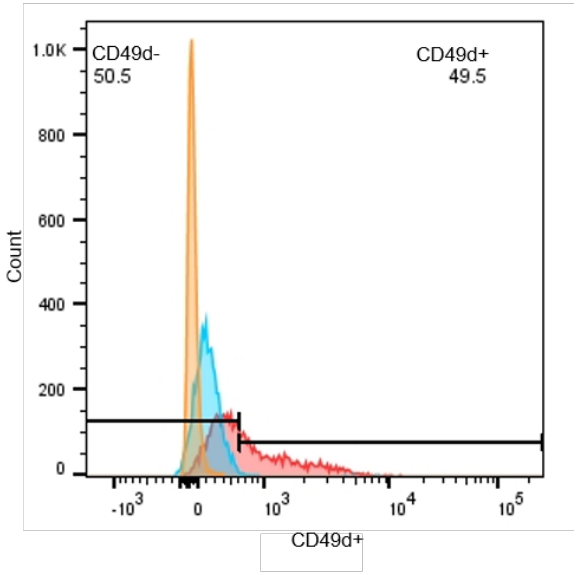

	Sample name	Subset name	Count
	ENCs 320 P0 stained	Single cells	5869
	ENCs 320 P0 isotype control	Single cells	5814
	ENCs 320 P0 unstained	Single cells	5686

b.

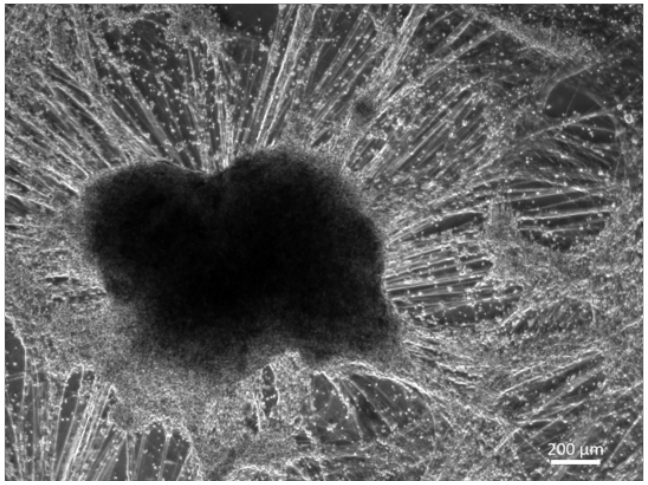

Figure 21. Enteric neuron derivation characterization.

a. Flow cytometry of enteric neuron precursors (ENCs) of cell line 232 (WT) after 3 passages, cell line 312 (WT-GFP) and cell line 320 (SNCA KO) (from left to right). **b.** Enteric neurons (ENS) from cell line 232 (WT) at 21 days of differentiation.

CD49d: Integrin α-4; P: passage; GFP: green fluorescent protein.

In regards to morphology, elongated cells were observed growing from the plated spheroids during ENS differentiation (Figure 21.b).

With the aim to establish the enteric neuronal identity of derived ENS, they were stained for different markers at 21, 38, and 50 days of differentiation. ENS were positive for the enteric neuron precursor markers PHOX2A and MASH1, specially at the earliest time points of differentiation (Figure 22.a & b). They were also positive for more specialized neuronal markers during different periods of differentiation. The serotonin receptor 5-HT_{2C} (5-hydroxytryptamine) was detected in similar levels through all the evaluated time points (Figure 22.b). Choline acetyltransferase (ChAT), the enzyme responsible for acetylcholine synthesis[49], and the neurotransmitter gamma-Aminobutyric acid (GABA) were mostly present at the latter stages of differentiation (Figure 22.c). Tyrosine hydroxylase (TH) an enzyme responsible for dopamine, norepinephrine, and epinephrine synthesis[49] was predominantly observed at 21 and 38 DoD, while AP-2α a transcription factor expressed in all GABAergic neurons[52] was detected in all time points (Figure 22.d). The neuronal-specific cytoskeletal markers MAP2, Neurofilament and TUJ1 (class III β-tubulin) were detected at all evaluated differentiation phases (Figure 22). It is also worth noting that ENS at all stages were positive for α-synuclein, the protein of interest for this project, and for Vasoactive Intestinal Peptide (VIP), a peptide neurotransmitter with a vasoactive function in the intestine[53] (Figure 22.e). ENS from cell line 320 (SNCA KO) were negative for α-synuclein, and positive for VIP and MAP2 (appendix 6.2).

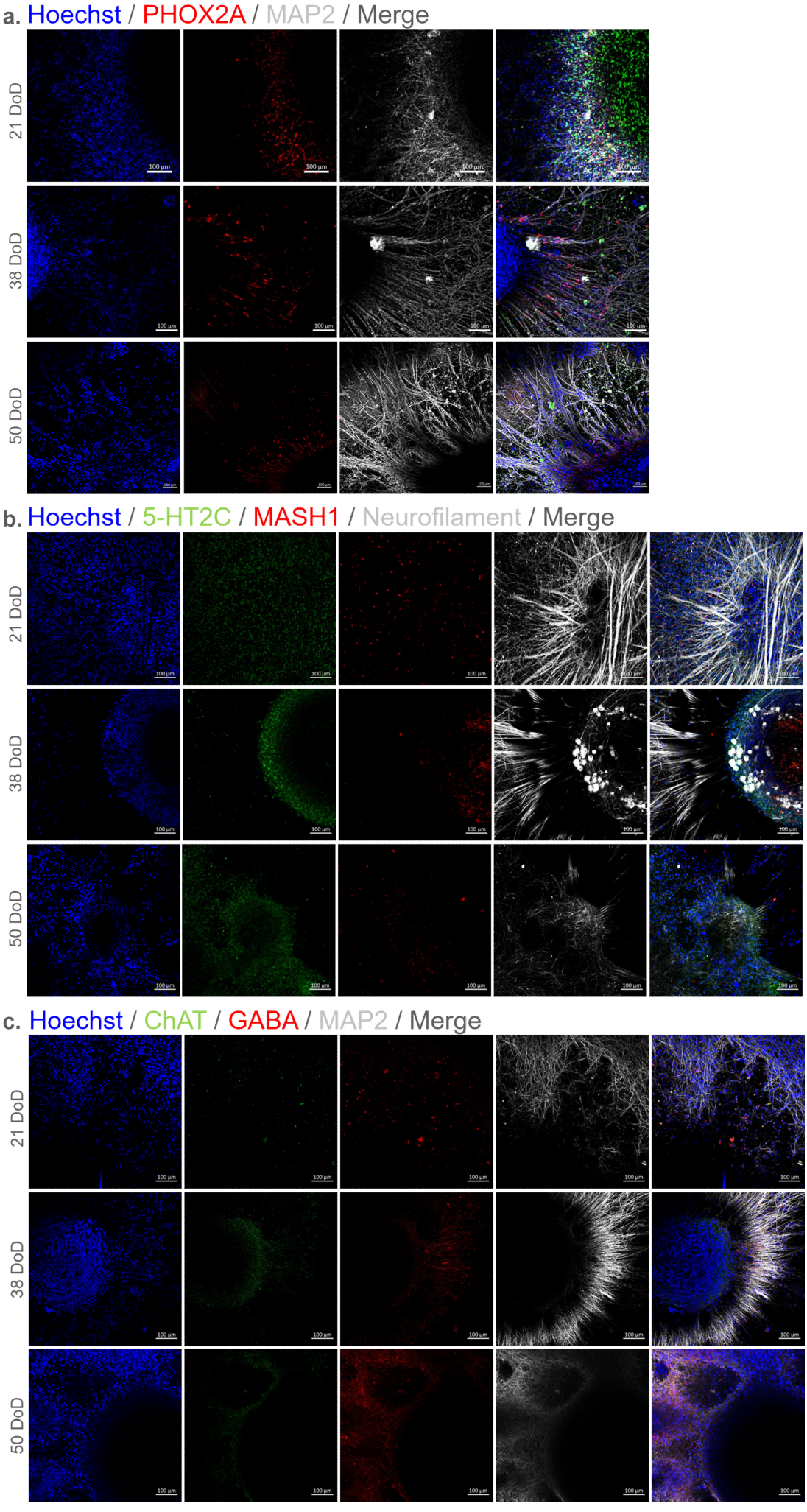
a. Hoechst / PHOX2A / MAP2 / Merge
21 DoD
38 DoD
50 DoD
b. Hoechst / 5-HT2C / MASH1 / Neurofilament / Merge
21 DoD
38 DoD
50 DoD
c. Hoechst / ChAT / GABA / MAP2 / Merge
21 DoD
38 DoD
50 DoD

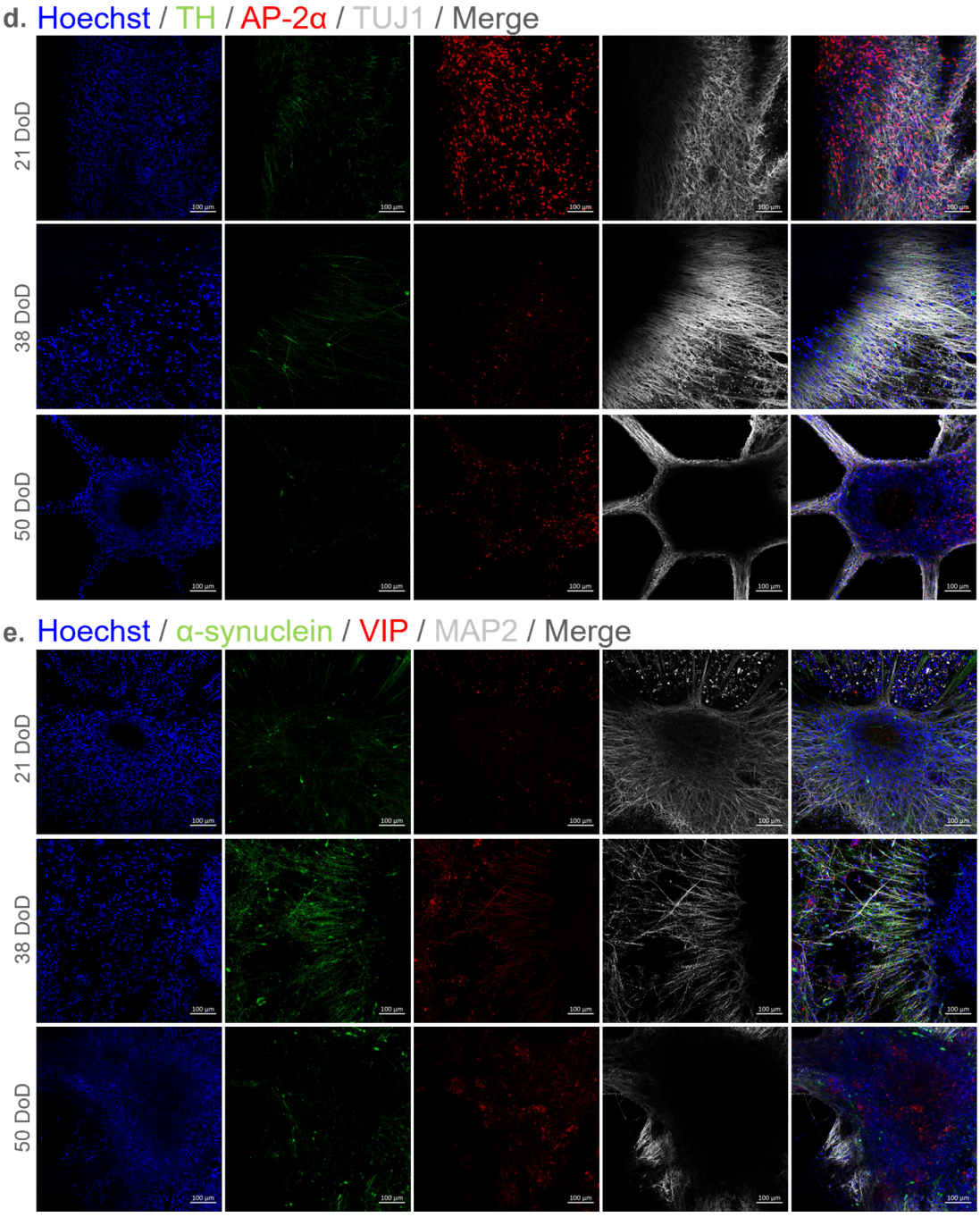

Figure 22. Enteric neuron characterization. ENS from cell line 232 (WT) were immunostained at 21, 38 and 50 DoD. **a.** Immunofluorescence stain for Hoechst, PHOX2A, and MAP2. **b.** Immunofluorescence stain for Hoechst, 5-HT_{2C}, MASH1, and Neurofilament. **c.** ENS immunostained for Hoechst, ChAT, GABA, and MAP2. **d.** ENS immunostained for Hoechst, TH, AP-2α, and TUJ1. **e.** Immunofluorescence stain for Hoechst, α-synuclein, VIP and MAP2. ENS: enteric neuron; PHOX2A: Paired Like Homeobox 2A; MAP2: Microtubule-associated Protein 2; 5-HT_{2C}: 5-hydroxytryptamine receptor; MASH1: Achaete-scute homolog 1; ChAT: Choline acetyltransferase; GABA: gamma-Aminobutyric acid; TH: Tyrosine hydroxylase; TUJ1: class III β-tubulin; VIP: Vasoactive Intestinal Peptide; WT: Wild Type; DoD: days of differentiation. Scale bar: 100 µm.

3.3 iHO-ENS contact was not detected and intracellular α-synuclein could not be quantified in iHO-ENS assembloids.

Once intestinal organoids and enteric neurons were derived, they were co-cultured together as detailed in section 2.1.4.1 for the iHO-ENS assembloids. As mentioned in the methodology section, two configurations of this assembloid were built: one in which the ENS were seeded on the plate one week before seeding the iHOs (Pre-plated-ENS) and one in which the ENS were seeded on the plate on the same day as the iHOs (ENS plated simultaneously). This was done to identify the configuration that allowed the best contact between the intestinal organoids and the enteric neurons.

Figure 23.a shows how the co-culture of ENS and iHOs, separated by the compartmentalizing insert, was observed after 8 days of co-culture (only the configuration of ENS plated simultaneously is shown as an example). ENS were attached to the plate surface, and both types of cells displayed their expected morphology. This was also confirmed by immunofluorescence staining 21 days after co-culture. Globular iHOs positive for Occludin were observed in the central compartment (Figure 23.b). Pre-plated ENS were present in the central compartment 21 days after co-culture (Figure 23.c, right) and ENS plated simultaneously with iHOs were able to cross the compartmentalizing insert (Figure 23.c, left). However, it was not possible to detect direct contact between the iHOs and the ENS; moreover, when doing the microscopy acquisitions, the iHOs were detected in a different plane than the ENS.

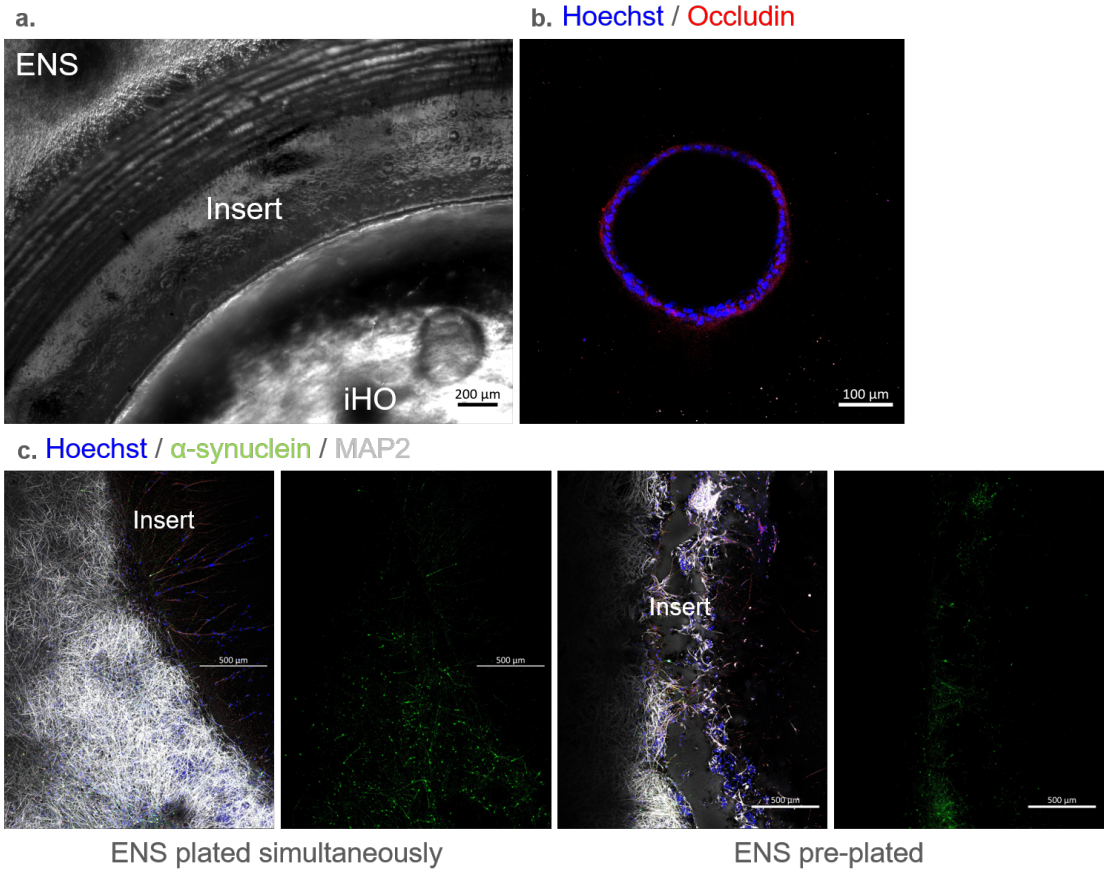

Figure 23. Growth of intestinal organoids and enteric neurons in iHO-ENS assembloids. a. ENS and iHOs eight days after initiating co-culture, both types of cells are separated by the compartmentalizing insert. **b.** Immunofluorescence stain of an iHO in the central compartment, 21 days after co-culture. **c.** ENS growth across the compartmentalizing insert for ENS plated simultaneously to iHOs (left) and ENS pre-plated (right), 21 days after co-culture. α-synuclein immunofluorescence is visible in green. ENS: enteric neurons; iHO: intestinal organoid; Paired Like Homeobox 2A; MAP2: Microtubule-associated Protein 2. Scale bar as indicated in each image.

With the aim to compare intracellular α-synuclein content in the enteric neurons co-cultivated with PD (336 SNCAx3) or healthy (232 WT) iHOs, ENS after 21 days of co-culture were analyzed through Western Blot (WB). Unfortunately, it was not possible to quantify α-synuclein through this technique (Figure 24.a), which contrasted with its (qualitative) detection through confocal microscopy as shown in Figure 23.c.

Extracellular α-synuclein levels in the two compartments of the assembloids was also studied to understand if the co-cultivation with PD (336 SNCAx3) or healthy (232 WT) iHOs affected the protein's concentration on the medium of the ENS. This was of interest since the requirement of cell-to-cell contact for α-synuclein transmission has not been proven (see section 4.2). It was observed that, on both types of co-culture (ENS plated simultaneously with iHOs and ENS pre-plated) extracellular α-synuclein

detected in central compartments with iHOs from cell line 232 (WT) increased in comparison to the first day of co-culture, while extracellular α-synuclein detected in central compartments with iHOs from cell line 336 (SNCAx3) remained constant, and sometimes decreased, throughout the co-culture period. Extracellular α-synuclein in the peripheral compartment behaved differently in both types of co-culture. In ENS plated simultaneously to iHOs, the α-synuclein concentration more than tripled at day 3 in comparison to ENS that were not in co-culture (control ENS), regardless of the cell line of the iHO. The α-synuclein concentration decreased at 10 days of co-culture and then returned to similar levels as the ENS that were not in co-culture. From days 7 to 21 of co-culture, the level of extracellular α-synuclein increased in a higher proportion in co-cultures containing iHOs from cell line 336 (SNCAx3) (Figure 24.c). In assembloids in which ENS were pre-plated, the concentration of α-synuclein was close to double from days 3 to 14 of co-culture, in comparison to ENS not in co-culture. This concentration returned to original levels at day 17 with a small decrease on day 21 of co-culture. This behavior did not differ between co-cultures with iHOs from cell line 232 (WT) or 336 (SNCAx3) (Figure 24.d). After 17 days of co-culture, ENS in both types of assembloids exhibited similar extracellular α-synuclein levels as the control ENS (Figure 24. c & d).

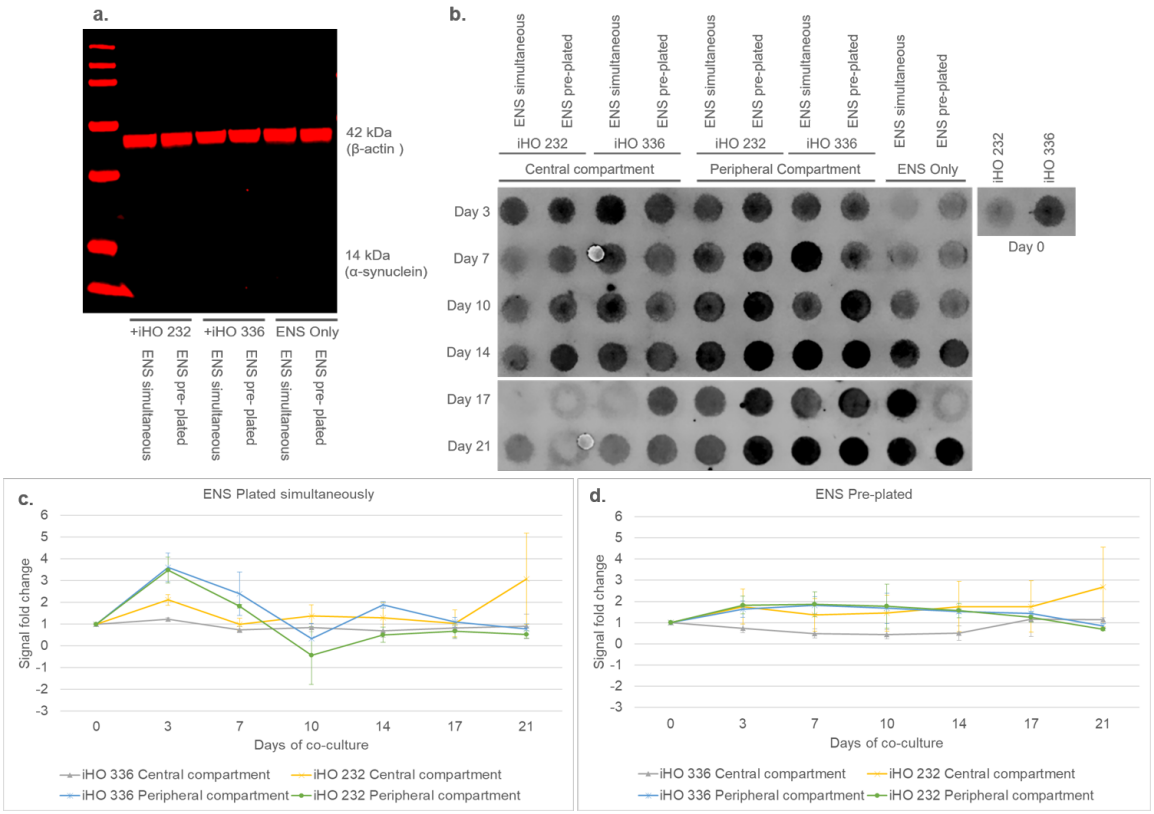

Figure 24. Intracellular and extracellular α-synuclein detection in iHO-ENS assembloids. a. Western blotting performed to detect intracellular α-synuclein in ENS from assembloids, only the reference protein, β-actin, is observed. **b.** Dot blot performed for the detection of extracellular α-synuclein in the iHO-ENS assembloids**. c.** Signal fold change in extracellular α-synuclein in the iHO-ENS assembloid in which the ENS was plated simultaneously as the iHOs. **d.** Signal fold change in extracellular α-synuclein in the iHO-ENS assembloid in which the ENS plated 7 days before the iHOs (pre-plated). All ENS were derived from cell line 232 (WT). ENS: enteric neurons; iHOs: intestinal organoids; kDa: kilodaltons. iHO 232: iHO derived from cell line 232 (WT). iHO 336: iHO derived from cell line 336 (SNCAx3); WT: Wild Type; SNCAx3: Triplication of the SNCA gene.

As further explained in the discussion section, the impossibility to detect contact between the iHOs and the ENS, the inconclusive results from the extracellular α-synuclein measurements, together with the impossibility to quantify intracellular α-synuclein, resulted in the discarding of this type of assembloid for the remaining analysis.

3.4 PD brain organoids exhibit higher p-α-synuclein at 30 DoD.

With the intention to be able to perform α-synuclein quantification through high content microscopy of the assembloids of intestinal organoids and enteric neurons, a computational algorithm was developed. However, due to the long period of time required to obtain the assembloids, this pipeline was first developed with readily available brain organoid sections. Immunofluorescence staining was performed and first visualized through confocal microscopy to verify the expression of α-synuclein. For these samples, staining for p-α-synuclein was of interest as a marker of α-synuclein aggregation. α-synuclein and p-α-synuclein were detected in brain organoids of 30, 60 and 90 DoD. Qualitatively, the signal for α-synuclein seemed greater in brain organoids from the cell line 336 (SNCAx3) for all time points (Figure 25). With regards to p-α-synuclein, a qualitative evaluation could not be performed due to positive p-α-synuclein staining on brain organoids from the negative control cell line 320 (SNCA KO), which indicated unspecific binding of the antibody (the presence of α-synuclein in the negative control was ruled out by the α-synuclein staining). MAP2 positive staining revealed the presence of neurons within the brain organoid.

a. 30DoD

Hoechst / MAP2 / p-α-synuclein / α-synuclein / Merge

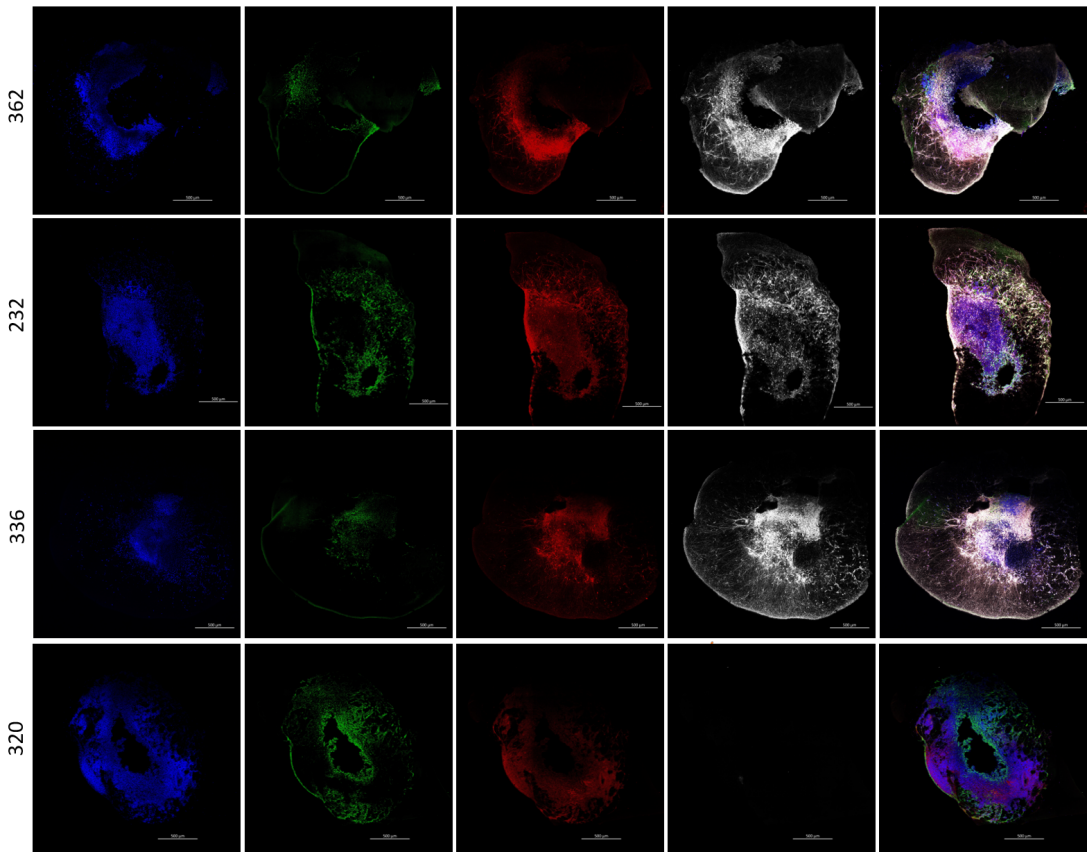

b. 60DoD

Hoechst / MAP2 / p-α-synuclein / α-synuclein / Merge

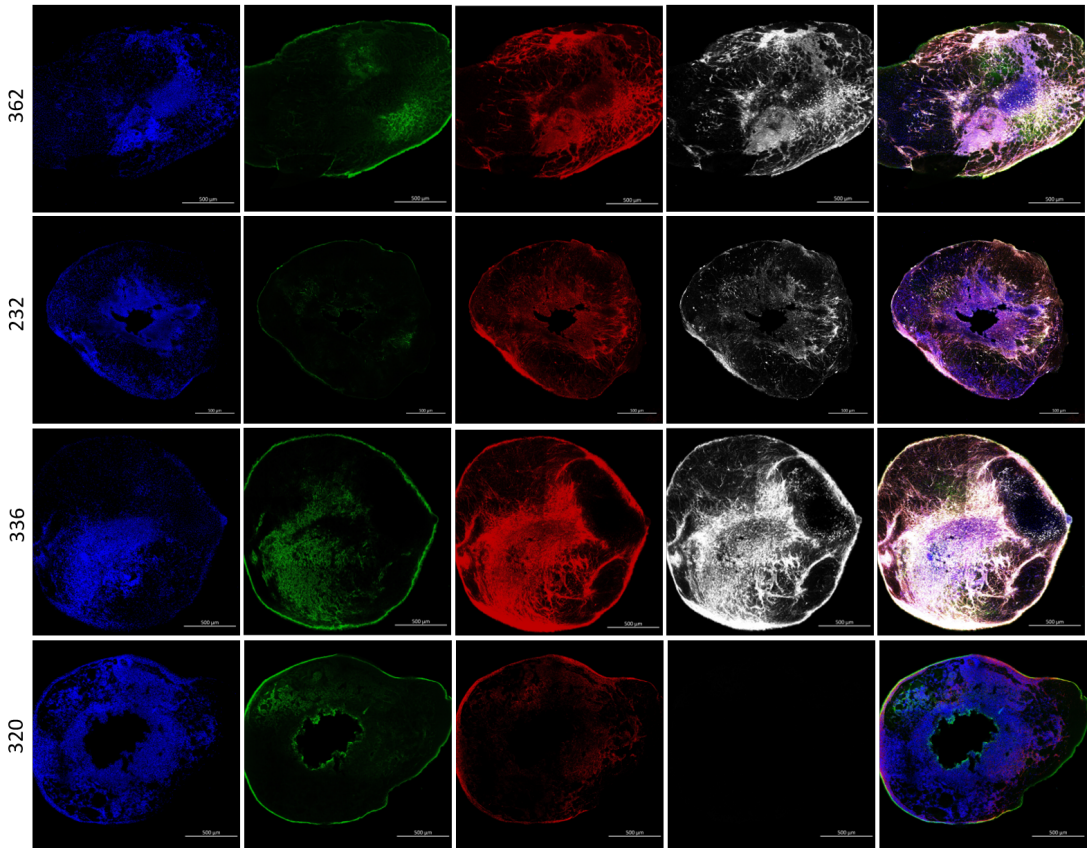

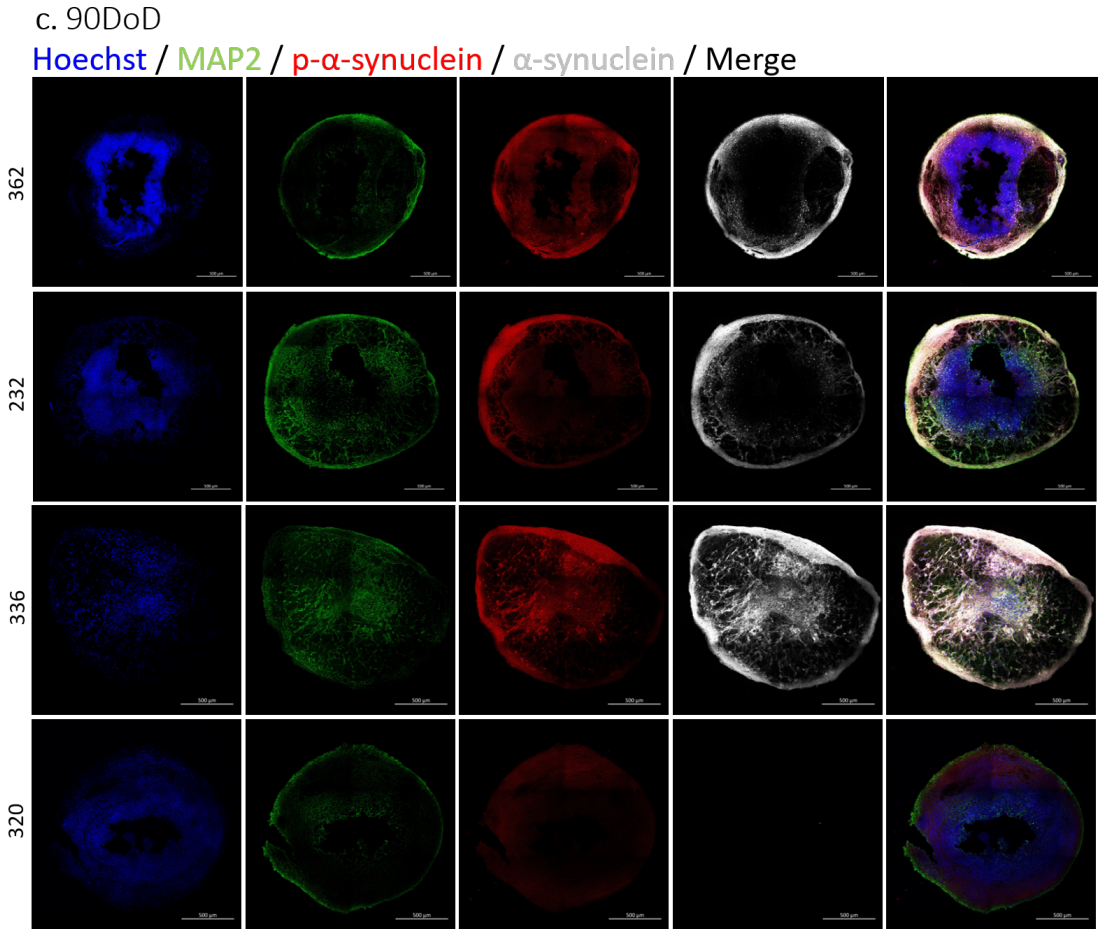

Figure 25. α-synuclein and p-α-synuclein in brain organoids. Organoids were Immunofluorescently stained for Hoechst, MAP2, α-synuclein, and p-α-synuclein. **a.** 30-day-old brain organoids. **b.** 60-day-old brain organoids. **c.** 90-day-old brain organoids. DoD: days of differentiation; MAP2: Microtubule-associated Protein 2. Scale bar: 500 µm.

Once the expression of the markers of interest was confirmed, high content imaging of the stained samples was performed to be able to quantify them. This revealed that the neuronal content of the brain organoids, as observed by MAP2+ staining, seemed to increase through time for the 336 (SNCAx3) and the 320 (SNCA KO) cell line, but not for the 232 and 362 (WT) cell lines (Figure 26.b). However, the difference between the PD (336 SNCAx3) and the healthy (232 & 362 WT) cell lines was not significant (Figure 26.a). α-synuclein and p-α-synuclein followed a tendency to increase in the 336 (SNCAx3) brain organoids over the evaluated time points, a behavior that was not observed in the WT cell lines 232 and 362 (Figure 26.b). The difference between these two groups was statistically significant for p-α-synuclein at 30 DoD (Figure 26.a). Calculations for all features were performed using the same data set, please refer to Table 6 for detail regarding replicate number for each type of organoid per time point.

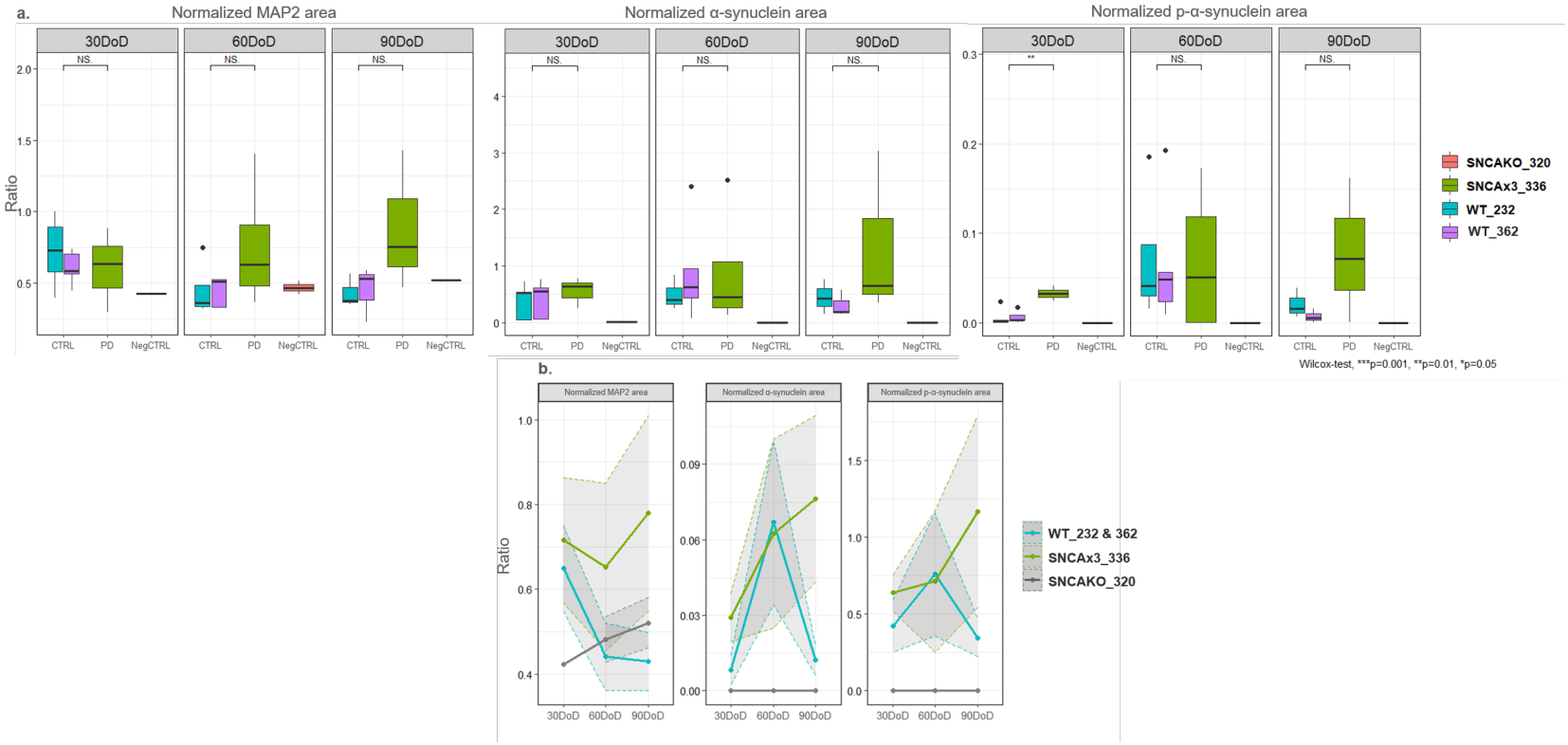

Figure 26. Quantitative analysis of α-synuclein and p-α-synuclein in brain organoids. a. Comparison of normalized MAP2, α-synuclein and p-α-synuclein area between cell lines. Statistical analysis by Wilcox test. Significance represented by p-value, ***p = 0.001, ** p = 0.01, * p = 0.05, and NS = not significant. **b.** Time tendency of normalized MAP2, α-synuclein and p-α-synuclein area. DoD: days of differentiation; MAP2: Microtubule-associated protein.

α-synuclein's known role as a pre-synaptic protein explains its localization at neuronal pre-synapses[54]. Still, subcellular localization studies confirm the presence of α-synuclein and p-α-synuclein in the nuclei and cell body of neurons[13,54] To understand if the PD phenotype affected their subcellular localization, α-synuclein and p-α-synuclein in the nuclei and the cytosol was quantified. α-synuclein showed a tendency to increase over time in brain organoids from cell line 336 (SNCAx3), and this was more evident in the cytosol than in the nuclei (Figure 27.b), but the difference remained not significant in comparison to the WT cell lines. On the contrary, p-α-synuclein detection in the nuclei increased over time (Figure 27.b) and the difference between PD (336 SNCAx3) and

healthy (WT 232 & 362) cell lines was significant at 30 DoD. This behavior was not observed for cytosolic p-α-synuclein. To attempt to control quantification issues of p-α-synuclein due to antibody unspecific binding, only p-α-synuclein colocalized with α-synuclein was taken into consideration. However, the issue remained for some quantifications at 60 DoD (Figure 27.a). Similar antibody issues have been experienced by other groups[13].

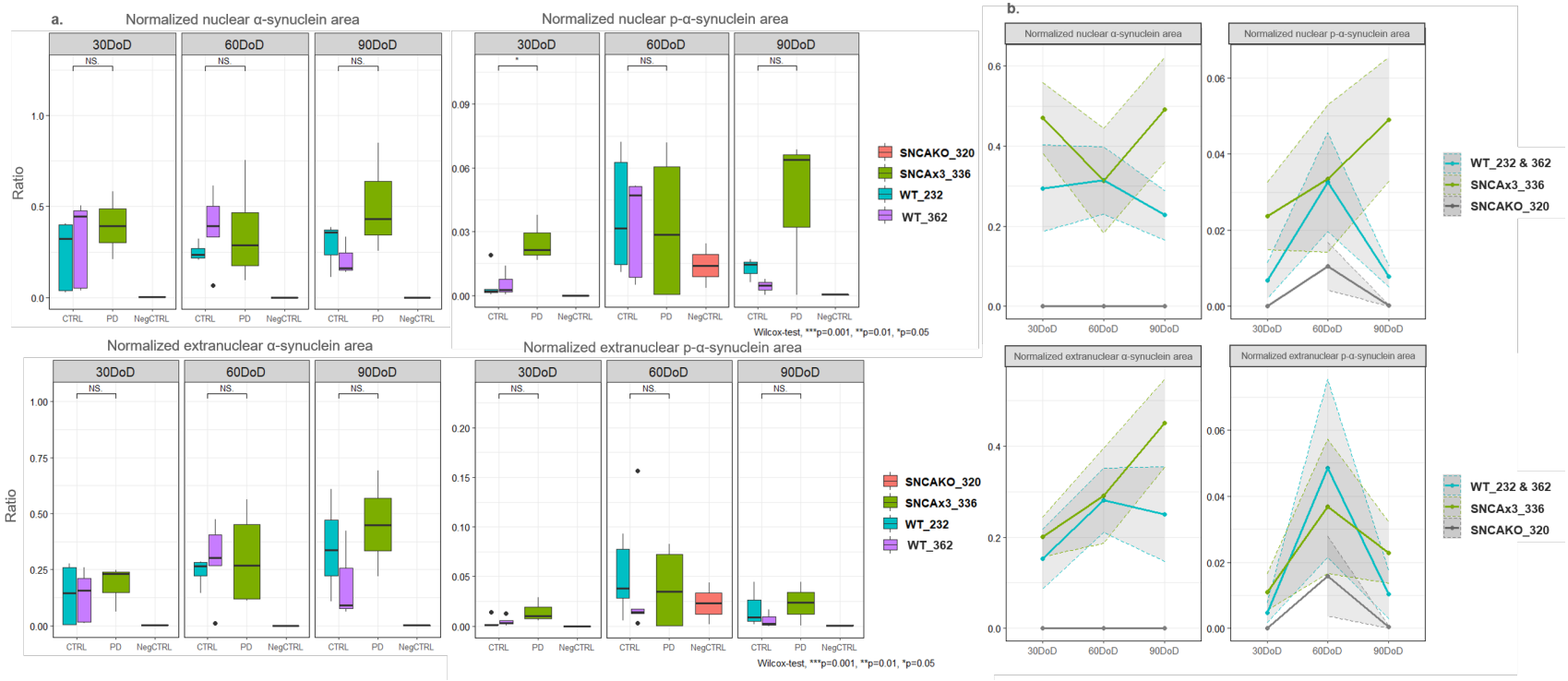

Figure 27. Subcellular localization of α-synuclein and p-α-synuclein in brain organoids. a. Comparison of normalized nuclear and extranuclear α-synuclein area as well as normalized nuclear and extranuclear p-α-synuclein area between cell lines. Statistical analysis by Wilcox test. Significance represented by p-value, ***p = 0.001, ** p = 0.01, * p = 0.05, and NS = not significant. **b.** Time tendency of normalized nuclear and extranuclear α-synuclein and p-α-synuclein area.

Next, and as explained in section 2.4.1, a spot detection method was implemented with the aim to characterize α-synuclein and p-α-synuclein aggregates in the nuclei and cytosol of neurons. Statistically significant differences were detected for the size of α-synuclein nuclear spots at 90 DoD and extranuclear spots at 60 DoD, with this size being larger in brain organoids from cell line 336 (SNCAx3) in comparison to the WT cell lines (232 and 362) (Figure 28.a.). In both subcellular localizations, the average size of α-synuclein spots increased over the evaluated time points (Figure 28.b). No significant difference was detected for the size p-α-synuclein spots, regardless of subcellular localization (Figure 28.a), however average size seemed to increase at 60 DoD (Figure 28.b).

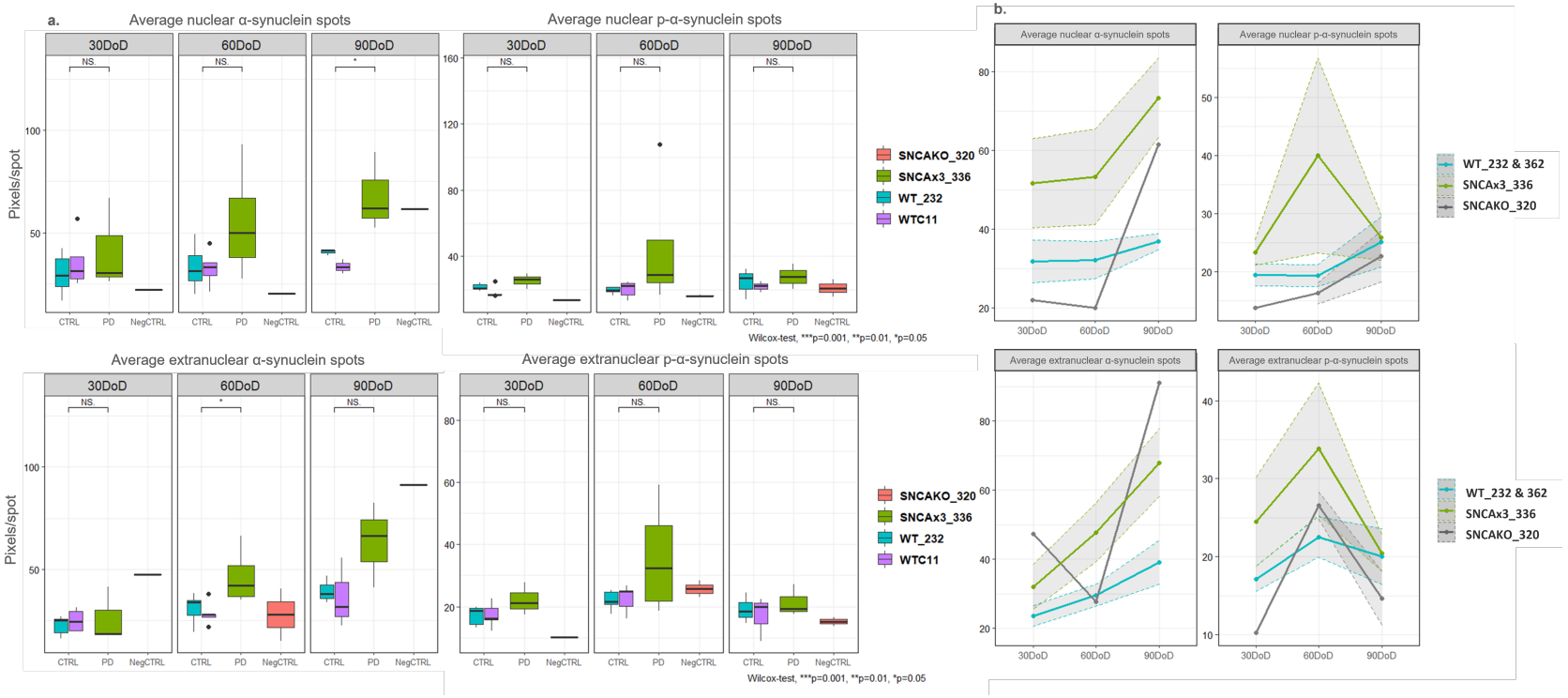

Figure 28. Subcellular localization of α-synuclein and p-α-synuclein spots in brain organoids. a. Comparison of average nuclear and extranuclear α-synuclein spots as well as average nuclear and extranuclear p-α-synuclein spots between cell lines. Statistical analysis by Wilcox test. Significance represented by p-value, ***p = 0.001, ** p = 0.01, * p = 0.05, and NS = not significant. **b.** Time tendency of average nuclear and extranuclear α-synuclein and p-α-synuclein spots. DoD: days of differentiation.

3.5 Greater α-synuclein intensities were detected in enteric neurons of iHO-ENC assembloids containing PD iHOs.

As an alternative approach to the iHO-ENS assembloids, intestinal organoids containing enteric neurons were derived following the protocol described by Workman *et al.* (2017) with adaptations. The obtained assembloids were referenced as iHO-ENC assembloids because, as detailed in section 2.1.4.2, they involved the incorporation of ENCs to hindgut spheroids.

In contrast with the iHO-ENS assembloids, in these assembloids contact between the enteric neuronal and the intestinal components of the iHO-ENC assembloids was evident through bright field imaging even after four passages, both in the assembloid containing-domes (Figure 29. a) and in the individual assembloids (Figure 29. b & c). The generation of assembloids containing ENCs derived from GFP-expressing iPSCs (cell line 312) allowed to confirm that the neuronal component seen in the assembloids was originated from the ENCs, as opposed to cells that came from the iHO derivation (Figure 29. d, e & f).

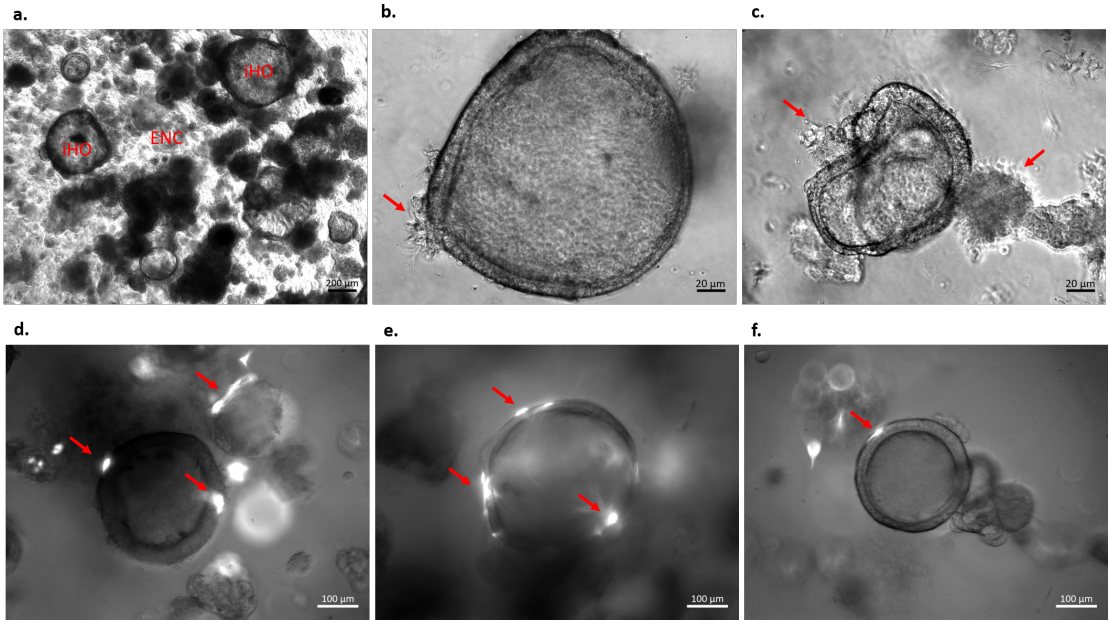

Figure 29. Intestinal organoids containing neurons. a. iHOs and ENCs grown together in a 3D extracellular matrix. **b. & c.** Individual iHOs with neurons and/or in contact with neurons. **d, e & f.** Intestinal organoids from cell line 232 (WT) with GFP-positive ENCs (cell line 312). Red arrows indicate neuronal components of the assembloids. iHOs: intestinal organoids; ENCs: enteric neuron precursors; GFP: Green Fluorescent Protein; WT: Wild Type. Scale bar as indicated in each image.

To be able to separately identify the intestinal and the neuronal component of each assembloid, they were immunostained for Villin and MAP2, respectively. They were also stained for the protein of interest, α-synuclein. Immunofluorescence staining further demonstrated the contact between the iHOs and the neurons and permitted to visualize the presence of α-synuclein within both types of cells (Figure 30).

Additional to the MAP2 staining, the neuronal component within iHO-ENC assembloids was further characterized as enteric neurons by immunostaining with VIP (Figure 31.a) and Neurofilament (Figure 31.b).

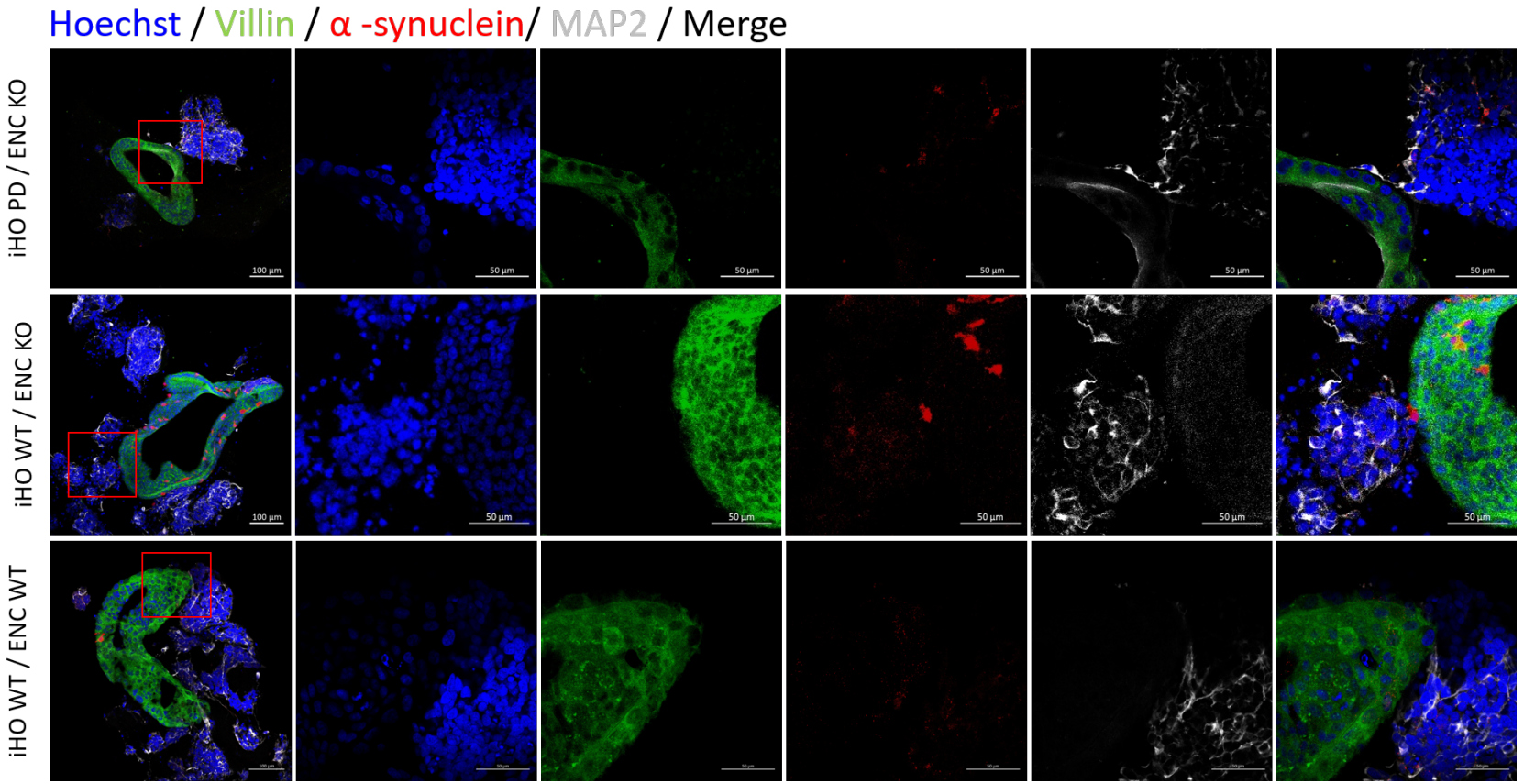

Figure 30. α-synuclein containing iHO-ENC assembloids. Contact between the neuronal (MAP2 positive) and intestinal (Villin positive) components of the asembloids was observed for the three types of assembloids generated: iHO PD / ENC KO, iHO WT / ENC KO, and iHO WT / ENC WT. The first image shows complete assembloids, while images to the right display a closer look of the region enclosed in red squares, points of contact between the ENCs and the iHO. Immunofluorescence staining done for Hoechst, Villin, α-synuclein, and MAP2. iHO PD: iHO from cell line 336 (SNCAx3); ENC KO: ENC from cell line 320 (SNCA KO); iHO WT: iHO from cell line 232 (WT); ENC

WT: ENC from cell line 232 (WT). ENC: enteric neuron precursor; iHO: intestinal organoid; MAP2: microtubule-associated protein 2; WT: Wild Type; SNCAx3: Triplication of the *SNCA* gene; SNCA KO: *SNCA* gene knock-out. Scale bar as shown in each image.

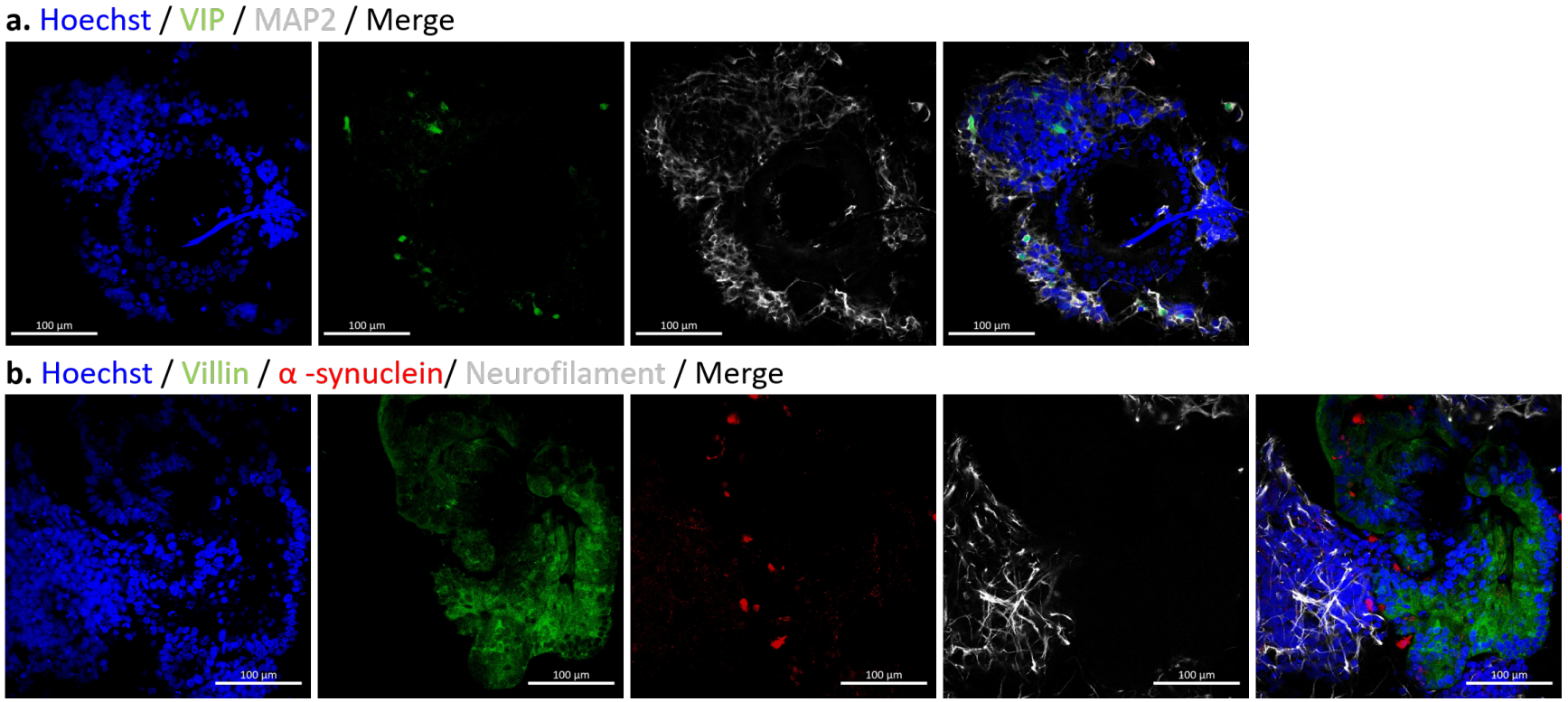

Figure 31. The neuronal component in iHO-ENC assembloids express VIP and neurofilament. a. iHO-ENC assembloid immunostaining for Hoechst, VIP, and MAP2. The neuronal component shows staining for VIP, and MAP2**. b.** iHO-ENC assembloid immunostaining for Hoechst, Villin, α-synuclein, and Neurofilament. The neuronal component shows staining for α-synuclein and Neurofilament. iHO: intestinal organoid; ENC: enteric neuron precursor; VIP: vasoactive intestinal peptide; MAP2: microtubule-associated Protein 2. Scale bar: 100µm.

After the qualitative detection of the markers of interest, immunostained assembloids were analyzed through high content microscopy to be able to quantify the of α-synuclein within each of the assembloid's components (intestinal and neuronal) and determine if co-cultivation of neurons with a PD (336 SNCAx3) iHO had an effect on the α-synuclein content of the enteric neurons. As seen in Table 2, only one replicate was obtained for the IHO PD / ENC KO assembloid, therefore, repetitions obtained for other assembloid combinations were pooled and analyzed as a single repetition. The performed quantification demonstrated that this protein showed a significantly greater intensity within the ENCs in assembloids containing PD iHOs (336 SNCAx3). It also showed that this intensity was not different between assembloids that had iHO WT (232) co-cultivated with ENCs KO (320 SNCA KO) or ENCs WT (232) (Figure 32. a & b). In relation to α-synuclein content within the iHOs, intensity was greater in iHOs WT (232) co-cultivated with ENCs KO (320 SNCA KO), this difference was only significant for the normalized α-synuclein intensity detected in the iHOs (Figure 32. c & d).

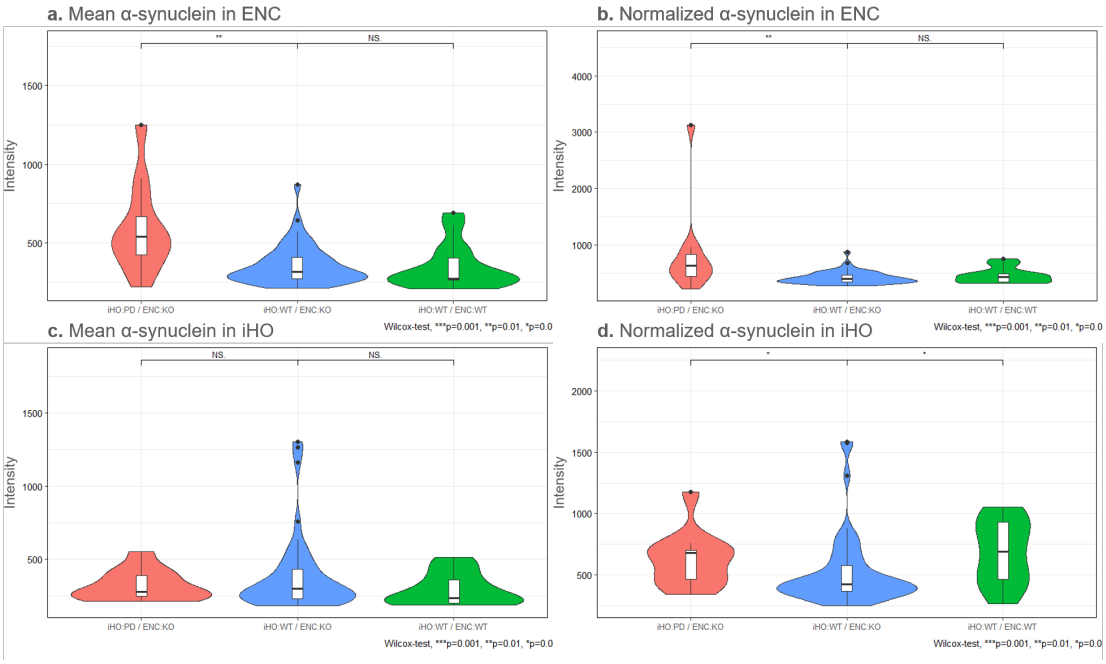

Figure 32. α-synuclein intensities were greater within the ENCs co-cultivated with PD iHOs. a. Mean α-synuclein intensities in the ENC component of the assembloids. **b.** Normalized α-synuclein intensities in the ENC component of the assembloids. **c.** Mean α-synuclein intensities in the iHO component of the assembloids. **d.** Normalized α-synuclein intensities in the iHO component of the assembloids. Statistical analysis by Wilcox test. Significance represented by p-value, ***p = 0.001, ** p = 0.01, * p = 0.05, and NS = not significant.

α-synuclein aggregates were also studied in these assembloids via the spot detection methodology. Count and area of spots were greater in ENCs co-cultivated with PD iHOs (336 SNCAx3) (Figure 33.a & b); however, this difference was not significant. Spot size was similar in ENCs from all assembloids (Figure 33.c). In contrast, spot size within the iHOs, it was significantly larger in WT iHOs (232) co-cultivated with ENCs KO (320 SNCA KO) in comparison to PD iHOs (336 SNCAx3) grown with the same type of ENCs (Figure 33.f). No significant difference was detected for spot count or area within the iHOs (Figure 33.d & e).

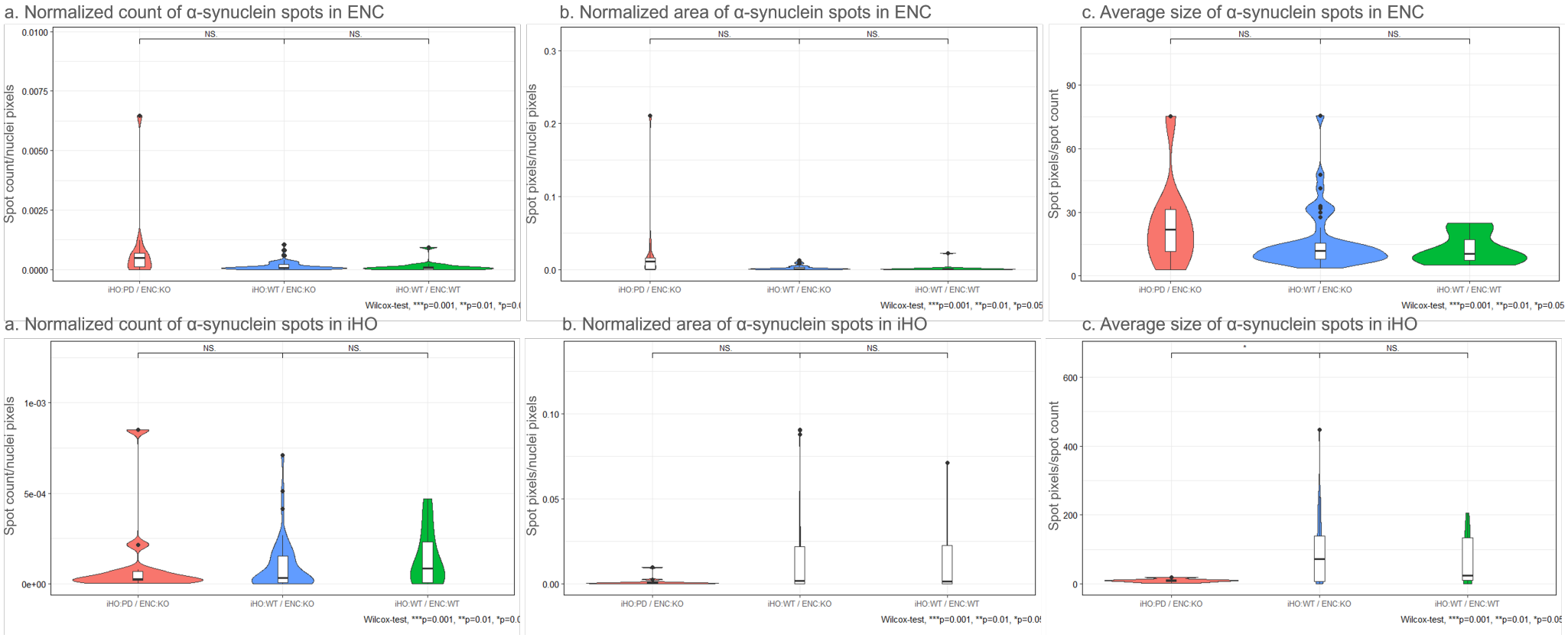

Figure 33. α-synuclein spots detected within the iHO-ENC assembloids. a. Normalized count of α-synuclein spots in the ENC component of the assembloids. **b.** Normalized area of α-synuclein spots in the ENC component of the assembloids. **c.** Average size of α-synuclein spots in the ENC component of the assembloids. **d.** Normalized count of α-synuclein spots in the Iho component of the assembloids. **e.** Normalized area of α-synuclein spots in the iHO component of the assembloids. **f.** Average size of α-synuclein spots in the iHO component of the assembloids. Statistical analysis by Wilcox test. Significance represented by p-value, ***p = 0.001, ** p = 0.01, * p = 0.05, and NS = not significant.

4 Discussion

4.1 Derivation of intestinal organoids and enteric neurons

In this project, considerable efforts were invested in the derivation of intestinal organoids and enteric neurons to achieve the construction of assembloids comprising these two components. For this, iPSCs were differentiated into the different cell types as explained in sections 2.1.2 and 2.1.3.2. In the case of iHO differentiation, the process was successfully achieved for cell lines 232 (WT) and 336 (SNCAx3), although less effectively for the latter, while no iHOs for cells 320 (SNCA KO) were obtained. Differentiation variations between cell lines were reported since iHO derivation from iPSCs was first established in 2011[36]. However, in this case, the challenging obtention of iHOs for cell lines with alterations in the *SNCA* gene indicate that it might play a role in iHO differentiation. Particularly since, as discussed below, this protein is highly expressed in one of the cell types of the iHOs. For future studies, an alternative to improve iHO derivation could be the usage of a commercially available kit for iHO derivation (e.g. STEMdiff™; STEMCELL Technologies, 05140), which could provide a validated and standardized methodology. Additionally, if the *SNCA* gene does interfere with iHO differentiation, PD cell lines with a different genetic back ground could be used (for example, iPSCs bearing a mutation in the *LRRK2* gene).

iHOs derived in this project displayed similar characteristics as the ones first derived from intestinal crypts by Sato and collaborators in 2009 [24] and from iPSCs by Spence and team in 2011: they were composed of a single layer of epithelial cells surrounding a lumen, as revealed by E-cadherin staining, they contained enterocytes (Villin+), with Globlet cells (Mucin+) and EECs (chromogranin A+) dispersed through the organoid. Sato *et al.* (2009) also described the presence of Paneth cells (Lysozyme+) and CBC stem cells (Lgr5+) concentrated in crypt-like progenitor niches. Although both cell types were present in the derived iHOs (using Ki67 for stem cells), this specific localization was not observed. This difference in development could be a result of the iPSC origin of the organoids, since Spence *et al.* (2011) described the presence of intestinal progenitor domains from 56 days of culture. It could also be a consequence of the different strategies used for iHO differentiation, since Sato *et al.* (2009) selected for Lgr5+ cells, consequently enriching this cell population. In contrast to both groups, in the derived iHOs Villin signal stained all the plasma membrane of cells identified as enterocytes while their

studies showed this staining localized facing the lumen of the organoid. This disparity might imply a lack of polarization of the enterocytes due to immaturity of the derived iHOs or could be the consequence of the use of a less specific antibody. Non-epithelial cells, such as mesenchymal cells, were absent in the crypt-derived iHOs; however, a mesenchymal tissue (Vimentin+) was detected surrounding many of derived iHOs, as well as in the iPSC-derived iHOs by Spence *et al.* (2011). These authors mention that mesenchyme probably comes from a low percentage of mesoderm cells that remain after definitive endoderm differentiation, developing into a mesenchymal layer along with the epithelial organoid. Mesenchymal cells were also present in the intestinal organoids derived by Workman *et al.* (2017), where they described that, during the generation of innervated iHOs, ENCs migrated into the iHOs' mesenchyme to differentiate into neurons. These results indicate that derived iHOs displayed the expected morphology and cell types of reported iPSC-derived intestinal organoids, although maybe with a lesser degree of maturity. It is worth noting that iHOs derived by Sato *et al.* (2009) came from crypts from the small intestine, while iHOs derived in this project and by Spence *et al.* (2011) are intended to mimic the large intestine, since they differentiate from hindgut. For future experiments, it is recommended to immunostain iHOs with hindgut markers, such as Caudal Type Homeobox 2 (CDX2)[36,39,40], to verify their regional identity.

Derived intestinal organoids also expressed α-synuclein, mostly localized within specific cells distributed throughout the iHO. Many of these cells were identified as EECs (flask-shaped and chromogranin A+). The expression of α-synuclein by EECs has previously been reported in samples of human duodenum and mouse colon[51], and, as discussed later, this could have a crucial implication on α-synuclein transmission from the gut to the enteric nervous system. As in this case, the referenced study also identified α-synuclein expression in other non-EEC cells, that remain to be identified. Meticulous literature review resulted in the identification of an RNA-seq data entry from the Expression Atlas that indicates that α-synuclein is up regulated in iHOs derived from the human embryonic stem cell line H9 in comparison to undifferentiated H9 stem cells[55], but no scientific publication related to this feature in this data set was found. To our knowledge, this is the first time that α-synuclein expression in intestinal organoids has been described.

In regard to ENS derivation, it was shown that the protocol by Barber *et al.* (2019) yielded a greater percentage of CD49d+ cells than the protocol by Fattahi *et al.* (2016). Both protocols were published by the same group, and the more recent one appears to be an improved version of the former one. Fattahi *et al.* (2016) identified

CD49d as a consistent surface marker for SOX10+ neural crest lineages. In turn, SOX10 had been previously identified as a marker of early multipotent neural crest stem cells[56]. Flow cytometry results aligned with the gene expression comparison done through RT-qPCR, since SOX10 was the most upregulated gene in ENCs derived with the protocol by Barber *et al.* (2019). Regarding other analyzed genes, Fattahi *et al.* (2016) mentioned that ENS maintained the expression of enteric neuron precursor markers (such as MASH1 and PHOX2B) until day 40 of differentiation, which corresponds with their considerable up regulation even at 21 DoD. The downregulation of the ENC marker PHOX2A was much less pronounced. Similarly, HOXB2 expression change was minor, suggesting that vagal neural crest identity of the ENCs was not affected by the change of protocol. Both protocols indicate that the down regulation of enteric neuron precursor markers is accompanied by an up regulation of neuronal commitment markers such as TUJ1. The down regulated levels obtained for MAP2 can imply that obtained ENCs and ENS stay at an undifferentiated stage for longer, since MAP2 expression is low in neuronal precursors but increases as neurons differentiate[57]. It should also be considered that the protocols reported higher expression levels of TUJ1 from 35DoD, which might explain why the neuronal commitment marker MAP2 was not so highly observed at 21DoD[42]. Altogether, the protocol by Barber *et al.* (2019) appears to promote the obtention of cells with a much stronger enteric neural precursor identity. Yet, this result should be confirmed by the execution of additional repetitions.

Concerning derivation efficiency between cell lines, the protocol's authors state that proportions of cells positive for enteric neuronal identifiers can vary, as observed in this project. Furthermore, they obtained percentages of CD49d+ cells ranging between 19 and 37% during the derivation of two iPSC cell lines[42] which is much lower than the percentages observed in this project for the three evaluated cell lines (97,8% for cell line 232 WT; 94,2% for 312 WT-GFP; and 49,5% for 320 SNCA KO) , and similar to the percentage obtained for ENCs that were three passages old (31,4%). Obtained results revealed that sorting for CD49d+ cells is strongly recommended when deriving a new cell line or using a later passage of a known cell line, to determine if CD49d sorting is required. Again though, obtained percentages should be corroborated by the execution of additional repetitions of the experiment.

Immunostaining of ENS at different time points, revealed a transition from the expression of enteric neural precursor markers at earlier stages of differentiation, to neuronal commitment and neuronal subtype specific markers at later stages, as reported by both referenced protocols. Abundant ENC populations were detected

until day 38 of differentiation in alignment with the 40-day stated period. Detection of the pan-neuronal markers MAP2, TUJ1, and Neurofilament at all studied time points confirmed the neuronal identity of the ENS; but more crucially, the range of observed neurotransmitter phenotypes, including serotonin, acetylcholine, GABA, and VIP, supported the enteric neuronal identity, maturity and functionality of the derived cells[41,42,58], especially after 38 DoD. Serotonin detection, in particular, allowed to confirm the enteric neural crest origin of the cells, since this neurotransmitter was not observed in other neural crest lineages in the consulted literature[41]. VIP presence was also relevant, since a previous study reported that in the enteric nervous system of PD patients LBs were mainly found in the cell body and processes of neurons that were VIP+[58]. The cholinergic neuron marker ChAT was detected at relatively low levels at all time points, which is in accordance to the fact that its highest levels of expression were reported after 60DoD[41,42]. On the contrary, AP-2α was strongly detected since 21DoD, and as this transcription factor is expressed in GABAergic neurons, its presence was expected at the later stages. Nevertheless, according to the consulted bibliography, AP-2α is also expressed in GABAergic precursors[52]. Similarly, dopaminergic neurons (TH+) were also detected since 21 DoD; in contrast with the referenced protocols which reported its expression at 60 DoD; however, other authors had observed its expression in ENS at earlier time points[38]. Although the reviewed literature and referenced protocols do not report the characterization α-synuclein in iPSC-derived enteric neurons, this protein has been previously been found to be expressed in myenteric neurons[59]. Importantly, it has also been detected in enteric nerves located between the villi of human duodenum[51]. Its detection in the derived ENS concretes their enteric neuronal identity and their usefulness for the aim of the study.

The enteric neuronal identity of the neuronal component of the iHO-ENC assembloids 4 weeks after co-culture was supported by the immunostaining with MAP2, Neurofilament and VIP. However, a more comprehensive characterization for neuronal and enteric markers, as done for the ENS, is recommended.

4.2 iHO-ENS assembloids

The main goal of this project was the establishment of an assembloid model of the intestine and the enteric nervous system that would allow to study α-synuclein spread under PD-pathological conditions. For this, two approaches were followed; the first one involved the co-culture of both cell types in a compartmentalized well (iHO-ENS assembloid) and the second one consisted in combining both cell types at

earlier differentiation stages and co-cultivating them under 3D conditions. Nonetheless, as showed in section 3.3, the first of these assembloids did not function as intended. In it, two factors are thought to have impeded contact between iHOs and ENS in this assembloid model: 1) the placement of intestinal organoids in a different (although connected) compartment than enteric neurons, and 2) the different growth configurations of each cell type, since the ENS grew in a two-dimensional manner as a monolayer, while iHOs were cultured in a 3D system, suspended in an extracellular matrix. Now, as further discussed later for the iHO-ENC assembloids, whether cell-to-cell contact is required for α-synuclein transmission is still under discussion. As reviewed in Rietdjik *et al.* (2017)[8] some *in vitro* studies using neuronal cells have shown that neurons are capable to secrete and uptake α-synuclein from their environment, while others show their neuron-to-neuron transmission. These two options would not be, in principle, mutually exclusive. However, a more relevant study between EECs and neurons assures that cell-to-cell contact is required[60].

Extracellular α-synuclein studies demonstrated α-synuclein presence in the media of both iHOs and ENS, whether this was a result of secretion or release due to cell death, remains to be determined. Extracellular α-synuclein has previously been detected in body fluids including serum, cerebrospinal fluid, and urine, as well as in the culture medium of neuronal cells, showing its excretion. Moreover, its secretion has been related to neuronal activity[10]. But no previous reports were found related to α-synuclein secretion by the intestinal epithelium or intestinal organoids. One review did mention that α-synuclein can be found in saliva, and that this can be a source for its presence in the intestinal lumen[61]. As described in previous sections, α-synuclein is expressed in EECs present in the intestine; accordingly, in the derived iHOs α-synuclein staining frequently colocalized with the marker for such cells. No publication explains whether EECs secrete α-synuclein, but they do secrete other molecules such as peptide YY and serotonin[61]. Additionally, EECs were the main cells expressing α-synuclein in the iHOs, and this expression has been reported to occur predominantly in their basal surface which also has synaptic vesicles and processes that appear to contact enteric neurons[51], implying that α-synuclein might be secreted basally. Therefore, we speculate that extracellular α-synuclein detected in iHO cultures, and in the central compartment of iHO-ENS co-cultures, was secreted by EECs. On the other hand, α-synuclein secretion by primary neurons and neuronal cell lines has been previously reported[8]. Therefore, the detected extracellular α-synuclein in ENS cultures, even when cultured independently, was expected.

Measurements suggested that the α-synuclein in the iHO medium modified this protein's concentration in the ENS medium. For example, in the iHO-ENS plated simultaneously, the increased extracellular α-synuclein of the ENS (peripheral compartment) during the first days, indicated that it might have originated from the iHOs. The low concentrations detected at day 10 pointed to an internalization by the ENS until an oversaturation level that led to a less prominent increase afterwards. In this configuration, PD (336 SNCAx3) iHOs seemed to cause higher levels of α-synuclein in comparison to healthy (232 WT) ones. In the case of iHO-ENS assembloids in which ENS were pre-plated, a single, less prominent, but more sustained-over-time increase of extracellular α-synuclein was observed in the peripheral compartment, with a decrease over the last days of co-culture. Similar to the previous configuration, these results suggested that iHOs caused an increase in α-synuclein in the ENS media that might have been later internalized by the ENS, but in this case no difference was observed between the assembloids with PD and healthy iHOs. The different tendencies between the two co-culture configurations are thought to be caused by the presence of the pre-plated ENS before the placement of the insert and the seeding of the iHOs (in the pre-plated ENS configuration), in which neurons constituted an additional physical barrier for the movement of α-synuclein between compartments, leading to a less pronounced, although more sustained, change over time. However, α-synuclein internalization explanations are built from assumptions, since unfortunately we could not evaluated intracellular α-synuclein in ENS via WB. Additionally, several questions remained unanswered, such as the increased levels of α-synuclein in the medium of healthy iHOs or the lack of effect of the type of iHO (PD or healthy) on the extracellular α-synuclein of the peripheral compartment in the pre-plated ENS configuration.

The lack of success in quantifying intracellular α-synuclein was thought to be a combination of several factors, including loss of neuronal material while attempting to separately retrieve the intestinal organoids and the enteric neurons from the co-culture plate. However, quantification of endogenous α-synuclein via WB, especially in cultured cells, has long been considered a challenge[62]. In accordance to what was observed in this project, one study pointed out that intracellular α-synuclein in neuroblastoma cells is easily detected by immunocytochemistry, but not by standard WB, even if the latter technique is assumed to be more sensitive[63]. Two independent studies have demonstrated that such difficulties occur because the protein is easily washed during routine blotting procedures[62,63]. One of the groups proposed the use of low concentrations of PFA to fix the proteins onto blotted membranes, as performed in the used protocol. However, this method does not seem to be

completely effective with different cell lines or different antibodies[62,64]. The second study demonstrated that pre-treatment of cell lysates with dithiobis(succinimidylpropionate)(DSP), a reducible amine-reactive-crosslinker, strongly increased α-synuclein immunoreactivity. They explained that the amine crosslinker neutralizes positive charges of the protein (which has 15 Lysines) and increases its hydrophobicity, promoting adhesion to the blotting membranes. Relevantly, a different group tested the proposed methodology in primary enteric neurons from rat and human intestinal homogenates, obtaining positive results[64]; this supports the method's effectiveness in a varied set of samples and with a wide range of antibodies. It is considered that the inclusion of a treatment with DSP in the WB protocol for α-synuclein detection would allow to quantify intracellular α-synuclein from enteric neurons in future studies.

The uncertain results obtained from the extracellular α-synuclein evaluations summed to the impossibility to quantify intracellular α-synuclein in the ENS, rendered this assembloid model unusable for the project's objectives. As a result, the research was continued with the development of iHO-ENC assembloids.

4.3 iHO-ENC assembloids

Concerning the second approach for generating assembloids of the intestine and the enteric nervous system, an assembloid comprised by neuron-containing intestinal organoids was constructed following a step-wise differentiation process as described in section 2.1.4.2. These assembloids formed three-dimensional structures that possessed a lumen-lining epithelium surrounded by neurons. The generation of innervated iHOs has been previously reported by Workman *et al.* (2017)[38], and the same research group later published a protocol[39] on which we based our own derivations. We followed the overall process described by this group, which consisted in generating iPSC-derived enteric neuron precursors (which they call vagal neural crest cells) and hindgut spheroids and combining them in a 3D culture system to form iHOs with a neuronal component. Visually, the generated assembloids resemble the ones reported by these researchers, as they kept the morphology of an intestinal organoid, but surrounded by neurons. Similar to this group, the usage of a GFP-expressing cell line allowed to confirm the ENC origin of the observed neurons. But in this project, the GFP-expressing cell line was only used once to confirm that the derivation process worked as intended. Therefore, the ENC-origin of the neurons obtained in other assembloids can not be 100% confirmed, as there is a possibility

that MAP2+ cells could have been originated from cells from the iHO derivation that unintendedly differentiated into a neuronal lineage.

Several organoid models have been developed to study PD, the most relevant ones being brain organoids[15]. Yet, as mentioned before, due to the multifaced aspects of PD, a need has surged to expand the complexity of existing models to include the interaction of different brain regions and diverse types of organoids. Some groups have studied intestinal organoids[65,66] and human neuroectodermal spheres[65] that have been derived from PD patient-specific iPSCs carrying an *LRRK2*-G2019S mutation; however, their interaction was not examined in these studies. To our knowledge, this is the first time that a PD-human organoid model that incorporates the intestine and the enteric nervous system has been built, and the first of such a model to be used to study α-synuclein transmission from the gut to the ENS.

The significantly different increase of α-synuclein and the tendency of α-synuclein spot area and count to increase in the enteric neurons co-cultivated with the PD iHO in comparison to the ones co-cultivated with a healthy iHO (Figures 32 & 33), might indicate that the pathological overexpression of this protein in the intestinal organoids caused an increase in its migration to the neighboring enteric neurons. It is considered that the α-synuclein detected in the enteric neurons proceeded from the intestinal organoids due to the fact the enteric neurons were derived from knock-out cell line for α-synuclein and therefore should not possess endogenous α-synuclein (as previously confirmed by staining of ENS derived from cell line 320 SNCA KO, appendix 6.2). The transmission of α-synuclein from the intestine to the ENS, the *vagus* nerve, and lastly to the brain has been previously demonstrated in animal models[8]. It is not possible to directly observe this process in humans; but, as summarized by Rietdijk *et. al* (2017), an increased staining for α-synuclein has been observed in the intestinal mucosa of PD patients, in association with increased permeability of the intestinal barrier, and Lewy bodies have been detected in the vagal nerves and the DMV before spreading to other areas of the brain. As further reviewed by these authors, studies have shown that α-synuclein is secreted by neurons as monomers, polymers, and fibrils through exocytosis (via vesicles or exosomes) and that neurons can take up α-synuclein from the environment by endocytosis (for polymers and fibrils) or through diffusion across the cell membrane[8]. Additionally, it has been reported that secreted α-synuclein is regulated by neuronal activity, displays cellular toxicity, impairs synaptic transmission[67], and activates inflammatory responses in microglia[68], all of which highlights its possible contribution to PD pathology. As shown for the iHO-ENS assembloid, iHOs appeared to secrete

α-synuclein to the medium, which means it could have been absorbed by neighboring neurons even if they were not in direct cell-to-cell contact. Nonetheless, neuron-to-neuron transmission of α-synuclein has also been proven *in vitro* using labeled human α-synuclein; after uptake, α-synuclein was shown to move through axons in an anterograde or retrograde fashion before transferring to other neurons[8]. As discussed before, immunostaining demonstrated the presence of α-synuclein in EECs of the iHOs (as well as in other uncharacterized epithelial cells). An interesting study by Chandra *et al.* (2017) reports that α-synuclein-expressing EECs connect to enteric neurons via fiber-like cellular processes; they describe that, besides sensing luminal contents of the intestine and producing hormones, EECs are linked to neurons, are electrically excitable, and hold many neuronal features, such as having presynaptic and post-synaptic proteins, neurofilaments, small secretory vesicles, and expressing TH. This team suggested that the EEC location at the interphase between the intestine and the enteric nervous system makes them a feasible target for the induction of abnormal α-synuclein aggregation and the initiation of its spread to the CNS that eventually leads to PD. In alignment to this, another study had previously revealed, via rabies viral tracing, a functional synaptic connection between EECs and enteric neurons in mice[69]. Furthermore, a recent publication demonstrated the spread of α-synuclein fibrils from the enteroendocrine cell line STC-1 and the neuronal cell line SH-SY5Y by a process dependent on cell-to-cell direct contact[60]. Even though no specific study was performed in this project to detect iHO-to-neuron synaptic connections, imaging of the iHO-ENC assembloids showed that neurons were frequently adjacent iHOs and often close to the α-synuclein-expressing cells hypothesized to be EECs (Figures 30 & 31). This leaves open the option that α-synuclein might have been directly transmitted to the enteric neurons via EECs and/or other types of α-synuclein-containing cells in the iHOs. Nonetheless, in previously derived innervated intestinal organoids, no apparent interaction between EECs and neurons was observed[38].

Another interesting finding was the lack of significance of α-synuclein content, or spot area, count or size, between ENCs from cell lines 232 (WT) and 320 (SNCA KO) co-cultivated with a 232 (WT) iHO (Figures 32 & 33). This comparison was performed with the aim to determine if a basal α-synuclein expression was required in enteric neurons to be recruited for aggregate formation by α-synuclein proceeding from neighboring iHOs, as proposed by the idea that aggregated α-synuclein spreads in a prion-like manner[8]. Nonetheless, the lack of significance in this comparison and the presence of α-synuclein in ENCs 320 (SNCA KO), besides supporting the hypothesis that it came from the iHOs, seems to indicate that this basal expression is not

required, and furthermore, it does not lead to greater α-synuclein accumulation in the neuronal component of the assembloid. The possibility of these observations being the result of a lack of antibody specificity was discarded by previously executed staining of ENS from cell line 320 (SNCA KO; appendix 6.2). Accordingly, other authors have also observed that PD does not fully fall in the definition of a prion-like disorder[15]. The made observations, however, must be taken cautiously, since the comparison should have also included a PD iHO / WT ENC combination; but due to derivation issues, no such assembloid was obtained. As a consequence to these same issues, only one replicate of the iHO-ENC assembloids could be quantified, which means that additional repetitions are needed to confirm the observed results. Also, immunostaining for p-α-synuclein should be done, to be able to more accurately characterize aggregated α-synuclein, as opposed to total α-synuclein.

In relation to spot detection in the assembloids, the obtained average α-synuclein aggregate (spot) size within the ENCs was around 10-20 pixels (Figure 33), equivalent to 3,2-6,4 µm. The critical diameter for α-synuclein aggregation has been experimentally defined as approximately 0.32µm[70], α-synuclein filaments have been described to have 5-10 nm in length, and Lewy bodies have been reported to measure 5-25 µm in diameter[71]. Therefore, the observed size is similar to the lower range of the reported diameter of LBs. And smaller aggregates, perhaps intermediates between filaments and LBs, seem to have also been quantified.

Now, when analyzing α-synuclein content within the iHOs, the greater content within 232 (WT) iHOs in co-culture with 320 (SNCA KO) ENCs in comparison to 232 (WT) ENCs was unexpected. This is hypothesized to be caused by a compensatory up regulation in the iHOs due to the lack of α-synuclein in the ENC; the connection of enteric nerves with α-synuclein-expressing EECs that takes place *in vivo*, could explain this type of cross-talk between the different cell types of the assembloid. Nonetheless, further studies would be required to understand this. On the other side, the greater α-synuclein content within 232 (WT) iHOs in comparison to 336 (SNCAx3) iHOs (both in co-culture with 320 SNCA KO ENCs) is thought to be due to the greater levels of secretion of this protein that was detected in iHOs from the latter cell line in the extracellular α-synuclein studies (section 3.3). This would also be in alignment with the obtained results for α-synuclein spot size in the iHO, which was significantly smaller in PD (336 SNCAx3) iHOs, but showed a tendency for an increased count (Figure 33).

In summary, the generated iHO-ENC assembloids successfully achieved the incorporation of an enteric nervous system to an intestinal organoid. More

importantly, these assembloids emulated the α-synuclein transmission from the gut to the enteric nervous system that is hypothesized to be a possible origin of PD pathology.

There are several ways in which the current study could be improved or expanded. It should be considered that only one biological replicate was obtained for the PD iHO / WT ENC assembloid, therefore, further testing is required to guarantee reproducibility of obtained results. With regard to the model characterization, further testing can be performed to prove iHO-ENC synaptic contact, such as rabies retrograde viral tracing or synaptic staining. The functionality of neurons in iHOs could be assessed through electrical-field stimulation to evaluate enteric neuron-mediated contractile activity[38]. Additionally, the generation of an isogenic-GFP expressing cell line to derive the ENCs could aid in ensuring the ENC origin of the observed neuronal component.

Concerning the study of α-synuclein transmission, the usage of cell lines with differentially labelled α-synuclein could help verify the origin of α-synuclein present in each of the subcomponents of the assembloid. Also, p-α-synuclein staining and imaging at higher resolution (63X) could be implemented to characterize aggregates more accurately.

Furthermore, it would be important to generate assembloids that model post natal (and ideally adult) human tissue. However, previous studies have shown that even with prolonged periods of culturing, *in vitro* iHOs continue to resemble the fetal intestine as opposed to the adult tissue[72]. It was only with the *in vivo* engraftment into immunocompromised mice that Workman and collaborators (2017) achieved the obtention of innervated iHOs with a more complex tissue structure (with e.g. vascularization, formation of villi and crypt structures, organization of neurons into ganglionated structures). An alternative to the use of an animal model could be the generation of an *in vitro*-aged iHO. A study by Uchida *et al.* (2018) showed that the stem cell marker *Lgr5* was epigenetically silenced in intestinal organoids derived from aged mice[73]. Creating an iHO in which this gene is silenced, via e.g. RNA interference or a knock-out cell line, could help derive an organoid that more accurately mimics adult tissue. The incorporation of other components to the assembloid, such as a microbiome, immune cells, or vasculature, could also make the model a more realistic version of a human intestine.

Leaving these observations aside, the generated model has a wide prospect of research applications. Differential expression, proteomic and metabolomic analysis of PD assembloids and healthy assembloids could help identify dysregulated genes or

pathways which could widen our understanding of the pathogenesis of PD in the gut context and deepen our insights for a potential therapeutic target. These targets could be verified by performing rescues via genetic modification or exposure of the assembloids to targeted drug treatments. Furthermore, the model could be used to mimic PD with a different genetic or environmental cause: the assembloids could be generated using cell lines with *LRRK2* mutations and idiopathic PD could be modeled via the exposure of iHOs to toxins known to induce α-synuclein aggregation, or to α-synuclein fibrils. Another next step would be to study other phases of the staging of LP in PD as proposed by Braak. A microbiome could be included in the lumen of the iHOs, to form a colonized and innervated intestinal assembloid, and the effects of a PD-related microbiome on the iHO-ENS assembloid could be elucidated. This is a particularly interesting option from the therapeutic point of view since the microbiome can be influenced in a relatively easy manner through dietary modifications or even fecal transplants. Going in the opposite direction, innervated intestinal organoids could be co-cultivated with brain organoids such as the ones studied in this project, to form iHO-ENS-CNS assembloids. This would aid to identify key processes or signals during α-synuclein transmission that could be interrupted or reversed to prevent further spread, and hopefully, alleviate symptomatology. In summary, the opportunities with such a model seem to be limited only by the researcher's creativity, as the tissue engineering technology is progressing at an unprecedented rate.

4.4 α-synuclein and p- α-synuclein analysis in brain organoids

As mentioned in the Introduction, organoids modeling diverse regions of the brain have been developed, and in relation to PD, MOs are highly relevant brain models. However, in the context of this project, the behavior of α-synuclein in different brain regions that connect to the *vagus* nerve and the enteric nervous system is of interest. As a result, α-synuclein and p-α-synuclein content was examined on brain organoids that posses a brainstem-related identity. But it has to be taken into account that their characterization has not been published yet.

Regarding the obtained results, the lack of difference between the neuronal content of PD (336 SNCAx3) and healthy (232 WT & 362 WT) organoids along time, indicated that PD organoids possessed the neuronal content expected for the brain model and were therefore valid for further comparison studies. It additionally evidenced the absence of neuronal loss in the PD brains during the evaluated time points. This resembles findings of an idiopathic PD study, in which increased levels

of α-synuclein were detected in the DMV and the SN, while neuronal loss was exclusively detected in the SN and not in the DMV[74], supporting the brainstem-like profile of the organoids. However, it could also mean that longer periods of cultivation are required to reproduce neuronal loss. Furthermore, staining for cell type-specific markers could allow to understand if loss of specific neuronal-subtypes, such as dopaminergic neurons, takes place. Considering the abundant α-synuclein expression as observed in immunostaining of sections of the organoids, it has long been known that, under physiologically normal conditions, α-synuclein is mainly expressed in the brain, constituting up to 1% of the total proteins[10]. Recently, deeper region-specific studies have revealed that this protein is mostly expressed in zones that are affected in early PD, such as the olfactory bulb, SN_C, and the dorsal motor nucleus of the *vagus*[75]. Thus, brainstem-like organoids exhibited the expected level of neuronal and α-synuclein content for the anatomical region they emulate.

Miller and collaborators showed in 2004[76] that patients with a triplication in the *SNCA* gene possessed higher levels of its protein and mRNA in serum and brain tissue. Therefore, it would be expected that the level of quantified α-synuclein in the PD brain organoids was higher than in the healthy organoids; however, despite of some tendencies that follow this behavior, only p-α-synuclein was significantly different at 30 DoD. As further explained in the mentioned research, *SNCA* mRNA in the brain was doubled, but concerning protein levels, a greater difference was observed in aggregates deposited in insoluble fractions rather than on total α-synuclein levels, a phenomenon that might have been reproduced in the brain organoids. This contrasts however, with published results in iPSC-derived MOs harboring a triplication for the *SNCA* gene, which depicted significantly different levels of α-synuclein and p-α-synuclein in comparison to healthy controls at 50, 100 and 170 DoD[35]. The observed differences might be a result of the different regional identities of the brain organoids, since α-synuclein pathology has been shown to have a more rapid initiation in the SN than in other brain regions[77], suggesting that brainstem-like organoids might need a longer culture time to exhibit a stronger PD phenotype.

PD brains did show an increase in α-synuclein and p-α-synuclein overtime, mimicking the progressive accumulation of α-synuclein[78], its oligomers[79] and fibrils[80] that occurs in PD brains. This was also observed for p-α-synuclein in the MO study, but on a later period of development (100 and 170 DoD) than the studied in this project.

Subcellular localization analysis showed that α-synuclein and p-α-synuclein behaved differently through time. α-synuclein increase was more noticeable in the cell body,

while p-α-synuclein increased continuously in the nuclei. However, the difference in comparison to healthy brain models was only significant for p-α-synuclein at 30DoD, implying that the significant difference observed in total p-α-synuclein was mostly influenced by its behavior in the nuclei. This is contrasts with a previous review that mentions that α-synuclein is mostly present in the cytoplasm of cells, associated with cellular membranes (synaptic vesicles, mitochondrial membranes, endoplasmic reticulum, Golgi apparatus, endosomes) and in interaction with various proteins and metal ions[10]. Nuclear α-synuclein has also been reported, presumably as a DNA-binding protein regulating gene expression[10]. But, as reviewed by Oueslati (2016)[13], an increasing number of studies show that p-α-synuclein accumulates significantly in the nucleus. Furthermore, the author exposes that phosphorylation of α-synuclein at Serine 129 may regulate its subcellular location by acting as a tag for its nuclear localization. As this type of phosphorylation is also a biomarker for PD, its function as a nuclear localization tag would explain the significantly different levels of p-α-synuclein observed in the nuclei of PD brain organoids. For the subcellular localization features though, it should be considered that all the nuclei detected in the organoids were accounted, while extranuclear detection was exclusively done within neurons. This could have affected the results obtained for the nuclear compartment, as it also could include the nuclei of glial populations. Regarding the physiological meaning of these results, the toxicity of phosphorylated α-synuclein, and particularly pS129, is still a highly debated topic. Its remarkably higher presence in brains of PD patients has led to believe that this PTM plays a key neuropathological role. However, *in vivo* studies in animal models have provided conflicting evidence, demonstrating p-α-synuclein-mediated toxicity in some studies, and neuroprotective effects in others[13].

The developed spot detection method revealed significantly greater sizes of the α-synuclein aggregates in PD organoids, both in the nuclei and the cell body, albeit at different time points. The lack of difference in size observed for p-α-synuclein suggests that aggregates were not exclusively conformed by the pS129 version of the protein and that other forms of α-synuclein contributed to its volume. These could have been for example, other types of phosphorylation, nitration, ubiquitination, and truncation, which have been detected in α-synuclein within LBs[13].

Average α-synuclein aggregate (spot) size was within 20-80 pixels (Figure 28), which is equivalent to 6,4-26 μm. Since Lewy bodies have been reported to measure 5-25 μm in diameter[71], it is reasonable to state that the detected spots encompassed aggregates of a similar size to LBs. As mentioned, the size of these LBs increased

through time, apparently following a process of progressively increased α-synuclein aggregation. Currently, it is impossible to directly observe the process of α-synuclein aggregate formation and growth in human brains, but aggregation stages have been measured experimentally *in vitro* and in living cells. *In vitro*, observations imply the appearance of a nucleus (nucleation) that progressively increases in size; while in studies using living cells, a preformed "nucleus" is usually seeded[70]. In either case, the described models of α-synuclein aggregation align with the increase of α-synuclein spot size in the brain organoids.

Lewy bodies are a pathological hallmark of PD, but their role in the disease remains unclear. As summarized by Narayanan *et al.* (2019), the presence of α-synuclein is not necessarily correlated with disease progression. They point out that a greater toxicity of aggregate intermediates that appear early in the aggregation process could explain these observations. This highlights the importance of performing additional studies in which high content imaging is done at a higher magnification (63X) to allow the quantification of α-synuclein aggregates of smaller sizes.

In summary, the brain organoids exhibited characteristics supporting a brainstem-like model of PD, by mimicking neuronal stability, progressive α-synuclein and p-α-synuclein accumulation, nuclear localization of p-α-synuclein, and α-synuclein aggregate growth. This model of course, has its limitations. Additional studies should be done that characterize specific neuronal subtypes as well as glial populations, and subcellular localization studies of α-synuclein should be done considering these other cell populations. Isogenic controls should be used to avoid the effect of a different genetic background. The model could be made more physiologically relevant by the incorporation of vascularization or an immune system. Still, the brainstem-like organoids have a wide range of applications for understanding PD. As a highly pertinent example for this project, disease progression could be studied by the co-cultivation with cortical organoids or with enteric neurons.

4.5 Conclusions and final remarks

The aim of this thesis was to build an assembloid model of PD comprising the intestine and the enteric nervous system and use this model to study α-synuclein transmission between these two tissues. This was accomplished through the development of an iHO-ENC assembloid which consisted of intestinal organoids with integrated enteric neurons and the creation of a computational algorithm to quantify α-synuclein detected through high content imaging. In the assembloid, an increased accumulation of α-synuclein was observed within the neurons grown together with

PD iHOs, suggesting a pathological transmission of the protein. Furthermore, aggregate size within the neurons conveyed early stages of LP. This constitutes, in a preliminary fashion, the foremost observation of α-synuclein propagation from the intestine to the enteric nervous system in a human organoid-based model. These findings provide a baseline for further understanding of the triggering of LP in the gastrointestinal tract.

Interestingly, α-synuclein expression within the iHOs was detected mostly within EECs, which has been previously reported human in duodenum and mouse colon, but has not been published for intestinal organoids. Besides the novelty in characterization of α-synuclein expression in iHOs, this observation has significant implications for the disease model, considering that EECs have been proposed as α-synuclein misfolding induction sites in the gut.

Additionally, analysis of PD brain organoids revealed an increased content of α-synuclein phosphorylated at Serine 129 in nuclei, supporting the function of this PTM as a nuclear localization tag, and providing insight into its pathological implications. This model further replicated PD phenotype by the observation of Lewy body-like aggregates that increased in size over time, mimicking pathological progression.

The cellular and computational models created in this project have a promising potential as a foundation for further disease modeling and drug screening studies, and can hopefully enable the identification of targets and therapeutical approaches to tackle Parkinson’s Disease.

5 References

1. Lebouvier, T. *et al.* The second brain and Parkinson's disease. *Eur. J. Neurosci.* **30**, 735–741 (2009).
2. Sveinbjornsdottir, S. The clinical symptoms of Parkinson's disease. *J. Neurochem.* **139**, 318–324 (2016).
3. Hirsch, L., Jette, N., Frolkis, A., Steeves, T. & Pringsheim, T. The Incidence of Parkinson's Disease: A Systematic Review and Meta-Analysis. *Neuroepidemiology* **46**, 292–300 (2016).
4. Schrag, A. & Schott, J. M. Epidemiological, clinical, and genetic characteristics of early-onset parkinsonism. *Lancet Neurol.* **5**, 355–363 (2006).
5. Tran, J., Anastacio, H. & Bardy, C. Genetic predispositions of Parkinson's disease revealed in patient-derived brain cells. *Npj Park. Dis.* **6**, 8 (2020).
6. Langston J. William, Ballard Philip, Tetrud James W., & Irwin Ian. Chronic Parkinsonism in Humans Due to a Product of Meperidine-Analog Synthesis. *Science* **219**, 979–980 (1983).
7. Tanner Caroline M. *et al.* Rotenone, Paraquat, and Parkinson's Disease. *Environ. Health Perspect.* **119**, 866–872 (2011).
8. Rietdijk, C. D., Perez-Pardo, P., Garssen, J., van Wezel, R. J. A. & Kraneveld, A. D. Exploring Braak's Hypothesis of Parkinson's Disease. *Front. Neurol.* **8**, 37 (2017).
9. Armstrong, M. J. & Okun, M. S. Diagnosis and Treatment of Parkinson Disease: A Review. *JAMA* **323**, 548 (2020).
10. Kawahata, I., Finkelstein, D. I. & Fukunaga, K. Pathogenic Impact of α-Synuclein Phosphorylation and Its Kinases in α-Synucleinopathies. *Int. J. Mol. Sci.* **23**, (2022).
11. Koh, Y. H., Tan, L. Y. & Ng, S.-Y. Patient-Derived Induced Pluripotent Stem Cells and Organoids for Modeling Alpha Synuclein Propagation in Parkinson's Disease. *Front. Cell. Neurosci.* **12**, 413 (2018).
12. Meade, R. M., Fairlie, D. P. & Mason, J. M. Alpha-synuclein structure and Parkinson's disease – lessons and emerging principles. *Mol. Neurodegener.* **14**, 29 (2019).
13. Oueslati, A. Implication of Alpha-Synuclein Phosphorylation at S129 in Synucleinopathies: What Have We Learned in the Last Decade? *J. Park. Dis.* **6**, 39–51 (2016).
14. Kingwell, K. Zeroing in on neurodegenerative α-synuclein. *Nat. Rev. Drug Discov.* **16**, 371–373 (2017).
15. Reiner, O., Sapir, T. & Parichha, A. Using multi-organ culture systems to study Parkinson's disease. *Mol. Psychiatry* **26**, 725–735 (2021).
16. Braak, H., Rüb, U., Gai, W. P. & Del Tredici, K. Idiopathic Parkinson's disease: possible routes by which vulnerable neuronal types may be subject to neuroinvasion by an unknown pathogen. *J. Neural Transm.* **110**, 517–536 (2003).
17. Braak, H. *et al.* Staging of brain pathology related to sporadic Parkinson's disease. *Neurobiol. Aging* **24**, 197–211 (2003).

18. Hawkes, C. H., Del Tredici, K. & Braak, H. Parkinson's disease: a dual-hit hypothesis. *Neuropathol. Appl. Neurobiol.* **33**, 599–614 (2007).

19. Hawkes, C. H., Del Tredici, K. & Braak, H. Parkinson's Disease: The Dual Hit Theory Revisited. *Ann. N. Y. Acad. Sci.* **1170**, 615–622 (2009).

20. Kim, J., Koo, B.-K. & Knoblich, J. A. Human organoids: model systems for human biology and medicine. *Nat. Rev. Mol. Cell Biol.* **21**, 571–584 (2020).

21. Lui, J. H., Hansen, D. V. & Kriegstein, A. R. Development and evolution of the human neocortex. *Cell* **146**, 18–36 (2011).

22. Sanoh, S. *et al.* Predictability of metabolism of ibuprofen and naproxen using chimeric mice with human hepatocytes. *Drug Metab. Dispos. Biol. Fate Chem.* **40**, 2267–2272 (2012).

23. Takahashi, K. *et al.* Induction of pluripotent stem cells from adult human fibroblasts by defined factors. *Cell* **131**, 861–872 (2007).

24. Sato, T. *et al.* Single Lgr5 stem cells build crypt-villus structures in vitro without a mesenchymal niche. *Nature* **459**, 262–265 (2009).

25. Lancaster, M. A. & Knoblich, J. A. Generation of cerebral organoids from human pluripotent stem cells. *Nat. Protoc.* **9**, 2329–2340 (2014).

26. Monzel, A. S. *et al.* Derivation of Human Midbrain-Specific Organoids from Neuroepithelial Stem Cells. *Stem Cell Rep.* **8**, 1144–1154 (2017).

27. Martins, J.-M. F. *et al.* Self-Organizing 3D Human Trunk Neuromuscular Organoids. *Cell Stem Cell* **26**, 172-186.e6 (2020).

28. Takasato, M. *et al.* Kidney organoids from human iPS cells contain multiple lineages and model human nephrogenesis. *Nature* **526**, 564–568 (2015).

29. Lancaster, M. A. *et al.* Cerebral organoids model human brain development and microcephaly. *Nature* **501**, 373–379 (2013).

30. Muguruma, K., Nishiyama, A., Kawakami, H., Hashimoto, K. & Sasai, Y. Self-organization of polarized cerebellar tissue in 3D culture of human pluripotent stem cells. *Cell Rep.* **10**, 537–550 (2015).

31. Zagare, A., Gobin, M., Monzel, A. S. & Schwamborn, J. C. A robust protocol for the generation of human midbrain organoids. *STAR Protoc.* **2**, 100524 (2021).

32. Qian, X. *et al.* Brain-Region-Specific Organoids Using Mini-bioreactors for Modeling ZIKV Exposure. *Cell* **165**, 1238–1254 (2016).

33. Makrygianni, E. A. & Chrousos, G. P. From Brain Organoids to Networking Assembloids: Implications for Neuroendocrinology and Stress Medicine. *Front. Physiol.* **12**, 661 (2021).

34. Smits, L. M. *et al.* Modeling Parkinson's disease in midbrain-like organoids. *Npj Park. Dis.* **5**, 5 (2019).

35. Mohamed, N.-V. *et al.* Midbrain organoids with an SNCA gene triplication model key features of synucleinopathy. *Brain Commun.* **3**, fcab223–fcab223 (2021).

36. Spence, J. R. *et al.* Directed differentiation of human pluripotent stem cells into intestinal tissue in vitro. *Nature* **470**, 105–109 (2011).

37. AU - Lees, E. A. *et al.* Using Human Induced Pluripotent Stem Cell-derived Intestinal Organoids to Study and Modify Epithelial Cell Protection Against Salmonella and Other Pathogens. *J. Vis. Exp.* e59478 (2019) doi:10.3791/59478.

38. Workman, M. J. *et al.* Engineered human pluripotent-stem-cell-derived intestinal tissues with a functional enteric nervous system. *Nat. Med.* **23**, 49–59 (2017).

39. Loffet, E., Brossard, L. & Mahe, M. M. Pluripotent stem cell derived intestinal organoids with an enteric nervous system. *Methods Cell Biol.* **159**, 175–199 (2020).

40. Davenport, C., Diekmann, U., Budde, I., Detering, N. & Naujok, O. Anterior–Posterior Patterning of Definitive Endoderm Generated from Human Embryonic Stem Cells Depends on the Differential Signaling of Retinoic Acid, Wnt-, and BMP-Signaling. *Stem Cells* **34**, 2635–2647 (2016).

41. Fattahi, F. *et al.* Deriving human ENS lineages for cell therapy and drug discovery in Hirschsprung disease. *Nature* **531**, 105–109 (2016).

42. Barber, K., Studer, L. & Fattahi, F. Derivation of enteric neuron lineages from human pluripotent stem cells. *Nat. Protoc.* **14**, 1261–1279 (2019).

43. Mead, B. E. & Karp, J. M. All models are wrong, but some organoids may be useful. *Genome Biol.* **20**, 66 (2019).

44. Vogt, N. Assembloids. *Nat. Methods* **18**, 27–27 (2021).

45. Garner, K. L. High content imaging for monitoring signalling dynamics in single cells. *J. Mol. Endocrinol.* **65**, R91–R100 (2020).

46. Buchser, W. *et al.* Assay Development Guidelines for Image-Based High Content Screening, High Content Analysis and High Content Imaging. in *Assay Guidance Manual (Internet)* (Eli Lilly & Company and the National Center for Advancing Translational Sciences, 2014).

47. CV8000 High-Throughput System | Yokogawa Europe. https://www.yokogawa.com/eu/solutions/products-and-services/life-science/high-content-analysis/cv8000/#Details.

48. Boutros, M., Heigwer, F. & Laufer, C. Microscopy-Based High-Content Screening. *Cell* **163**, 1314–1325 (2015).

49. The UniProt Consortium. UniProt: the universal protein knowledgebase in 2021. *Nucleic Acids Res.* **49**, D480–D489 (2021).

50. Cummins, P. M. Occludin: one protein, many forms. *Mol. Cell. Biol.* **32**, 242–250 (2012).

51. Chandra, R., Hiniker, A., Kuo, Y.-M., Nussbaum, R. L. & Liddle, R. A. α-Synuclein in gut endocrine cells and its implications for Parkinson's disease. *JCI Insight* **2**, e92295 (2017).

52. Zainolabidin, N., Kamath, S. P., Thanawalla, A. R. & Chen, A. I. Distinct Activities of Tfap2A and Tfap2B in the Specification of GABAergic Interneurons in the Developing Cerebellum. *Front. Mol. Neurosci.* **10**, (2017).

53. Iwasaki, M., Akiba, Y. & Kaunitz, J. D. Recent advances in vasoactive intestinal peptide physiology and pathophysiology: focus on the gastrointestinal system. *F1000Research* **8**, F1000 Faculty Rev-1629 (2019).

54. Taguchi, K. *et al.* Differential expression of alpha-synuclein in hippocampal neurons. *PloS One* **9**, e89327 (2014).

55. Papatheodorou, I. *et al.* Expression Atlas update: from tissues to single cells. *Nucleic Acids Res.* **48**, D77–D83 (2020).

56. Mica, Y., Lee, G., Chambers, S. M., Tomishima, M. J. & Studer, L. Modeling neural crest induction, melanocyte specification, and disease-related pigmentation defects in hESCs and patient-specific iPSCs. *Cell Rep.* **3**, 1140–1152 (2013).

57. Dehmelt, L. & Halpain, S. The MAP2/Tau family of microtubule-associated proteins. *Genome Biol.* **6**, 204 (2004).

58. Li, W. *et al.* Characterization and transplantation of enteric neural crest cells from human induced pluripotent stem cells. *Mol. Psychiatry* **23**, 499–508 (2018).

59. Phillips, R. J., Walter, G. C., Wilder, S. L., Baronowsky, E. A. & Powley, T. L. Alpha-synuclein-immunopositive myenteric neurons and vagal preganglionic terminals: autonomic pathway implicated in Parkinson's disease? *Neuroscience* **153**, 733–750 (2008).

60. Rodrigues, P. V. *et al.* Transcellular propagation of fibrillar α-synuclein from enteroendocrine to neuronal cells requires cell-to-cell contact and is Rab35-dependent. *Sci. Rep.* **12**, 4168 (2022).

61. Lerner, A. The intestinal luminal sources of α-synuclein: a gastroenterologist perspective. *Nutr. Rev.* **80**, 282–293 (2022).

62. Newman, A. J., Selkoe, D. & Dettmer, U. A New Method for Quantitative Immunoblotting of Endogenous α-Synuclein. *PLOS ONE* **8**, e81314 (2013).

63. Lee, B. R. & Kamitani, T. Improved Immunodetection of Endogenous α-Synuclein. *PLOS ONE* **6**, e23939 (2011).

64. Preterre, C. *et al.* Optimizing Western Blots for the Detection of Endogenous α-Synuclein in the Enteric Nervous System. *J. Park. Dis.* **5**, 765–772 (2015).

65. Son, M.-Y. *et al.* Distinctive genomic signature of neural and intestinal organoids from familial Parkinson's disease patient-derived induced pluripotent stem cells. *Neuropathol. Appl. Neurobiol.* **43**, 584–603 (2017).

66. Sim, H. *et al.* Iroquois Homeobox Protein 2 Identified as a Potential Biomarker for Parkinson's Disease. *Int. J. Mol. Sci.* **21**, (2020).

67. Yamada, K. & Iwatsubo, T. Extracellular α-synuclein levels are regulated by neuronal activity. *Mol. Neurodegener.* **13**, 9 (2018).

68. Kim, C. *et al.* Neuron-released oligomeric α-synuclein is an endogenous agonist of TLR2 for paracrine activation of microglia. *Nat. Commun.* **4**, 1562 (2013).

69. Bohórquez, D. V. *et al.* Neuroepithelial circuit formed by innervation of sensory enteroendocrine cells. *J. Clin. Invest.* **125**, 782–786 (2015).

70. Narayanan, A. *et al.* A first order phase transition mechanism underlies protein aggregation in mammalian cells. *eLife* **8**, (2019).

71. Spillantini, M. G., Crowther, R. A., Jakes, R., Hasegawa, M. & Goedert, M. alpha-Synuclein in filamentous inclusions of Lewy bodies from Parkinson's disease and dementia with lewy bodies. *Proc. Natl. Acad. Sci. U. S. A.* **95**, 6469–6473 (1998).

72. Finkbeiner, S. R. *et al.* Transcriptome-wide Analysis Reveals Hallmarks of Human Intestine Development and Maturation In Vitro and In Vivo. *Stem Cell Rep.* **4**, 1140–1155 (2015).

73. Uchida, R. *et al.* Epigenetic silencing of Lgr5 induces senescence of intestinal epithelial organoids during the process of aging. *NPJ Aging Mech. Dis.* **5**, 1 (2019).

74. Pan-Montojo, F. *et al.* Progression of Parkinson's disease pathology is reproduced by intragastric administration of rotenone in mice. *PloS One* **5**, e8762 (2010).

75. Taguchi, K., Watanabe, Y., Tsujimura, A. & Tanaka, M. Expression of α-synuclein is regulated in a neuronal cell type-dependent manner. *Anat. Sci. Int.* **94**, 11–22 (2019).

76. Miller, D. W. *et al.* α-Synuclein in blood and brain from familial Parkinson disease with SNCA locus triplication. *Neurology* **62**, 1835 (2004).

77. Henderson, M. X. *et al.* Spread of α-synuclein pathology through the brain connectome is modulated by selective vulnerability and predicted by network analysis. *Nat. Neurosci.* **22**, 1248–1257 (2019).

78. Chu, Y. & Kordower, J. H. Age-associated increases of alpha-synuclein in monkeys and humans are associated with nigrostriatal dopamine depletion: Is this the target for Parkinson's disease? *Neurobiol. Dis.* **25**, 134–149 (2007).

79. Roshanbin, S. *et al.* Age-related increase of alpha-synuclein oligomers is associated with motor disturbances in L61 transgenic mice. *Neurobiol. Aging* **101**, 207–220 (2021).

80. Canron, M.-H., Perret, M., Vital, A., Bézard, E. & Dehay, B. Age-dependent α-synuclein aggregation in the Microcebus murinus lemur primate. *Sci. Rep.* **2**, 910 (2012).

6 Appendix

6.1 Antibodies used in immunocytochemistry studies.

Antibody	Source	Catalog number
α-synuclein	NOVUS Biologicals	NBP1-05194
α-synuclein	ab138501	Abcam
p- α-synuclein	Cell Signaling	23706S
Villin	Santa Cruz	sc-58897
Anti-Uvomorulin/E-Cadherin	Sigma	U3254
CDX2	ThermoFisher	PA5-13122
Chromogranin A	ThermoFisher	MA5-13096
Vimentin	Abcam	ab24525
Mucin	Santa Cruz	sc-59859
Ki-67	GenScript	A01495-40
Occludin	Abcam	ab31721
Lysozyme	ThermoFisher	PA5-16668
PHOX2A	Abcam	ab155084
ChAT	Thermo Fisher	PA5-29653
GABA	Abcam	ab17413
MAP2	Abcam	ab92434
Serotonin	Millipore	MAB352
Tyrosine Hydroxylase (TH)	Abcam	ab112
TUJ1	Abcam	ab41489
TUJ1	BioLegend	801201
SOX10	DSHB	PCRP-SOX10-1D8
MASH1	BD Bioscience	556604
5-HT2C Receptor	Abcam	ab137529
AP-2α	DSHB	3B5

TPH2	Abcam	ab111828
GAD67	Sigma	G5419
Neurofilament	Abcam	ab7794
HuC/HuD	Thermofisher/Invitrogen	A-21271
VIP	Santa Cruz	sc-25347
Goat anti- mouse IgG1 488	Thermo Scientific	A-21121
Goat anti- mouse IgG1 568	Invitrogen	A21124
Goat anti- mouse IgG1 647	Invitrogen	A-21240
Goat anti- Rabbit IgG 488	Invitrogen	A11034
Goat anti- Rabbit IgG 568	Invitrogen	A11036
Goat anti- Rabbit IgG 647	Invitrogen	A-21244
Goat anti- Rat IgG 568	Invitrogen	A-11077
Goat anti- guinea pig IgG 568	Invitrogen	A11075
Goat anti- chicken IgG 488	Invitrogen	A-11039
Goat anti- chicken IgY 647	Invitrogen	A-21449
Goat anti- mouse IgG 568	Invitrogen	A-21043
Goat anti- mouse IgG2b 568	Invitrogen	A-21144
Goat anti- mouse IgG2a 647	Invitrogen	A-21241
Hoechst	Invitrogen	62249

6.2 α-synuclein staining of ENS from cell line 320 (SNCA KO)

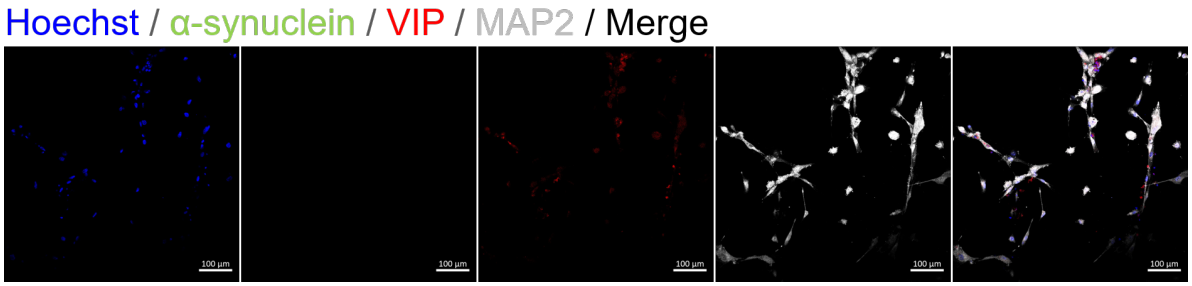

Figure 34. ENS from cell line 320 (SNCA KO) do not express α-synuclein. 50 DoD enteric neurons (ENS) derived from iPSCs from cell line 320 (SNCA KO) immunostained for Hoechst, α-synuclein, VIP, and MAP2. DoD: days of differentiation; VIP: Vasoactive Intestinal Peptide; MAP2: Microtubule-associated Protein 2. Scale bar: 100 µm.